

**Development and application of Crystal
Digital PCR-based single pollen nucleus
genotyping to measure meiotic recombination
rates in barley (*Hordeum vulgare*) in high-
throughput**

Dissertation

zur Erlangung des

Doktorgrades der Naturwissenschaften (Dr. rer. nat.)

der

Naturwissenschaftlichen Fakultät III

Agrar- und Ernährungswissenschaften,

Geowissenschaften und Informatik

Martin-Luther-Universität Halle-Wittenberg

vorgelegt von

Frau Yun-Jae Ahn

Geboren am 21.01.1993 in Daegu, Republic of Korea

Gutachter:

1. Prof. Dr. Andreas Houben
2. Prof. Dr. Eugenio Sanchez-Moran

Tag der öffentlichen Verteidigung: 02 Mai 2022, Halle (Salle)

Table of Contents

1. Introduction	1
1.1. <i>Overview of meiosis</i>	1
1.2. <i>Meiotic recombination</i>	1
1.2.1. Pathways to meiotic recombination	1
1.2.2. Meiotic chromosome axis and synaptonemal complex	2
1.2.3. Meiotic recombination landscapes	5
1.2.4. Meiosis in barley	7
1.3. <i>Manipulation of meiotic HR outcome in plants</i>	8
1.3.1. Genetic modifiers	8
1.3.2. Epigenetic modifiers	9
1.3.3. Environment, abiotic/biotic factors and “stresses”	10
1.3.4. Chemical compounds	12
1.4. <i>Measuring meiotic recombination rates in plants</i>	13
2. Aim of this study	16
3. Materials and Methods	17
3.1. <i>Plant material</i>	17
3.2. <i>Plant cultivation</i>	17
3.3. <i>Cytology</i>	17
3.3.1. Fixation of anthers for cytological analysis	17
3.3.2. Acetocarmine stain preparation of chromosomes for meiotic stage detection	17
3.3.3. Male meiotic chromosome spread preparations	18
3.3.4. EdU detection	18
3.4. <i>In planta injection of chemical compounds</i>	19
3.5. <i>Chemical compounds screening using germinated barley seeds</i>	19
3.6. <i>Crossing of plants and hybrid confirmation</i>	20
3.7. <i>Pollen nuclei isolation</i>	23
3.8. <i>Flow-sorting of isolated pollen nuclei</i>	23
3.9. <i>Single pollen nucleus genotyping with InDel markers</i>	24
3.10. <i>Pre-amplification of target sites from a single pollen nucleus</i>	24
3.11. <i>Single pollen grain genotyping using germinated pollen</i>	25
3.12. <i>Single pollen nucleus genotyping via Crystal Digital PCR</i>	26
3.12.1. Crystal Digital PCR statistics	26
3.12.2. Crystal dPCR genotyping	27
3.12.3. Improving Crystal dPCR efficiency	28
3.12.4. Nuclei encapsulation efficiency employing different plant species	28
3.12.5. Measuring the nuclear size	28
4. Results	29
4.1. <i>In planta delivery of chemical compounds</i>	29
4.1.1. Phenotype analysis of barley hybrids	29
4.1.2. <i>In planta</i> injection	30
4.1.3. Chemical compound pre-screening	35

4.2. PCR-based single pollen nucleus genotyping	40
4.2.1. Direct PCR-based genotyping of flow-sorted single pollen nuclei.....	40
4.2.2. Targeted pre-amplification and subsequent PCR-based genotyping of flow-sorted single pollen nuclei	41
4.2.3. PCR-based genotyping employing entire pollen grains	42
4.2.4. Crystal digital PCR: Encapsulation and genotyping of flow-sorted single haploid pollen nuclei	43
4.2.4.1. Refining a Crystal dPCR-based single pollen nucleus genotyping approach.....	47
4.2.4.2. Crystal dPCR-based single pollen nucleus genotyping: Measuring meiotic recombination rates within four defined chromosomal intervals.....	55
4.2.4.3. Reliable meiotic recombination rate measurements in pollen nuclei samples.....	59
4.2.5. Measuring meiotic recombination rates for plants grown under different environmental conditions, in different spikes of single plants as well as chemical-treated and untreated plants ...	60
4.2.5.1. Meiotic recombination rates in plants grown under different environmental conditions	60
4.2.5.2. Measuring meiotic recombination rates in different spikes of single plants.....	61
4.2.5.3. Measuring meiotic recombination rates simultaneously within two chromosomal intervals after <i>in planta</i> chemical compound injections	62
5. Discussion.....	66
5.1. <i>When and how to deliver chemical compounds in planta</i>	66
5.1.1. Phenotype analysis of barley hybrids	66
5.1.2. Selected chemical compounds and pre-screening of their impact	68
5.2. <i>Comparison of different PCR-based single pollen nucleus genotyping methods</i>	70
5.2.1. Gel-based genotyping of a single pollen nuclei with or without pre-amplification	70
5.2.2. Gel-based genotyping of single pollen grains with or without prior germination	71
5.2.3. Crystal Digital PCR-based genotyping of single pollen nuclei	71
5.3. <i>Establishment and optimization of Crystal dPCR-based genotyping of single pollen nuclei</i>	72
5.3.1. Improving sample throughput	72
5.3.2. Increasing efficiency of Crystal Digital PCR.....	73
5.3.3. Data quality and analysis.....	74
5.3.4. Reliable measurements of meiotic recombination rates in pollen nuclei using Crystal Digital PCR ...	75
5.4. <i>Meiotic recombination rates in plants grown under different environmental conditions</i>	76
5.5. <i>Measuring meiotic recombination rates in different spikes of single plants</i>	76
5.6. <i>Impact of chemical compounds on meiotic recombination rates in barley</i>	77
6. Outlook.....	80
7. Summary	81
8. Zusammenfassung.....	83
9. References.....	85
10. Abbreviations.....	98
11. Acknowledgements.....	99
12. Curriculum vitae	100
Eidesstattliche Erklärung / Declaration under Oath.....	103
13. Appendix	104

1. Introduction

1.1. Overview of meiosis

A distinct feature of sexual reproduction is the alternation between haploid and diploid generations. Chromosome sets are segregated into half through meiosis resulting in the formation of haploid gametes (Mercier *et al.*, 2015). Meiosis is a specialized cell division that involves two successive rounds of chromosome segregation after one round of DNA replication. After the first meiotic division (meiosis I) homologous chromosomes are separated, and after the second meiotic division (meiosis II) sister chromatids are separated. During prophase I, comprised of leptotene, zygotene, pachytene, diplotene and diakinesis (**Figure 1**), chromosomes start to condense, and homologous chromosomes are physically aligned, enabling the crossover (CO; a reciprocal genetic exchange between parental chromosomes) formation. After further condensation until metaphase I, homologous chromosomes are dragged to the opposite poles of the cell by spindle microtubules during anaphase I halving the number of chromosomes. During anaphase I, arm cohesion is lost while centromeric cohesion is maintained, thus sister chromatids are still connected (Mercier *et al.*, 2015). After meiosis I a typically rather short interphase, the interkinesis, follows. During interkinesis, telophase I and prophase II separated chromosomes decondense to form nuclei and the cytoplasm is divided forming two individual cells. During meiosis II, chromosomes condense again, and centromeric cohesion is released, allowing sister chromatids to be pulled by spindle microtubules to opposite poles forming four haploid cells that will give rise to the gametes (**Figure 1**).

By halving somatic ploidy through meiosis, organisms can sustain ploidy level consistently through generations after the fusion of male and female gametes (Mercier *et al.*, 2015). Moreover, homologous recombination (HR) can result in homologous chromosomes reciprocally exchanging their genetic information in the form of CO. Thus, the significance of meiosis for sexual reproduction is two-fold: it assures genetic variation by HR and the random assortment of homologous chromosomes during the first meiotic division as well as it assures somatic diploidy after fusion of male and female gametes.

1.2. Meiotic recombination

1.2.1. Pathways to meiotic recombination

Meiotic HR is initiated by the formation of numerous meiotic DNA double strand breaks (DSBs) during prophase I that are repaired either into CO or non-crossover (NCO; either via inter sister repair leaving no genetic trace or by using the homologous chromosome as repair template) (**Figure 1**).

The fundamental aspects of meiotic recombination are conserved between species, including plants. During leptotene, chromosomes are marked by numerous DSBs catalyzed by the topoisomerase-like protein SPO11 and additional factors (Mercier *et al.*, 2015) (**Figure 1**). DSB ends are resected from 5' ends towards 3' ends and resulting 3' single stranded DNA tails are coated with the recombinases DMC1 and RAD51. These nucleoprotein filaments can either use the sister chromatid as a repair template as in somatic cells, leaving no genetic trace. Or, they can invade the homologous chromosome (strand invasion), acting as a template to restore the DNA sequence leading to the formation of a structure called displacement loop (D-loop) (Mercier *et al.*, 2015; Wang and Copenhagen, 2018). Considering the fact that excessive numbers of DSBs are generated compared to the number of actual COs in various species, the majority of meiotic DSBs are repaired as NCO either using the sister chromatid as repair template or recombination intermediates are channelled into NCOs in particular through synthesis-dependent strand annealing (SDSA) after D-loop disassembly (**Figure 1**) (Wang and Copenhagen, 2018). When, however, the D-loop region is extended by DNA synthesis enabling the second DSB end to anneal (second end capture), a double Holliday junction (dHj) is formed. This maturation of recombination intermediates into a dHj is mediated by so-called ZMM proteins (**Figure 1**). ZMMs initially described in yeast as Zip1-4, Msh 4-5 and Mer3, recognize and stabilize D-loops and enable their further maturation as COs (Mercier *et al.*, 2015). The resolution of recombination intermediates through the ZMM-dependent pathway can result in the formation of so-called class I COs, that are sensitive to CO interference. CO interference refers to the non-random placement of COs related to each other during meiosis, i.e., the formation of one CO reduces the probability of another CO close by (Wang and Copenhagen, 2018). Typically, ZMM-dependent COs account for ~70-85% of total COs among mammals, yeast and plants (Wang and Copenhagen, 2018). Mechanisms and players involved in class I CO formation seem to be conserved among plants, including *A. thaliana*, rice, wheat and barley (Wang *et al.*, 2012; Barakate *et al.*, 2014; Desjardins *et al.*, 2020). The second type of CO is called class II CO which constitutes 10-20% of the total number of CO. These are not sensitive to interference and in plants either require the activity of MUS81 (Berchowitz and Copenhagen, 2008), FANCD2 (Kurzbaue *et al.*, 2018) or arise via other pathways (**Figure 1**) (Higgins *et al.*, 2008).

1.2.2. Meiotic chromosome axis and synaptonemal complex

Meiotic recombination occurs in the context of meiotic chromosomes and chromatin (Mainiero and Pawlowski, 2014; Mercier *et al.*, 2015). During leptotene, sister chromatids are held together by cohesin and are organized in chromatin loops anchored to a proteinaceous structure, called the meiotic chromosome axis (Blat *et al.*, 2002) (**Figure 1**). This axis structure is comprised of DNA-binding and DNA organizing cohesin complexes such as REC8 and axis-associated proteins such as ASY1, ASY3 and ASY4 in *Arabidopsis* (Caryl *et al.*, 2000; Ferdous *et al.*, 2012; Chambon *et al.*, 2018; Onn *et al.*, 2008).

Across organisms, the meiotic chromosome axis structure plays an important role not only for chromatin condensation but also for DSB and CO formation. DSBs are generated along the chromatin loops and are tethered later on to the axis to facilitate their repair (Wang and Copenhaver, 2018; Blat *et al.*, 2002). Similar to other organisms, studies in plants have reported aberrant meiotic DNA repair, including limited CO formation when axis proteins are defective (Ross *et al.*, 1997; Ferdous *et al.*, 2012). Furthermore, axis proteins can antagonize CO formation in a dosage-dependent manner (Lambing *et al.*, 2020).

During zygotene, aligned homologous chromosomes start to synapse, i.e., the homologs get physically connected along their length culminating in the formation of the synaptonemal complex (SC) (Mercier *et al.*, 2015) (**Figure 1**). The SC forms a tripartite proteinaceous structure: transverse filaments (TF) in the center, connected to two lateral elements (LE; axial elements of each homolog), forming a zipper-like structure between homologous chromosome axes (Zickler and Kleckner, 1999). The SC structure is highly conserved among species (Mercier *et al.*, 2015). ZIP1 orthologs were identified in plants such as Arabidopsis, rice, maize, wheat and barley, and their impact on CO formation has been reported (Higgins *et al.*, 2005; Wang *et al.*, 2010; Golubovskaya *et al.*, 2011; Khoo *et al.*, 2012; Barakate *et al.*, 2014). In rice, *zep1* mutants (ZEP1: rice ZYP1 homolog) showed an increase in CO rates in some chromosome regions, while RNAi-mediated downregulation of ZYP1 in barley indicated that ZYP1 is critical for WT (wild type) CO levels (Higgins *et al.*, 2005; Wang *et al.*, 2010). In Arabidopsis *zyp1* mutants, SC formation is absent while homologous chromosomes undergo pairing together with increased CO rates (including redistribution of COs towards distal chromosome regions), indicating that ZYP1 is not critical for CO formation (Capilla-Pérez *et al.*, 2021; France *et al.*, 2021).

In summary, axis and SC formation and their regulation are tightly linked to meiotic recombination progression and thus play a pivotal role in the frequency and distribution of meiotic recombination events (meiotic recombination landscape).

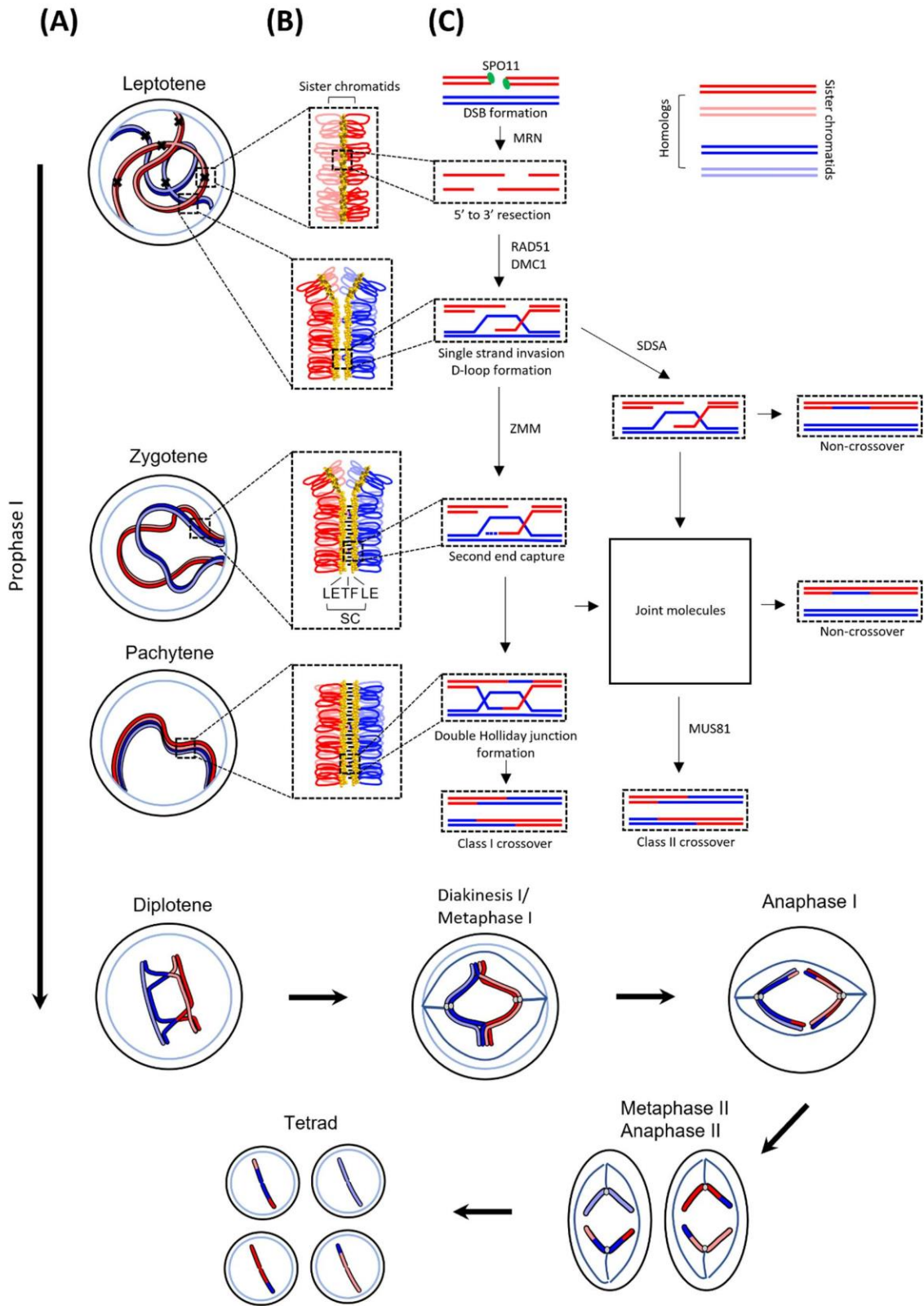


Figure 1. A scheme on meiotic recombination with a pair of homologous chromosomes (blue and red). Newly replicated sister chromatids are indicated as light red and light blue. Modified from Lambing *et al.* (2017). (A) Meiotic chromosome behavior: Prophase I consists of leptotene, zygotene, pachytene, diplotene and diakinesis. During leptotene, DSBs (black crosses) induced by SPO11 initiate the meiotic homologous recombination process. Homologous chromosomes start to

synapse during zygotene reaching full synapsis at pachytene. CO sites are visible as chiasmata by diplotene. Homologous chromosomes are separated and divided by microtubules attached to kinetochores (grey circles) during metaphase I and anaphase I. During meiosis II, sister chromatids are separated, resulting in tetrads (four haploid cells). **(B)** Meiotic chromosome axis remodeling: During leptotene, meiotic chromatids are coordinated in arrays of loops anchored to a proteinaceous structure, called the chromosome axes (yellow circles) and presynaptic alignments take place at late leptotene, indicating single strand invasion events. At zygotene, homologous chromosomes start to synapse by the formation of the synaptonemal complex (SC), a tri-partite structure consisting of transverse filaments (TF) and lateral elements (LE). The homologs are fully synapsed by pachytene. **(C)** Homologous recombination during meiosis: To repair the nicks introduced by SPO11 (green circles), the MRN complex (Mre11-Rad50-Nbs1 in plants) performs 5' to 3' strand resections. Resected 3' ends are then coated with the recombinases DMC1 and RAD51 enabling single end invasion and D-loop formation. The second ends of the DSBs are then annealed with the D-loop strand (second end capture). A double Holliday junction is formed with the help of ZMM proteins, which can be resolved into class I CO. Class II CO can be resolved through MUS81-dependent or other pathways.

1.2.3. Meiotic recombination landscapes

Meiotic DSBs initiate meiotic recombination processes resulting in CO or NCO events. CO-repair is an important source of genetic diversity. Therefore, how and where meiotic DSBs are formed as well as determined to be resolved as COs or NCOs are of interest.

In diverse species, independent of chromosome size and despite excessive numbers of meiotic DSBs, typically only one or two DSBs are repaired as CO per homologous chromosome pair forming a bivalent critical for faithful meiotic chromosome segregation (**Table 1**) (Zelkowski *et al.*, 2019; Wang and Copenhaver, 2018). Moreover, CO (and NCO) including meiotic DSB positions are unevenly distributed along chromosomes forming so-called recombination hot and cold spots. DSBs preferentially form at “open” chromatin devoid of nucleosomes (fundamental unit of chromatin, DNA segment wrapping a histone octamer) (Berchowitz *et al.*, 2009). In Arabidopsis and maize, a high correlation between DSB hot spots and chromatin organization is found, in particular, DNA methylation and specific histone methylation marks (He *et al.*, 2017; Choi *et al.*, 2013).

Tight regulation of meiotic HR results in three general phenomena regulating meiotic recombination landscapes: CO assurance, CO interference and CO homeostasis. CO assurance describes the formation of an ‘obligate CO’ per homologous chromosome pair critical for accurate chromosome segregation during meiosis I (Wang and Copenhaver, 2018). CO interference describes the phenomenon that the presence of one CO is reducing the possibility of another CO being formed in its vicinity along a given chromosome. Sensitivity to CO interference also distinguishes the two major types of CO found (see 1.2.1.). CO homeostasis describes the phenomenon that even in case the number of meiotic DSBs is decreased, the number of CO is preserved. However, in Arabidopsis and maize, the number of CO increased as the number of DSBs increased, indicating CO homeostasis being weak or absent (Sidhu *et al.*, 2015; Xue *et al.*, 2018). Together, three general principles (homeostasis, interference and assurance) of CO formation (co-)operate, regulating the meiotic recombination landscape at the genome-wide and/or chromosome-scale level.

Table 1. Recombination landscape in selected species modified from Zolkowski *et al.* (2019).

Species	Genome size	Chromosome no.	Average DSB no.	Average CO no.	Most common DSB location	Most common CO location	References
<i>Arabidopsis thaliana</i>	157 Mb	5	300 (male)	10 (male) 6 (female)	Gene promoters and terminators	Genes	(Bennett <i>et al.</i> , 2003; Yant <i>et al.</i> , 2013; Choi <i>et al.</i> , 2018)
<i>Zea mays</i> (maize)	2.4 Gb	10	500	18	All genome regions	Genes	(He <i>et al.</i> , 2017)
<i>Homo sapiens</i> (human)	3.3 Gb	23	150 (male) 350 (female)	50 (male) 70 (female)	Intergenic	Intergenic	(Pratto <i>et al.</i> , 2014; Paigen and Petkov, 2018)
<i>Hordeum vulgare</i> (barley)	5.1 Gb	7	400-500	15	All genome regions	Genes	(Higgins <i>et al.</i> , 2012)

Along chromosomes, differences in CO rates occur. Regions flanking chromosome ends, i.e., telomeres which protect chromosome ends from nucleolytic degradation, have a higher gene density and GC content, a relatively low density of transposable elements and higher CO rates compared to other chromosome regions in *Arabidopsis* (Giraut *et al.*, 2011). Additionally, heterochiasmy in *Arabidopsis* is characterized by a higher CO frequency in subtelomeric regions in male compared to female meiosis. An uneven distribution of COs along chromosomes is particularly found in cereal crops with large and complex genomes such as wheat, maize and barley, displaying recombination hot spots preferentially clustered towards telomeric regions (Liu *et al.*, 2009; Saintenac *et al.*, 2011; Higgins *et al.*, 2012). COs within (peri-)centromeres are highly suppressed in most monocentric species including plants possibly to avoid impaired meiotic chromosome segregation (Mercier *et al.*, 2015). In *Arabidopsis*, DNA methylation negatively correlates with CO distribution, not frequency, especially in (peri-)centromeric regions (Mirouze *et al.*, 2012; Yelina *et al.*, 2012).

At the fine scale, for instance, the DNA sequence context or heterozygosity shapes meiotic recombination landscapes. In plants, certain DNA sequences positively correlate with CO formation, e.g. a (G/C)-rich motif in maize is abundant at DSB hotspots in genic regions similar to *Arabidopsis* (He *et al.*, 2017; Giraut *et al.*, 2011). Moreover, in *Arabidopsis*, a positive correlation between sequence heterozygosity and CO frequency was found (Zolkowski *et al.*, 2015) with increased CO rates in heterozygous regions and decreased CO rates in exchange in flanking homozygous regions (Zolkowski *et al.*, 2015). Blackwell *et al.* also reported an association between differences in pericentromeric CO

rates and SNP density (Blackwell *et al.*, 2020). Thus, the DNA sequence context can impact meiotic CO formation.

1.2.4. Meiosis in barley

Barley (*Hordeum vulgare*) is an important cereal crop and the fourth most abundantly cultivated crop worldwide due to its versatile usage and adaptability to various environments. It has a haploid genome size of 5.1 Gb, comprising seven chromosomes bearing a putative number of 53,220 genes (Mayer *et al.*, 2012). Similar to other cereal crops such as wheat, in barley meiotic recombination events preferentially cluster at distal chromosome regions. While (peri-)centromeric regions, that occupy roughly half of the entire physical map with almost 30 % of the entire genes, being virtually suppressed for COs (Mayer *et al.*, 2012; Künzel *et al.*, 2000). Based on this skewed CO distribution, new allelic combinations arise mainly through shuffling distal chromosome regions during meiosis. Hence, naturally available genetic variation located in the proximal chromosome region can not be harnessed by breeders to develop superior barley varieties. It also limits trait introgression, creates linkage drag (undesirable traits cannot be separated from useful traits), and impairs gene isolation as well as marker-assisted selection of important agronomical phenotypes. Therefore, to improve and accelerate barley breeding programs, approaches to modify the recombination landscape in barley hold great promise.

Various studies have shown the conservation of many key meiotic aspects in barley (Higgins *et al.*, 2012; Higgins *et al.*, 2014; Barakate *et al.*, 2014; Colas *et al.*, 2016; Colas *et al.*, 2017). In plants, tight regulation of HR results in only ~5% of DSBs maturing into a CO; e.g. in barley 400-500 DSBs result in 15-22 COs (dependent on accession, CO scoring method or growth condition; (Higgins *et al.*, 2012; Phillips *et al.*, 2015)). Higgins *et al.* (2012) indicated a spatiotemporal asymmetrical regulation of meiotic recombination initiation and progression, chromosome axis formation and synapsis in barley, suggesting that the skewed distribution of COs towards distal chromosome parts is associated with DNA replication in euchromatic regions, which occurs earlier than DNA replication in interstitial regions. In other words, COs designated early inhibit additional COs formed nearby in accordance with CO interference. Therefore, COs in distal regions already fulfill the obligatory CO and interstitial regions undergoing DNA replication later than distal region have a reduced probability of acquiring a CO. Higgins *et al.* (2012) observed also an almost twofold increase of COs within interstitial regions when plants were exposed to a higher temperature (30°C), while the total number of COs was reduced. Elevated temperature led to chromosome axis protein ASY1 loading on both interstitial and distal regions synchronously. Thus meiotic progression was spatiotemporally similar, likely contributing to increased CO frequency in interstitial regions. Additionally, Phillips *et al.* (2015) reported an effect of temperature on meiotic recombination only during male meiosis. In a nutshell, COs are likely not

physically predetermined in barley despite their skewed distribution towards distal chromosome regions.

1.3. Manipulation of meiotic HR outcome in plants

The frequency and distribution of meiotic recombination events are tightly regulated by diverse factors at the genome-wide, chromosome-scale and local level (see 1.2.3). Additionally, also e.g. chromatin structure, post-translational modifications (PTMs) of meiotic proteins, epigenetic modifications, environmental conditions, biotic or abiotic factors, certain “stresses” or chemical compounds can influence meiotic recombination landscapes in plant and non-plant species (**Figure 2**) (Choi *et al.*, 2017; Lambing *et al.*, 2017; Blary and Jenczewski, 2019).

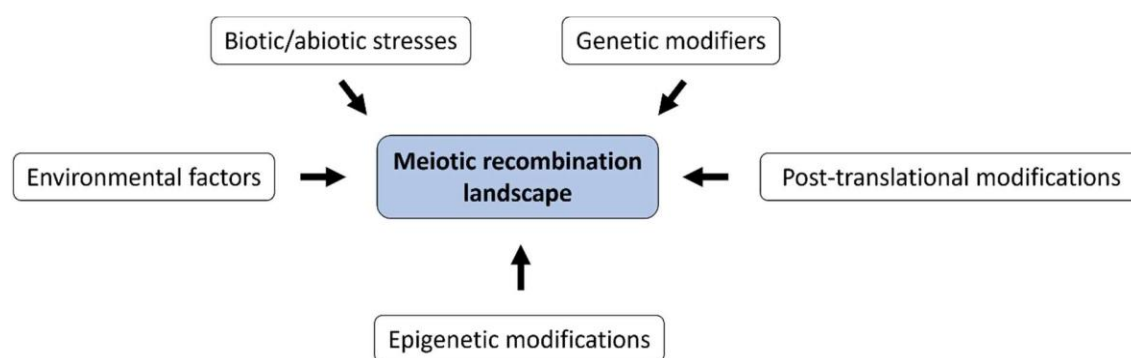


Figure 2. Factors described impacting meiotic recombination landscapes.

1.3.1. Genetic modifiers

In *Arabidopsis* three main classes of so-called anti-CO factors were identified, that limit the number of MUS81-dependent class II CO: i) The helicase FANCM and its cofactors MHF1 and MHF2 (Crismani *et al.*, 2012; Girard *et al.*, 2014), ii) the RTR complex (BTR/STR complex in mammals/yeast, respectively) consisting of the helicase RECQ4, TOP3 α and RMI1 (Knoll *et al.*, 2014), and iii) FIGL1 and its associated cofactor FLIP (Girard *et al.*, 2015). Similar to *Arabidopsis*, in various crop plants such as Brassica, rice, pea and lettuce, these anti-CO factors also regulate meiotic CO landscapes. However, in the few tested crops so far, mutation in some of the anti-CO factors can lead to complete or partial sterility upon their full knock-out (Zhang *et al.*, 2017; Blary *et al.*, 2018; de Maagd *et al.*, 2020; Li *et al.*, 2021). Moreover, typically in anti-CO factor mutants, the increase in CO is found in chromosome regions with naturally high recombination rates, while regions that are typically devoid of meiotic recombination remain recalcitrant for CO formation.

In addition to factors limiting class II CO formation, pro-CO factors such as HEI10 regulate the number of ZMM-dependent class I CO in a dosage-dependent manner (Choi *et al.*, 2017; Toby *et al.*, 2003; De Muyt *et al.*, 2014). In *Arabidopsis* increased dosage of HEI10 resulted in a twofold increased CO

frequency (Ziolkowski *et al.*, 2017). Whether HEI10 dosage also regulates CO numbers in other plants, including crops, is unclear. By combining increased HEI10 dosage and depletion of anti-CO factor *recq4*, CO frequency was dramatically increased based on a parallel increase in class I and II CO formation (Serra *et al.*, 2018). However, this CO increase was still restricted to already recombining distal chromosome regions. In summary, genome regions naturally devoid of CO formation remain recalcitrant for meiotic recombination in *hyperrecombination* plants (anti-CO factor mutants, increased HEI10 dosage) and thus do not enable breeders to access natural genetic variation in large interstitial genome regions.

1.3.2. Epigenetic modifiers

CO formation and patterning are associated with epigenetic modifications. DNA cytosine methylation is found in various DNA sequence contexts classified into CG, CHG (H=A, T, C) and CHH methylation (Wang and Copenhaver, 2018). In plants, DNA methylation is abundant at transposable elements (occupy 50-80% of some grass genomes (Meyers *et al.*, 2001)) and at repetitive DNA sequences including (peri-)centromeric heterochromatic chromosome regions that are commonly devoid of COs. In Arabidopsis loss of DNA CG methylation maintenance in *ddm1* results in increased CO numbers along subtelomeric regions while not within (peri-)centromeric chromosome regions (Colomé-Tatché *et al.*, 2012; Melamed-Bessudo and Levy, 2012). In *met1* (methyltransferase1, mediates CG DNA methylation), while the total number of COs was similar to WT, a redistribution of COs towards centromere-proximal and distal regions away from pericentromeric regions was found (Mirouze *et al.*, 2012; Yelina *et al.*, 2012; 2015a; Choi *et al.*, 2018). In addition to CG methylation, also non-CG methylation in concert with histone modifications impacts the CO landscape in Arabidopsis (Underwood *et al.*, 2018). Underwood *et al.* (2018) observed increased frequencies of DSBs and COs along pericentromeric chromosome regions in hybrid and inbred lines when non-CG methylation and H3K9me2 (histone H3 dimethylated at lysine 9) are disrupted. Hence, at the chromosome scale, DNA methylation impairs CO formation.

In mammals, meiotic recombination hot spots are associated with specific DNA sequence motifs mediated by PRDM9 (zinc finger domain protein) acting as an H3K4me3 (H3 trimethylated at lysine 4) methyltransferase (Baudat *et al.*, 2010; Berg *et al.*, 2010). While PRDM9 is absent in budding yeast, meiotic recombination sites are also within “open chromatin” characterized by low nucleosome density, and the distribution of H3K4me3 positively correlates with recombination hot spots (Borde *et al.*, 2009; Sommermeyer *et al.*, 2013; Berchowitz *et al.*, 2009). CO patterning in Arabidopsis, lacking PRDM9, shows to some extent similar tendencies as in budding yeast; recombination hot spots are associated with open chromatin or active chromatin modifications such as H2A.Z (abundant in

promoter regions), H3K4me3, low nucleosome density and low DNA methylation levels (Choi *et al.*, 2013).

Various histone or post-translational modifications of proteins involved in axis, SC and CO formation are tightly linked to meiotic recombination regulation. In yeast, H3K9ac (H3 acetylated at lysine 9) marks recombination hotspots, and when the histone acetyltransferase SpGcn5 is depleted, the frequency of DSBs is decreased (Yamada *et al.*, 2004; Yamada *et al.*, 2013). In Arabidopsis, when the GCN5-related histone *N*-acetyltransferase *MCC1* is over-expressed, causing histone hyperacetylation, global redistribution of COs was found while the total CO number per cell was unchanged (Perrella *et al.*, 2010). In rice MEL1, a homolog of Arabidopsis AGO5, redirects histone H3 modifications including H3K9me2, H3K9ac, and H3S10ph. In *mel1* with decreased H3K9me2 levels HR and synapsis are impaired (Nonomura *et al.*, 2007; Komiya *et al.*, 2014; Liu and Nonomura, 2016).

Modification of meiotic proteins with SUMO (small ubiquitin-like modifier) is involved in meiotic recombination regulation (Nottke *et al.*, 2017). SUMOylation is a reversible mark that can regulate/modify transcription, nuclear transport, maintenance of genome integrity and signal transduction in a substrate-specific manner. Red1 in budding yeast undergoes SUMOylation (Cheng *et al.*, 2006; Eichinger and Jentsch, 2010) mediated by the meiosis-specific SUMO E3 ligase Zip3. SUMOylated Red1 along lateral elements interacts with the SC protein Zip1. Hence, SUMOylated Red1 functions as a “zipping glue” for a zipper-like SC structure, ensuring the timely formation of the SC. Additionally, Zhang *et al.* reported that SUMOylation of Red1 and Topoisomerase II (TOPOII) are required for CO interference mediated by TOPOII (Zhang *et al.*, 2014). Whether ASY3 as a homolog of Red1 in plants undergoes SUMOylation is unclear. However, in Arabidopsis SUMOylation is an abundant mark found along meiotic chromosome axes during prophase I and mutation of a SUMO E3 ligase encoding gene results in meiotic chromosome fragmentation and missegregation, suggesting that SUMOylation is also important for plant meiosis (Liu *et al.*, 2014).

1.3.3. Environment, abiotic/biotic factors and “stresses”

Various environmental and abiotic/biotic factors or “stresses” including temperature, nutrient availability, radiation, light, water supply or pathogen attack, have been implicated to influence the the meiotic recombination landscape (Lambing *et al.*, 2017; Wang and Copenhaver, 2018).

The temperature was shown to influence meiotic recombination landscapes in several organisms, including *Drosophila*, Arabidopsis and barley (Plough, 1917; Bomblies *et al.*, 2015; Phillips *et al.*, 2015). Interestingly, species react differently to altered temperatures. Increased temperatures result in excessive interstitial COs in Arabidopsis and barley (Higgins *et al.*, 2012; Phillips *et al.*, 2015; Modliszewski *et al.*, 2018). However, extra COs in Arabidopsis are derived from class I COs, whereas in

barley from class II COs. In barley, a positive correlation between SC length and elevated temperature is found, suggesting that a longer SC length under higher temperature conditions may enable a higher frequency of COs (Phillips *et al.*, 2015). In contrast, in *Arabidopsis* the SC length showed a negative correlation towards elevated temperature (Lloyd *et al.*, 2018). Moreover, while under elevated temperature barley shows heterochiasmy with higher CO numbers in male, while not in female meiosis (Phillips *et al.*, 2015). *Arabidopsis* plants briefly exposed to elevated temperatures showed a higher CO frequency in female meiosis (Saini *et al.*, 2017). Elevated temperature in wheat led to a shift in CO localization along chromosomes. However, especially centromeric regions remained devoid of CO (Coulton *et al.*, 2020). Altering temperature is a promising tool; however, considering the negative impact of high temperature on meiotic progression and overall plant fertility, the actual application of a temperature treatment needs to be thoroughly defined for a given plant species.

In *Drosophila* and *S. cerevisiae*, the nutritional composition of the environment e.g. food or growth medium can influence meiotic recombination (Parsons, 1988; Abdullah and Borts, 2001). In plants, elevated potassium or phosphate levels in soil or culture media resulted in increased meiotic recombination rates in barley, rye and *Lolium temulentum* (Law, 1963; Bennett and Rees, 1970; Fedak, 1973). In wheat, irrigating plants with Hoagland solution without macronutrients revealed that the application of magnesium restored the CO frequency of *zip4* (*Ph1, Pairing homologous 1*) mutants (Rey *et al.*, 2018). Likely, a deficit or abundance of macro-/micronutrients can influence meiotic recombination rates based on their possible direct and indirect impact on the activity of key meiotic proteins.

In *Vicia faba* or *Crotalaria intermedia*, irradiation increased or decreased meiotic recombination frequencies (MATHER, 1934; Sybenga, 1960). Irradiation of plants to influence meiotic recombination rates can be an efficient tool when the dosage, timing and type of radiation are established. In addition to irradiation, biotic stress can impact recombination frequency. An increased somatic recombination rate was found in *Arabidopsis* infected with the pathogen *Peronospora parasitica* (Lucht *et al.*, 2002) and in tobacco infected with tobacco mosaic virus or oilseed rape mosaic virus (Dong, 2004; Filkowski *et al.*, 2004; Boyko *et al.*, 2007; Marii and Chiriac, 2009; Kovalchuk *et al.*, 2003). Chiriac *et al.* reported an increased number of total chiasmata events in interstitial chromosome regions in tomatoes infected with the tomato aspermy virus, potato virus X or tobacco mosaic virus (Chiriac *et al.*, 2006). Additionally, an increased number of total chiasmata, especially in interstitial chromosome regions, was found in barley infected with the barley stripe mosaic virus (Andronic, 2012). Pathogen infection might be one tool to manipulate meiotic recombination landscapes, however, pathogenicity and potential negative impacts of infection need to be considered. Additionally, numerous studies have implicated abiotic and biotic stresses such as drought, salinity, heat and cold to impact the chromatin

structure, which is a crucial determinant for meiotic recombination landscapes (Kim *et al.*, 2015; Asensi-Fabado *et al.*, 2017).

1.3.4. Chemical compounds

Chromatin modifications in response to chemical compounds can influence the meiotic recombination landscape. Chemical agent ethylenediamine tetra-acetic acid (EDTA) treatment in *Drosophila* and *Chlamydomonas reinhardtii* resulted in an increased CO frequency (Eversole and Tatum, 1956). EDTA-induced Ca^{2+} and Mg^{2+} cation deficiency and increased CO rates imply a relationship between macronutrient availability and meiotic recombination rates (Steffensen, 1955; Eversole and Tatum, 1956). In tomato, foliar spraying of 3-indoleacetic acid and benzthiazoleoxyacetic acid increased CO frequency while barbituric acid, streptomycin, ribonucleic acid lowered CO frequency (Griffing and Langridge, 1963). Sinha and Helgason observed almost a threefold increase of CO rates within two linked loci after injection of actinomycin D and diepoxybutane into barley stems bearing young spikes undergoing meiosis (Sinha and Helgason, 1969). In *Pisum sativum* increased and decreased numbers of chiasmata were found when sprayed with 0.2% and 0.4% of the fungicide Balvin, respectively, possibly the application of Balvin remodeled the chromatin structure (Choudhary and Sajid, 1986).

Inhibition or promotion of histone modifications by epigenetic drugs can be applied to alter chromatin state, possibly contributing to redistribution or induction of meiotic COs (Soppe *et al.*, 2002; Saze *et al.*, 2012). For instance, BIX-01294 inhibits histone H3K9 methylation *in vitro* and promotes microspore totipotency and embryogenesis initiation in Brassica and barley, by decondensing the chromatin (Tachibana *et al.*, 2002; Kubicek *et al.*, 2007; Berenguer *et al.*, 2017). Similarly, UNC0642 can induce “open” chromatin structures by inhibiting H3K9 methylation (Kim *et al.*, 2017). In maize, Trichostatin A (TSA) and 5-azacytidine were functional as inhibitors of histone H4 deacetylation and DNA/histone H3K9 methylation (Yang *et al.*, 2010). TSA is a well-known histone deacetylase inhibitor in mammals and plants (Yoshida *et al.*, 1990; Tian and Chen, 2001; Li *et al.*, 2014). Perrella *et al.* observed that TSA-dipped Arabidopsis flower buds can phenocopy meiotic alterations based on hyperacetylation in *mcc1* overexpression plants (see 1.3.2.), indicating a possible application of TSA to influence histone acetylation and thus to promote chromosome remodeling leading to changes in CO distribution (Perrella *et al.*, 2010). In addition to the impact of histone modifications on chromatin structure via chemical compounds, DNA methylation inhibitors such as Zebularine or 5-Azacytidine can also induce chromatin decondensation (Ma *et al.*, 2016; Solís *et al.*, 2015).

To identify influences of epigenetic drugs or chemical compounds on PTMs during meiosis and possible impacts on meiotic recombination, the drugs need to be introduced/delivered into meiocytes *in planta* before or during meiosis. Typically, *in planta*, delivery of chemical compounds to impact meiotic

recombination landscapes were performed by e.g. dipping cut *Arabidopsis* stems or cereal tillers or foliar spraying (Griffing and Langridge, 1963; Knight *et al.*, 2010; Perrella *et al.*, 2010). Recently, the delivery of compounds or genetic materials to targeted organs or cells in plants has been explored based on so-called nanomaterials (nano-sized particles) (Wang *et al.*, 2019; Santana *et al.*, 2020).

Delivery of chemical compounds into reproductive organs of cereal crops such as barley is challenging when compared to e.g. *Arabidopsis* with visible and easily accessible reproductive structures. Young barley spikes containing cells that undergo meiosis are embedded in the stem/tiller surrounded by several layers of leaf sheaths. Thus, they are not visible or easily approachable from outside being “hidden” (Reid, 2015). Therefore, the injection of chemical compounds into cereal tillers is more suitable than dipping or spraying methods (Sinha and Helgason, 1969; Higgins *et al.*, 2012; Osman *et al.*, 2021). To estimate when to deliver the compounds, developmental scales such as Zadoks or Waddington scales (Zadoks *et al.*, 1974; Tottman, 1987; Waddington *et al.*, 1983) can be helpful to estimate meiotic stages of young spikes inside the stems. However, relying on these indications can be challenging since plant development and meiotic stages differ between genotypes, growing conditions, etc. As an alternative, Tracy *et al.* demonstrated a non-destructive detection method of floral stages in barley tillers using X-ray (Tracy *et al.*, 2017), that however requires special equipment enabling only a limited number of plants to be analyzed.

1.4. Measuring meiotic recombination rates in plants

Methods to detect meiotic recombination outcomes are crucial during breeding programs to identify desired genotypes and also to trace and better understand meiotic recombination dynamics including e.g. frequency of COs vs NCOs or strength and occurrence of CO interference (Mercier *et al.*, 2015; Lambing and Heckmann, 2018). Several approaches are available to detect COs in plants. COs can be detected cytologically by scoring chiasmata or performing immunolocalization of meiotic proteins (Lukaszewski, 1992; Chelysheva *et al.*, 2012; Higgins *et al.*, 2012; Martín *et al.*, 2014). Cytological approaches to study CO landscapes also provide an overview of meiotic chromosome dynamics, however, they are time-consuming and provide comparatively low sample throughput and resolution. Another approach to study plant meiotic CO landscapes is based on genotyping-by-sequencing (GBS) (Saintenac *et al.*, 2009; Yelina *et al.*, 2015b). GBS analysis enables deciphering genome-wide meiotic CO rates and also CO interference by low-coverage sequencing of F₂ populations derived from F₁ hybrids based on polymorphisms between the two parental genomes (Rowan *et al.*, 2015). This approach provides an overview of the genome-wide CO distribution and also enables to focus on selected regions along the genome in high resolution. However, the approach can be expensive in the case of large and/or complex genomes (Bastien *et al.*, 2018). Alternatively, recombination profiles can be deciphered without screening segregating populations based on linked-read sequencing of male

gametes as shown for Arabidopsis or tomato (Sun *et al.*, 2019; Rommel Fuentes *et al.*, 2020). Sequencing plant microspores (tetrad or pollen nuclei) from F₁ hybrids enables detection of meiotic recombination events at the genome-wide level and possibly CO interference according to polymorphisms between parental genomes or allele-specific marker genotyping (Dreissig *et al.*, 2015; Dreissig *et al.*, 2017; Li *et al.*, 2015). Furthermore, measurements of meiotic CO rates within selected short regions of distinct chromosomes through pollen typing have been performed with high numbers of Arabidopsis pollen (Yelina *et al.*, 2012; Yelina *et al.*, 2015b; Choi *et al.*, 2016; Lim *et al.*, 2020). Additionally, the meiotic recombination outcome in Arabidopsis can be detected in high-throughput based on fluorescent transgenic lines (FTLs) in pollen or seeds (Melamed-Bessudo *et al.*, 2005; Berchowitz and Copenhaver, 2008; Wu *et al.*, 2015). FTL analysis in pollen is based on transgenic lines bearing genes for a fluorescent protein (red, cyan or yellow) in the *qrt* background. *QRT* genes (*QRT1* and *QRT2*) are needed for pollen grain separation; in *qrt* mutants all four male meiotic products stay attached as a tetrad, allowing all four male meiotic products to be analyzed in parallel (Preuss *et al.*, 1994; Copenhaver *et al.*, 2000). The recombination events are detected based on the segregation ratio/behavior of different linked fluorescent protein markers in the tetrads (Berchowitz and Copenhaver, 2008). FTL analysis allows generating large data sets rapidly since COs are detected in pollen grains or seeds. Yelina *et al.* analyzed the meiotic CO frequency of high numbers of fluorescent pollen via flow cytometric analysis (Yelina *et al.*, 2013). Unfortunately, FTLs are not available for crops due to the laborious and expensive generation of FTL lines in crops with particularly large-genome sizes or even due to different crops or certain genotypes being recalcitrant for genetic transformation.

In barley and other crops, cost-effective, rapid and high-throughput methods to decipher meiotic recombination rates are limited compared to *A. thaliana*. To overcome some of the limitations in measuring meiotic recombination rates in crops, single pollen genotyping combined with fluorescence-activated cell sorting (FACS) has been conducted to measure meiotic recombination rates in barley and citrus pollen nuclei (Dreissig *et al.*, 2015; Garavello *et al.*, 2020). In this approach, individual haploid pollen nuclei were isolated through FACS and amplified by whole-genome amplification (WGA) followed by genotyping with allelic KASP (Kompetitive Allele-Specific PCR) markers. Dreissig *et al.* also measured meiotic recombination events in barley genome-wide by analyzing single-cell sequencing data from isolated pollen nuclei amplified by WGA (Dreissig *et al.*, 2017). Single pollen genotyping assays without FACS are also used in Arabidopsis, citrus and pear, however with difficulties in isolating single gametes in high-throughput and inefficient genotyping frequencies due to the low DNA content of haploid gametes (Khademian *et al.*, 2013; Mase *et al.*, 2014; Honsho *et al.*, 2016). Measurement of CO rates in pollen nuclei offers the opportunity to analyze a large number of samples from a single plant and to save time by measuring CO events directly in pollen nuclei while not depending on (large) segregating plant populations. Additionally, measuring CO events in pollen nuclei avoids segregation

distortion since the analysis takes place in gametes before fertilization. However, so far genotyping of single pollen nuclei in barley relies on a prior whole genome amplification (WGA) step. Unfortunately, WGA is rather expensive and laborious, inhibiting its application as a high-throughput tool to measure meiotic recombination rates.

2. Aim of this study

Meiotic recombination events are limited in numbers and skewed towards chromosome ends in cereal crops such as barley (*Hordeum vulgare*). However, various reports have indicated plasticity of the meiotic recombination landscape (frequency and chromosomal distribution of meiotic recombination events) in response to the environment, biotic/abiotic factors or stresses. Moreover, epigenetic or post-translational protein modifications have a profound impact on the meiotic recombination landscape.

To explore whether chemical compounds impacting epigenetic marks or post-translational protein modifications could be employed in barley to alter the chromatin (status) and accordingly the meiotic recombination landscape, a set-up is required to deliver chemical compounds *in planta* during the time cells undergo meiosis and to test the applicability of the selected compounds *in planta*. In addition, to assess whether this *in planta* delivery of the chemical compounds, different growth conditions or the developmental stage of a plant impacts the meiotic recombination landscape, a reliable system is required to measure recombination rates at the level of an individual plant in high throughput.

In plants, cost-effective and high-throughput methods to measure meiotic recombination rates are so far limited to *Arabidopsis thaliana*. In barley, single pollen nucleus genotyping enables to measure meiotic recombination rates in gametes before fertilization without the need for segregating populations. However, so far, established methods rely on whole-genome amplification of individual single pollen nuclei due to their limited DNA content, thus restricting the number of analyzable samples.

Hence, the aims of this study are:

1. the development of a method to deliver chemical compounds *in planta* during the time cells undergo meiosis in barley,
2. to test the *in planta* applicability of selected chemical compounds in barley,
3. the establishment of a method to measure meiotic recombination rates in barley pollen nuclei in high-throughput from individual plants, and
4. to compare meiotic recombination rates in barley plants grown under different growth conditions, within different tillers from the same plant and in plants treated with selected chemical compounds in contrast to untreated plants.

3. Materials and Methods

3.1. Plant material

For all experiments *H. vulgare* cv. Morex, cv. Barke and hybrid plants cv. Barke x cv. Morex were used. For leaf nuclei encapsulation, plant material of *A. thaliana*, *Glycine max*, *Petroselinum crispum*, *Capsicum annuum*, *H. vulgare*, and *Vicia faba* was kindly provided by Dr. Jörg Fuchs (research group: Chromosome Structure and Function, IPK Gatersleben).

3.2. Plant cultivation

Barley seeds were germinated in pre-cultivation soil (substrate 1) in a growth chamber [12 h light (~200 $\mu\text{mol}/\text{m}^2\text{s}$), 80 % relative humidity, 14°C day/12°C night] for 2 weeks. After repotting into 18 cm (\varnothing) pots, they were transferred to a greenhouse [16 h light (~600 $\mu\text{mol}/\text{m}^2\text{s}$), 60-70 % relative humidity, 17°C day/13°C night]. At ~3 leaf stage, Plantacote depot 4M granulate was added to the surface of the soil. Fertilizer (1% Hakaphos blue) was applied once per week, two weeks after the repotting, according to the manufacturer's instruction. After flowering, 1% Hakaphos red was applied once per week.

In a phytochamber (Climatic Grow Systems, Polyklima), plants were grown under the following conditions: [16 h light (Lamp bank 1: warm white 40%, cold white 25%, Lamp bank 2: warm white 40%, cold white 25%)], 60% humidity, 19°C day/17°C night. Seeds were germinated on two filter papers in a petri dish soaked in 8 mL of water for 5 days and transferred into 9 cm square pots. Fertilizers were applied in the same manner as in greenhouse growing conditions.

3.3. Cytology

3.3.1. Fixation of anthers for cytological analysis

Isolated barley spikes were fixed in ice-cold fixative (3 parts ethanol, 1 part glacial acetic acid) in a glass vial. Three hours later, the fixative was replaced with a newly prepared fixative, and spikes were incubated in the fixative overnight at RT. Fixed materials were used for chromosome spread preparations or stored at 4°C until further use.

3.3.2. Acetocarmine stain preparation of chromosomes for meiotic stage detection

After placing a fixed spike on a clean petri dish (94 mm \varnothing), individual spikelets were detached by forceps under a stereo microscope (Stemi SV 11 equipped with KL 1500 halogen light source, Zeiss). Considering the gradual spikelet developmental along the barley spike, central spikelets were studied first. The three anthers in a spikelet develop synchronously including their meiotic stage. Using forceps, one anther per spikelet was isolated and mounted onto a clean slide in one to two drops of acetocarmine solution (Morphisto). After a brief heat treatment of the specimen using an alcohol lamp,

a coverslip was added, and the anther material was pressed between folded filter papers (90 mm \emptyset) by thumb. Meiocytes released from the anther were evaluated under a light microscope (BA310 Biological Light Microscope, Motic) at 20X or 40X magnification.

3.3.3. Male meiotic chromosome spread preparations

Once the meiotic stage was identified by acetocarmine staining, the remaining two anthers of the spikelet were washed twice for 5 mins at RT in 300 μ L of citrate buffer (444 μ L of 0.1 M citric acid monohydrate and 556 μ L of 0.1 M trisodium citrate dehydrate in 9 mL of dH₂O, freshly prepared). After removing the citrate buffer, anthers were incubated in 200 μ L of enzyme digestion mix (333 μ L of 1% cellulase and 1% pectolyase in 0.01 M citrate buffer, pH 4.5, diluted with 667 μ L of 0.01 M citrate buffer) for 45 min at 37°C in a humid chamber. Anthers were washed in 500 μ L of citrate buffer and kept on ice. The anther material was transferred to a slide and macerated in 3 μ L of citrate buffer using a brass rod. 10 μ L of 60% acetic acid was added to the specimen, and the slide was heated on a hot block for 1 min at 52°C while spreading the drop by moving the needle horizontally. 100 μ L of ice-cold fixative was added to the slide surrounding the squashed anther specimen, the excess was discarded by inverting the slide a few times, and the residual fixative was dried using a blow-dryer. Using a cover slip, the slides were mounted in 18-20 μ L of 1.5 μ g/mL of DAPI (4',6-diamidino-2-phenylindole) in VECTASHIELD (Vector Laboratories) and evaluated under a fluorescence microscope (Eclipse Ni-E fluorescence microscope equipped with a DS-Qi2 camera and NIS-Elements-AR version 4.60 software, Nikon).

3.3.4. EdU detection

EdU (5-ethynyl-2'-deoxyuridine) was detected by the EdU click reaction (Sigma-Aldrich) (Kolb *et al.*, 2001). EdU detection cocktail was prepared according to the manufacturer's instructions (Sigma-Aldrich, 50 μ L of reaction buffer (10X), 20 μ L of catalyst solution, 1 μ L of 6-FAM-azide (10 mM), 50 μ L of buffer additive (10X) and deionized water up to 500 μ L). Slides (prepared as in 3.3.3.) were washed three times in 1X PBST (0.1% Triton X-100 in 1X PBS) for 15 min and briefly placed on tissue paper to remove the excessive buffer. 50 μ L of EdU detection cocktail was added to each slide. Slides covered by parafilm were incubated at 37°C for 30 min in a dark humid chamber. After removing the parafilm, slides were washed for 2 min in 1X PBS buffer and air-dried in darkness. Slides were observed under a fluorescence microscope after staining with 18-20 μ L of 1.5 μ g/mL of DAPI in VECTASHIELD and covering them with a cover slip.

3.4. *In planta* injection of chemical compounds

In barley plants, within primary tillers early meiosis occurs roughly at 5-6 weeks after germination. By softly pressing along the stem using the thumb and index finger, two nodes roughly at two-thirds of the entire stem length were identified. A part of the stem above these two nodes is packed with several leaf sheaths that surround the young developing spike. Another lump ~3-4 cm above these two nodes was identified by touching, representing the leaf ear of the inner leaf sheath below the most outer leaf sheath. A young barley spike is located between this leaf ear and the two bottom nodes. After estimating the developmental stage of a young barley spike, i.e., whether cells in anthers undergo early meiosis, based on the distance between the leaf ear and two bottom nodes, 0.5 mL of a selected chemical compound was injected into each spike using a syringe (1 mL single use syringe) and injection needle (25 G× 1", size 17/23, Ø 0.50 ×25 mm) when the distance was between 2.8 and 5 cm to impact early meiosis. The needle was injected diagonally at the upper point between the leaf ear and the two bottom nodes. Injection protocol: plant selection based on internode distance, 0.5 mL of injection volume with 0.05% Silwet L-77, 3 days injections with 24-hour intervals and one more injection after 1 hour after the first initial injection. The selected chemical compounds were injected at following concentrations: EdU (10 mM), Zebularine (0.5 mM), Trichostatin A (0.5 nM) and BIX-01294 (0.5 mM).

3.5. Chemical compounds screening using germinated barley seeds

Barley cv. Morex seeds were germinated in a petri dish with two filter papers soaked in 8 mL of water in a phytochamber ([16 h light (Lamp bank 1: warm white 40%, cold white 25%, Lamp bank 2: warm white 40%, cold white 25%)], 60% humidity, 19°C day/17°C night) after sealing with parafilm. After three days, uniformly grown seedlings (root length ~1 cm) were transferred to a new petri dish with two filter papers soaked in 8 mL of Zebularine (100, 10, 1 and 0.1 µM), Trichostatin A (1, 0.1, 0.01 and 0.001 µM), BIX-01294 (40, 20, 10 and 5 µM), 5-Azacytidine (100, 50, 25 and 12.5 µM) or UNC0642 (40, 20, 10 and 5 µM) solution and pictures of petri dishes were taken directly. Zebularine, Trichostatin A and 5-Azacytidine were dissolved in DMSO, while BIX-01294 was dissolved in distilled water. None of the treatments included detergents or surfactants. Control plates were treated with 8 mL of distilled water or distilled water with 1% DMSO (used to dissolve the highest concentrations of Zebularine, Trichostatin A, 5-Azacytidine and UNC0642). All Petri dishes were sealed with parafilm. After three days, pictures of Petri dishes were taken again. The impact of chemical compounds on root length was measured from pictures taken before and after chemical compound treatment with ImageJ. To measure the impact of chemical compounds on relative mitotic cell cycle values, root meristems were chopped using a razorblade on a petri dish with 500 µL of Galbraith buffer with PI (50 µg/mL) and filtered through a 50 µm filter mesh (Celltrix, Sysmex-Partec). Cell cycle profiles were recorded on a BD Influx cell sorter (BD Biosciences) equipped with a 150 mW 532 nm laser (Cobolt) and analysed

using the software ModFit 3.0 (Verity Software House). The relative percentage of nuclei in each cell cycle phase (G1, S and G2) was determined using the optimized 'Auto Analysis' function. Per chemical treatment and concentration, three independent experiments with 10 measurements each were performed.

3.6. Crossing of plants and hybrid confirmation

Eight to nine (cv. Barke) or seven to eight (cv. Morex) weeks after germination in the greenhouse, plants were ready for crossing to produce F₁ hybrid seeds. A Barke spike was selected when the entire spike was still wrapped inside the leaf sheath and ~1 cm of the awns was visible. Flag leaf, leaf sheath and awns were removed by scissors. Four rows of sterile lateral spikelets were removed by forceps. Emasculation was performed in three ways (**Figure 3**): i) cutting the upper half of each spikelet by scissors and removing three anthers (Thomas *et al.*, 2019), ii) making a ~2 mm vertical incision in each spikelet using one side of forceps and emasculating three anthers by forceps, or iii) sliding with the tip of closed forceps vertically between palea and lemma and removing the three anthers inside. After emasculation, spikes were covered with a glassine bag closed using a paper clip until fertilization. Three to eight days later, emasculated spikelets were fertilized using mature Morex anthers when spikelets were swollen and bigger with the stigma being elongated. Similar to emasculating Barke, flag leaf, leaf sheath and awns were removed by scissors. By opening the palea of each spikelet, three mature Morex anthers (plumed and yellow) were harvested and placed inside the emasculated Barke spikelets using forceps. The fertilized spikes were labeled and covered again with a glassine bag closed using a paper clip. The glassine bag was removed two weeks after fertilization to avoid excessive humidity. Crossed seeds harvested when they were dry and yellow were stored at 4°C.

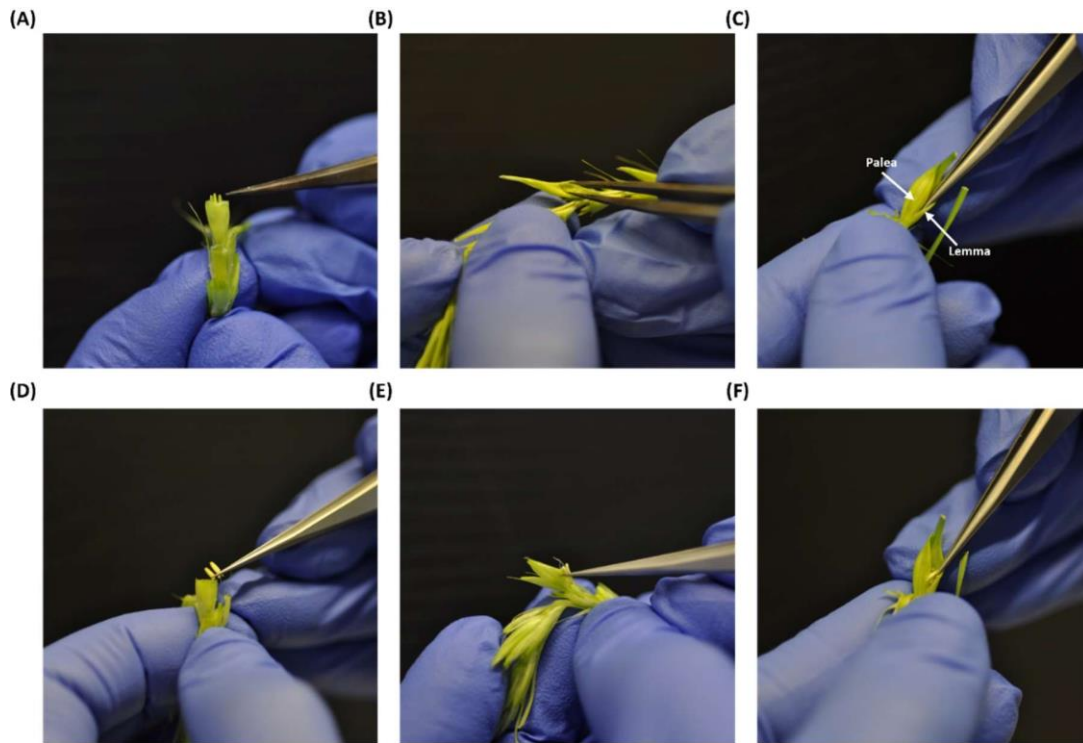


Figure 3. Emasculation and crossing of barley plants. (A) The upper half of a spikelet was cut using scissors (Thomas *et al.*, 2019) and the three anthers were removed by forceps. (B) ~2 mm vertical incision made using forceps and anthers removed through the incision. (C) Closed forceps were inserted between lemma and palea to open the spikelet and to remove the anthers inside. (D-F) Three to eight days after emasculating, mature anthers from pollen donor inserted through the opening.

To confirm the hybrid status of the obtained offspring, harvested seeds from the crossed plants were germinated, 200-400 mg of young leaf material was collected and frozen in 2 mL microcentrifuge tubes together with two metal beads (2.4 mm \varnothing) in liquid nitrogen. The material was ground using a homogenizer (Mixer Mill MM 400, Retsch) at 28 Hz for 45 sec. After adding 700 μ L of genomic DNA extraction buffer (5 mL of 1% N-Lauryl-Sarcosin 100 mM of Tris (pH 8), 10 mM of EDTA (pH 8) and 100 mM of NaCl), samples were vortexed vigorously for 2 min at RT. 700 μ L of phenol-chloroform-isoamyl alcohol (25:24:1, v/v) was added and the samples were vortexed again for 2 min. After centrifugation at $16,000 \times g$ for 3 min at RT, 700 μ L of supernatant was transferred to a new 1.5 mL microcentrifuge tube. 70 μ L of 3 M sodium acetate and 700 μ L of isopropanol were added to the supernatant. After inverting the tubes ten times, DNA was pelleted by centrifugation at $16,000 \times g$ for 10 min at 4°C. The supernatant was removed, and the pellet was washed by adding 500 μ L of 70% ethanol. After centrifugation at $16,000 \times g$ for 5 min at 4°C, the ethanol was removed and the pellet was air-dried. The pellet was re-suspended in 20 μ L of dH₂O and samples were stored at -20°C until further use.

The hybrid status of plants was confirmed by quantitative PCR (qPCR) using allele-specific (cv. Barke or cv. Morex) InDel and SNP Taqman markers for the selected polymorphic sites (**Tables 2** and **3**) employing extracted genomic DNA samples. The PCR mix contained: 1X Perfecta Multiplex qScript

Toughmix (Quantabio), 1.5 μ mol of each oligonucleotide primer, 1.25 μ mol of each Taqman probe, 0.6 μ mol of ROX (Promega, CXR reference dye), 100 ng of genomic DNA and dH₂O to 5 μ L. The PCR was performed in a QuantStudio 6 Flex Real-Time PCR system (ThermoFisher Scientific) using the following program: 95°C for 3 min, 45 cycles of 95°C for 15 sec and 54°C for 30 sec.

Table 2. List of primers of the selected markers polymorphic between barley cv. Barke and cv. Morex.

Primers	Genetic pos. (cM)	Sequence	T _m (°C)	Polymorphism (bp)	Sequence of polymorphism
InDel 1029 F	43.2	TGCCACCGAAGACAT GGAAA	65.6	144/137	ACCACCAAGC[<u>CTTGTC</u> A]CTTGTGTGC G
InDel 1029 R		CAAGGCACCACAATC CCGTA	65.7		
InDel 1076 F	49.86	ACCGGCCACTACTGT AACCA	66.5	202/186	CTTGGCTGCA[<u>CCGCACCAGACTGACA</u>] GGTGACAGCA
InDel 1076 R		CCAGTGCAGCGATCA GTTAG	63.8		
InDel 3039 F	46.03	GGTGTGCCCCAGTC ATAAT	65.5	128/135	CCCCTGCCAA[<u>CTTGTA</u> T]ATATAAAATT
InDel 3039 R		TCACATCCCATTTTTG CAAGCA	65.2		
SNP 6 F	54.53	CCGTGTGTCTGTTGG TTAGC	64.2	82	GCAAGGCATT[<u>T/C</u>]TTGTTCTAA
SNP 6 R		CGGTTCTTCTGTCCA TCCT	64.7		
InDel 3118 F	132.22	TGCAACTGGTTCTGG TTCTG	63.9	200/177	CAGGTGTGTC[<u>TGCTGTGGCCTGTGGG</u> <u>CTTCCTC</u>]CTCTGGTACG
InDel 3118 R		GGGGTCACCAAGTGA TCAGTG	65.1		
InDel 3135 F	143.91	GGTGTGGCATTGGT GAGA	65.7	93/90	CGAGAAGAAG[<u>AAG</u>]GGTGTGGCAT
InDel 3135 R		GAGGCACCATCCCCA TCAAA	65.7		
InDel 3152 F	155.02	GCTGGTCCTAATGAT GCACG	64.2	207/189	AACAGAGGCA[<u>ACATTTGTAGAAAATG</u> <u>CA</u>]TGGTAAGAGT
InDel 3152 R		TCCATCATCGAAGGC ACAGA	64.6		

Table 3. List of selected fluorophore markers polymorphic between barley cv. Barke and cv. Morex.

Probes	Target allele	5' Fluorophore	Sequence	3' Quencher	T _m (°C)
InDel 1029	cv. Morex	FAM	ACACGGTGTGGCAACCACCAAGCCTTGTC	BHQ-1	76.3

	cv. Barke	HEX	ACACGGTGTGGCAACCACTAAGCCTTGAT	BHQ-1	73.1
InDel 1076	cv. Morex	FAM	CACCTTGGCTGCACCGCACCAGACTGACAG	BHQ-1	75.9
	cv. Barke	HEX	TGCACCTTGGCTGCAGGTGACAGCAACACA	BHQ-1	76.5
InDel 3039	cv. Morex	FAM	TCCGCCCTGCCAAATATAAAATTACATGC	BHQ-1	69.9
	cv. Barke	HEX	CTGGGTCCGCCCTGCCAACTTGATATAT	BHQ-1	72.5
SNP 6	cv. Morex	FAM	AGTTGGCAAGGCATTTTTGTTCTAACGGA	BHQ-1	71.3
	cv. Barke	HEX	AGTTGGCAAGGCATTCTTGTTCCTAACAGA	BHQ-1	70.6
InDel 3118	cv. Morex	FAM	TTAGCATAGTCCAACCTCAGGTGTGCTCTCT	BHQ-1	70.4
	cv. Barke	HEX	TTAGCATAGTCCAACCTCAGGTGTGCTGCT	BHQ-1	70.8
InDel 3135	cv. Morex	FAM	TTGGCGGCAGCTCCTCCGAGAAGAAGGGTG	BHQ-1	76.6
	cv. Barke	HEX	TTGGCGGCAGCTCCTCCGAGAAGAAGAAGG	BHQ-1	75.2
InDel 3152	cv. Morex	FAM	CACTAATCCGCGCCTTGAACAGAGGCATGG	BHQ-1	73.3
	cv. Barke	HEX	CACTAATCCGCGCCTTGAACAGAGGCAACA	BHQ-1	73.3

3.7. Pollen nuclei isolation

Mature barley hybrid (cv. Barke x cv. Morex), cv. Barke or cv. Morex pollen were collected when anthers were plump and bright yellow around six to seven or eight to nine weeks after germination in the greenhouse or phytochamber, respectively. In total 48 anthers from the third to the tenth flower from the top of the main tiller were collected with forceps into 500 μ L of nuclei isolation buffer (Galbraith *et al.*, 1983) and isolated as described (Kron and Husband, 2012). In brief, anthers were vortexed vigorously for \sim 1 min until the pollen was released and visible with naked eyes. The anthers were then removed by filtering the suspension through a 100 μ m mesh filter (CellTrics, Sysmex-Partec). Afterwards, the suspension was transferred on a 20 μ m filter mesh (CellTrics, Sysmex-Partec), and the pollen grains were burst using a plastic pestle. 500 μ L of nuclei isolation buffer was added again to wash off pollen nuclei from the mesh. Isolated pollen nuclei were stained with PI (Propidium Iodide) (50 μ g/mL).

3.8. Flow-sorting of isolated pollen nuclei

PI-stained barley pollen nuclei were flow-sorted using BD Influx cell sorter (BD Biosciences) equipped with an 86 μ m nozzle and a 200 mW 488 nm laser (Coherent). A dot plot of the PI fluorescence intensity log (575/30) versus the side scatter log signal (488/10) enabled the separation of the pollen nuclei fraction from the debris background. The sorting gate was defined in a histogram showing the PI fluorescence intensity (610/20). The pollen nuclei were flow-sorted into an Eppendorf tube containing either a PCR, qPCR or dPCR mix (see below) using 1X PBS as sheath fluid. In case separation of

vegetative and sperm nuclei was required, a dot plot of the PI fluorescence intensity versus the forward scatter log signal (488/10) was used to define the corresponding sorting gates.

3.9. Single pollen nucleus genotyping with InDel markers

Polymorphic sites were genotyped using single barley pollen nuclei as PCR templates. Single pollen nuclei were flow-sorted individually into the PCR mix including selected InDel primers between barley cv. Barke and cv. Morex (InDel 1029 F, InDel 1029 R, InDel 1076 F and InDel 1076 R; **Table 2**). Amplicons were analyzed on a 3% Phor agarose gel (Biozym, prepared in 1X TBE) at 100 V for 180 min.

3.10. Pre-amplification of target sites from a single pollen nucleus

To pre-amplify genomic regions containing either the marker InDel 1029 or 1076 defining together the interval Ic 1 (interval at centromeric region of chromosome 1, 6.7 cM, 344.7 Mbp) (Zhou *et al.*, 2015), two pairs of pre-amplification primers were designed (**Table 4** and **Figure 4**). Amplicons were between 974-1269 bp for InDel 1029 and 917-1097 bp for InDel 1076. Pollen nuclei were flow-sorted individually into a well of a 384 micro-well plate containing 10 μ L of PCR mix: 1X Perfecta Multiplex qScript Toughmix, 3 pmol of each oligonucleotide primer and dH₂O to 10 μ L. In an Eppendorf Mastercycler Ep 384 PCR system, the following program was used: 95°C for 3 min, 45 cycles of 95°C for 15 sec and 54°C for 30 sec. 1 μ L of each pre-amplification product was transferred to a new 384 micro-well plate containing 9 μ L of PCR mix for a nested PCR with the same conditions as for the pre-amplification: 1X Perfecta Multiplex qScript Toughmix, 3 pmol of each oligonucleotide primer (InDel primers: InDel 1029 F, InDel 1029 R, InDel 1076 F and InDel 1076 R, **Table 2**) and dH₂O to 10 μ L. Nested PCR products were analyzed by gel electrophoresis on a 3% Phor agarose gel at 100 V for 180 min.

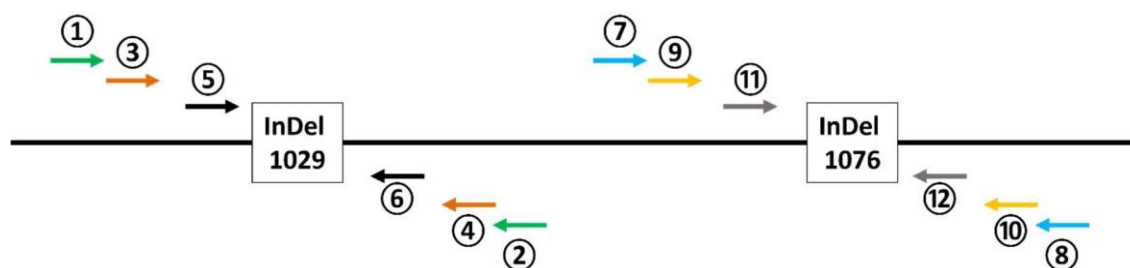


Figure 4. Scheme of pre-amplification primers for InDel 1029 and InDel 1076. ① InDel 1029_binding_1F ② InDel 1029_binding_2R ③ InDel 1029_binding_2F ④ InDel 1029_binding_3R ⑤ InDel 1029 F ⑥ InDel 1029 R ⑦ InDel 1076_binding_1F ⑧ InDel 1076_binding_1R ⑨ InDel 1076_binding_2F ⑩ InDel 1076_binding_2R ⑪ InDel 1076 F ⑫ InDel 1076 R. After pre-amplification of InDel 1029 and InDel 1076 using pre-amplification primers: ① to ④ and ⑦ to ⑩, InDel primer ⑤, ⑥, ⑪ and ⑫ were used for nested PCR.

Table 4. List of primers for pre-amplification of InDel 1029 and InDel 1076.

Primers	Genetic pos. (cM)	Sequence	Tm (°C)
InDel 1029_binding_1F	43.2	TCCAGTCGAATTCAGGGCAA	65.1
InDel 1029_binding_2R		CCTACCCCTTAGTGTGCCAT	64.4
InDel 1029_binding_2F		TGCCCTGCTTTTATTGCGA	64.5
InDel 1029_binding_3R		CCTCCAATCCCCTTCTCCTC	64.4
InDel 1076_binding_1F	49.86	CAATCAACGGTCGTGATGGG	64.3
InDel 1076_binding_1R		ATGGAAAGGCGAGGGTGATT	65.3
InDel 1076_binding_2F		CTGTTCTTGCCATCTCTCGC	64.0
InDel 1076_binding_2R		ACGATACGAACCAGCAGTCG	65.1

3.11. Single pollen grain genotyping using germinated pollen

To possibly improve the efficiency of pollen nuclei genotyping, all three pollen nuclei (two sperm and one vegetative nuclei) from a pollen grain were used as PCR template. Pollen germination was assessed in pollen germination media modified according to Burke *et al.*, (2004): 20 g of sucrose, 10.3 mg of H₃BO₃, 5.3 mg of KNO₃, 10.3 mg of Ca(NO₃)₂, 51.7 mg of MnSO₄ and 10.3 mg of MgSO₄·7H₂O in 100 mL of ddH₂O. Pollen was shattered into 3 mL of 1X, 0.5X, 0.2X or 0.1X of germination media in a well of a 6-well plate (Thermofisher) and evaluated after 15 min under a stereo microscope for germination (**Figure 14**).

To employ all nuclei of a single pollen grain for genotyping, fresh pollen were shattered on a clean petri dish, individual pollen grains were picked by a human hair (or a sterile tooth brush hair) attached to a Pasteur pipette and transferred into a well of a 384-well plate containing either 2 µL of 0.2X pollen germination media for germination before PCR or 10 µL of PCR mix (1X Perfecta Multiplex qScript Toughmix, 3 pmol of each oligonucleotide primer: InDel 1029 F, InDel 1029 R, InDel 1076 F and InDel 1076 R (**Table 2**), dH₂O to 10 µL) for direct PCR amplification without germination (**Figure 5**). Successful transfer of a single pollen grain was assessed using a stereo microscope. After 15 min of incubation at RT, 8 µL of PCR mix was added to the germination media containing a pollen grain. The 384-well plate was sealed using ThermalSeal RTS™ Sealing Films (Sigma-Aldrich) and transferred to an Eppendorf Mastercycler Ep 384 PCR system. PCR conditions were 95°C for 3 min, 45 cycles of 95°C for 15 sec and 54°C for 30 sec. PCR products from germinated/not germinated pollen were analyzed by gel electrophoresis on a 3% Phor agarose at 100 V for 180 min.

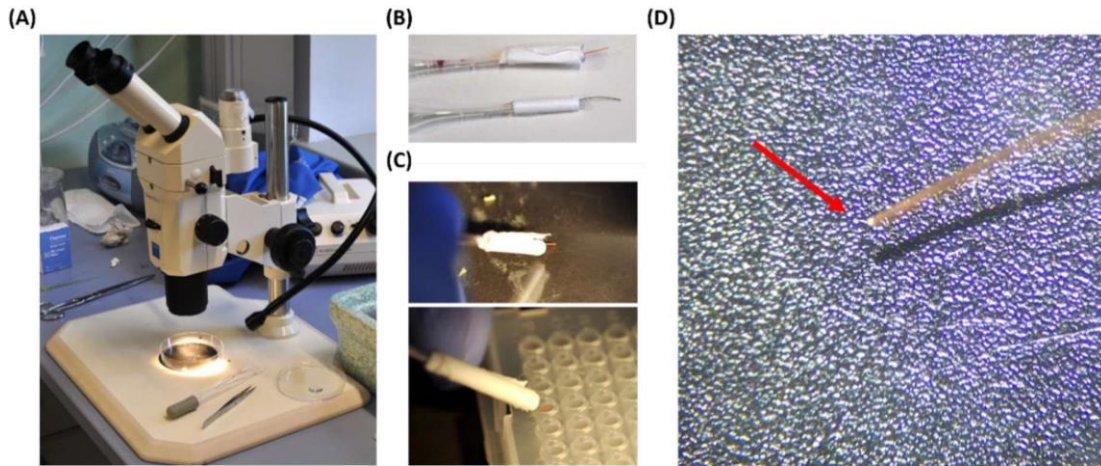


Figure 5. Pollen selection and transfer into a 384-well plate containing pollen germination media. (A) Pollen grains shattered on a petri dish were transferred into wells of a 384 well plate under a stereo microscope. **(B)** Hand-made tools for the transfer of pollen grain using a human hair or a toothbrush hair (both sterile) attached with tape to a Pasteur pipette. **(C)** Pollen grain was picked using the hand-made tool. **(D)** Single pollen grain attached to human hair is indicated by a red arrow.

3.12. Single pollen nucleus genotyping via Crystal Digital PCR

3.12.1. Crystal Digital PCR statistics

To determine the nuclei encapsulation rate of the Crystal dPCR system (Stilla Technologies®) defined numbers of nuclei (from 2,000 to 6,000) were flow-sorted into a 1.5 ml Eppendorf tube as described above, diluted to a final volume of 28 μL with distilled water, loaded in one of the four chambers of a Sapphire chip (Stilla Technologies®), transferred onto the Geode of the Naica® system and subjected to the droplet generation. Afterward, the chips were scanned on the Naica® Prism3 and the number of droplets with successful nuclei encapsulation were counted. The observed number of nuclei was compared to the predicted number of encapsulations according to the Poisson distribution. PI-stained nuclei were visible in the HEX channel even after thermocycling which enabled manual counting of the number of encapsulated nuclei. According to Crystal dPCR statistics based on the Poisson distribution, the putative number of encapsulated nuclei (N_{max}) per chamber was calculated based on the total number of droplets formed per chamber (N_{D}), the volume of the individual droplets (V_{D}), and the concentration of sorted nuclei (C_{N}).

$$N_{\text{max}} = N_{\text{D}} \times V_{\text{D}} \times C_{\text{N}} \quad (V_{\text{D}} = 0.00059 \mu\text{L})$$

Finally, the probability of the number of droplets encapsulating zero, one, two, or even more nuclei, ($P(k)$) was calculated as below:

$$P(k) = \frac{\lambda^k}{k!} e^{-\lambda}$$

$$\lambda = C_{\text{N}} \times V_{\text{D}} = \text{average number of target molecules per droplet in the chamber}$$

$$e = \text{Euler's constant} \approx 2.71828$$

Hence, the number of probable droplets ($N_{\text{ExD}}(k)$) was predicted as follows:

$$N_{\text{ExD}}(k) = N_{\text{max}} \times P(k)$$

3.12.2. Crystal dPCR genotyping

Crystal Digital PCR™ was performed on a Naica® System digital PCR platform (Stilla Technologies®). The Crystal Digital PCR™ mix consisted of 1X Perfecta Multiplex qScript Toughmix, 2.8 pmol of fluorescein (Sigma-Aldrich), 14 pmol of each oligonucleotide or 7 pmol of each TaqMan probe for multiplexing four markers to detect two InDels in parallel (e.g. only Ic 1 or Id 3-1). For multiplexing eight markers to detect four InDels in parallel, 8.4 pmol of each oligonucleotide and 4.2 pmol of each TaqMan probe were added to the mix. After sorting the desired number of nuclei (in the employed setup 1,000 flow-sorted nuclei using an 86 µm nozzle resulted in a volume of ~1.7 µL) or pipetting desired concentration of genomic DNA directly into the pre-mixed Crystal Digital PCR™ mix, distilled water was added to a final volume of 28 µL. Out of this, 25 µL of the Crystal Digital PCR™ mix was loaded in one of the four chambers of a Sapphire chip. After closing the lids of all chambers, the Sapphire chips were transferred onto the Geode of the Naica® system. The thermocycling conditions were 40°C for 40 min for droplet generation (partitioning) and nuclei encapsulation, 95°C for 10 min and 45 cycles of 95°C for 30 sec and 54-56°C for 15 sec. Air pressure used for partitioning was released at the final step. After thermocycling, the chips were transferred from the Geode to the scanner (Naica® Prism3 or Prism6). Before loading the chip onto the scanning tray, the bottom of the chips was thoroughly cleaned by a lint-free tissue (Stilla Technologies®). Any contamination of the bottom surface of the chip was removed by 70% ethanol if needed. The Naica® Prism3 scanner allowed scanning of chips in three different channels: FAM, HEX and Cy5. The Naica® Prism6 scanner enabled scanning in FAM, Yakima Yellow, Cy3, ROX, Cy5 and Atto700. The exposure time for each channel used was 65 ms for FAM, 125 ms for HEX and 50 ms for Cy5 in Prism3 (Focus: 0.78 mm). The initial exposure times in Prism6 were 200 ms for FAM, 350 ms for Yakima Yellow, 350 ms for Cy3, 350 ms for ROX, 250 ms for Cy5 and 350 ms for Atto 700 (Focus: 0.2 mm). Exposure time was adjusted in the scanning software (CrystalReader v.2.4.0.3, Stilla Technologies®), if necessary, and applied throughout individual assays. Scanned chip images were visualized as a plot and analyzed in Crystal Miner v.2.4.0.3 software (Stilla Technologies®).

3.12.3. Improving Crystal dPCR efficiency

To explore possible improvements of the Crystal dPCR nucleus genotyping efficiency, the thermostable restriction enzyme *TaqI* and Proteinase K were tested for nuclei digestion. *TaqI* (optimal incubation temperature at 65°C) was tested by adding 5 U to each Crystal dPCR reaction prior to pollen nuclei sorting. After droplet generation and encapsulation at 40°C, an incubation step at 65°C for 30 mins was added to the thermocycling program (see 3.12.2). In case of a Proteinase K treatment, pollen nuclei were flow-sorted into 300 µL of 0.3 µg/mL Proteinase K solution, incubated at 37°C for 15 min and diluted by adding 200 µL of nuclei isolation buffer (Galbraith *et al.*, 1983). Then desired numbers of digested pollen nuclei were flow-sorted again into the Crystal dPCR mix.

3.12.4. Nuclei encapsulation efficiency employing different plant species

Leaf nuclei of *A. thaliana*, *G. max*, *P. crispum*, *C. annuum*, *H. vulgare*, and *V. faba* (see section 3.1.) were isolated by chopping roughly 1 cm² of fresh leaf tissue in 1 ml of nuclei isolation buffer (Galbraith *et al.*, 1983) with a razorblade in a Petri dish. The nuclei suspensions were filtered through 50 µm mesh filters and stained with PI (50µg/ml). 3,000 leaf nuclei from all species were flow-sorted into the Crystal dPCR mix using a BD Influx cell sorter. The populations of the nuclei were identified and sorted as described above (see 3.8.). Encapsulation rates of flow-sorted leaf nuclei were manually counted and compared to encapsulation rates predicted according to the Poisson distribution.

3.12.5. Measuring the nuclear size

Fresh leaf material of *A. thaliana*, *G.max*, *P. crispum*, *C. annuum*, *H. vulgare* and *V. faba* was fixed in 4% formaldehyde (in Tris buffer: 10 mM Tris, 10 mM Na₂EDTA, 100 mM NaCl, pH 7.5) for 30 min on ice under vacuum. After three washes with Tris-buffer, fixed leaf tissue was chopped with a razorblade in nuclei isolation buffer (LB01; (Doležel *et al.*, 1989)) in a petri dish and filtered through a 50 µm CellTrics filter, stained with DAPI (1 µg/mL) and the 2C nuclei were flow-sorted into an Eppendorf tube using a BD Influx cell sorter equipped with a 200 mW 355 nm laser (Coherent). 15 µL of the flow-sorted nuclei suspension was pipetted into a drop of 15 µL of sucrose buffer (100 mM Tris-HCl, 50 mM KCl, 2mM MgCl₂, 0.05% Tween 20, 5% sucrose) mounted on a microscopic slide. After air-drying overnight, slides were stained with DAPI (1 µg/mL) in antifade solution, covered with a coverslip and evaluated under a fluorescence microscope (Axiophot 2, Zeiss). Images were captured with a cooled CCD camera (ORCA-ER, Hamamatsu). 50 2C nuclei were measured in size from each species using the software Image J.

4. Results

4.1. *In planta* delivery of chemical compounds

To study a possible effect of chemical compounds on the barley recombination landscape, it was essential to set-up a procedure to deliver chemical compounds *in planta* during and/or shortly before cells undergo meiosis as well as to set-up a platform to select chemical compounds and their active concentrations in barley.

4.1.1. Phenotype analysis of barley hybrids

To introduce chemical compounds *in planta* during the time cells undergo meiosis, it was critical to identify when to deliver the compounds *in planta* under given environmental conditions. To do so, in initial pilot experiments 48 barley hybrid plants (Barke x Morex) were grown in a greenhouse under controlled growth conditions. At various time points (28-51 days after germination) primary spikes were fixed, and anthers in the center of the spike were cytologically studied for the presence of meiotic cells. Four categories were defined: Pre-meiotic (cells before meiosis), Leptotene-Zygotene (cells in leptotene or zygotene), Pachytene-Tetrad (cells from pachytene until tetrad stage) and Pollen (developing/mature pollen) (**Figure 6**). Furthermore, the height of the plants, the length of the spikes and the length of the anthers were recorded (**Figure 6A**). A positive correlation between spike/anther length and the four defined stages was found: 0.48 ± 0.2 cm spike/ 0.3 ± 0.1 mm anther (Pre-meiotic), 1.02 ± 0.64 cm spike/ 0.6 ± 0.2 mm anther (Leptotene-Zygotene), 2.46 ± 1.01 cm spike/ 1.1 ± 0.3 mm anther (Pachytene-Tetrad) and 4.08 ± 1.88 cm/ 1.8 ± 0.5 mm anther (Pollen). However, large variation among plants was found in terms of height/age and (meiotic) stage. For instance, anthers in the center of a spike containing cells undergoing leptotene or zygotene were found in plants that were 29 and 55 days old and that were between 19 and 44 cm in height.

To identify whether, compared with a greenhouse under more controlled growth conditions, a better correlation between plant age/height and spikes containing cells undergoing meiosis was found, in small-scale experiments 33 barley hybrid plants were grown in a phytochamber (**Figure 6B**). Similar to greenhouse conditions, a positive correlation between spike/anther length and the four defined stages was found: Pre-meiotic (0.57 ± 0.07 cm spike/ 0.39 ± 0.08 mm anther), Leptotene-Zygotene (1.22 ± 0.28 cm spike/ 0.69 ± 0.09 mm anther), Pachytene-Tetrad (2.47 ± 0.26 cm spike/ 1.17 ± 0.21 mm anther) and Pollen (2.83 ± 0.05 cm spike/ 1.52 ± 0.08 mm anther). Compared with greenhouse conditions, plant development was delayed with plants being shorter in appearance and older at the time spikes contained cells undergoing meiosis. For instance, anthers in the center of a spike containing cells undergoing leptotene or zygotene were found in plants that were between 43 and 49 days old and between 23 and 26.8 cm in height. Due to the large variation among plants grown in particular in a

greenhouse but also in the phytochamber in terms of (meiotic) stage and plant height/age, a possible *in planta* delivery scheme of chemical compounds during the time cells undergo meiosis based on only plant height or age was considered not reliable under both tested growth regimes. Nevertheless, cultivation in the phytochamber was considered more suitable for future experiments aiming to measure a potential increase or decrease of meiotic recombination rates after *in planta* delivery of compounds due to the lower variation observed between plants when compared with greenhouse conditions.

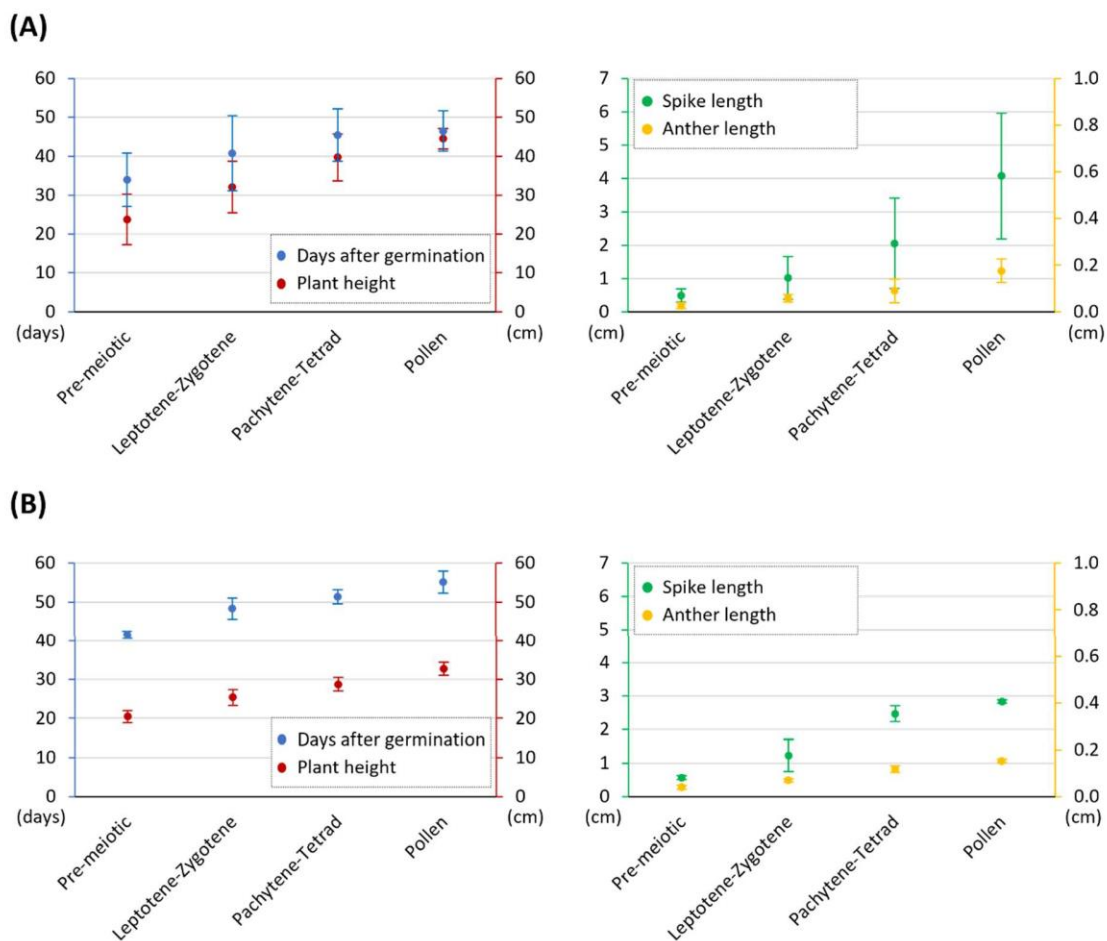


Figure 6. Phenotype analysis of barley hybrid plants (Barke x Morex) grown under greenhouse or phytochamber conditions. (A) Phenotype evaluation of 48 plants grown in a greenhouse and **(B)** 33 plants grown in a phytochamber. Days after germination/plant height (left) and spike/anther length (right) in relation to cytological defined (meiotic) stages.

4.1.2. *In planta* injection

It was explored whether independent of the plant age and/or height, plants could be identified that contain developing spikes in the size range of 0.5-1.0 cm (greenhouse) or 0.6-1.2 cm (phytochamber) with cells before or undergoing meiosis suitable for chemical compound delivery. Among the analyzed plants above (**Figure 6**), the internode distance below the spike and the distance between the bottom

node and the leaf auricle of 22 plants from the greenhouse and 10 plants from the phytochamber were measured to check for a correlation with the meiotic stages in a given spike. Typically, in both the greenhouse and the phytochamber spikes/anthers containing cells before or undergoing meiosis were found when the two nodes right below the spike were close to each other (less than 1 cm), and the distance between the two nodes and the leaf auricle was in the range of 2-4.5 cm regardless of plant height and/or age (**Figures 7A** and **7B**). This rough estimation of meiotic stages according to the distance of internode and distance from bottom nodes to leaf auricle did not guarantee to find spikes with cells undergoing early meiosis. However, this estimate was more accurate than relying on other phenotypic traits (plant height, days after germination, etc.). Thus, all following *in planta* injections were performed when the distance between the two bottom nodes and the leaf auricle was 2-4.5 cm and the internode distance between the two bottom nodes was below 1 cm.

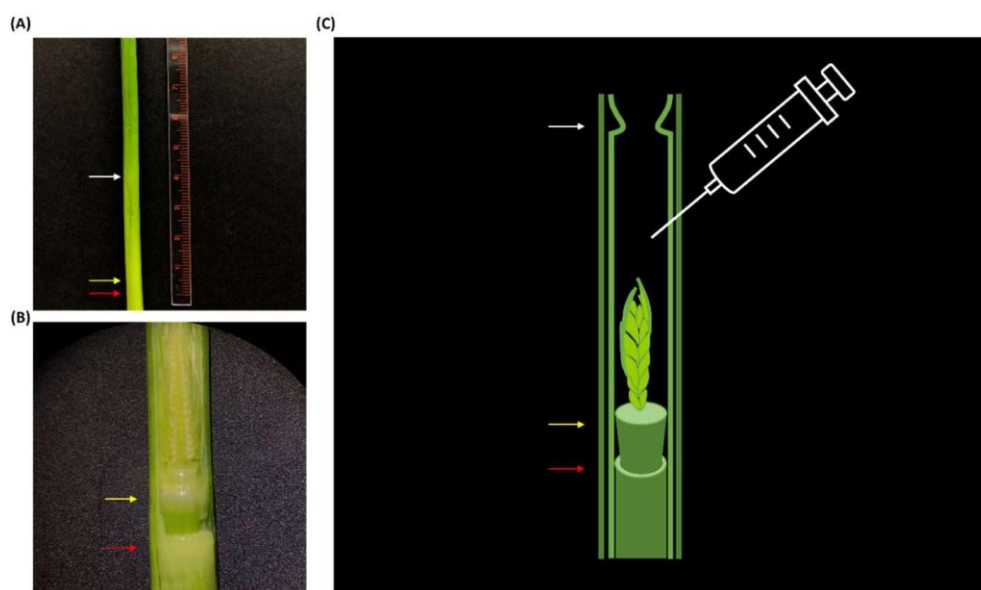


Figure 7. Tiller and spike morphology of barley cv. Barke during the time of *in planta* EdU/compound injection grown in the greenhouse and phytochamber. Modified from Ahn *et al.* (2020). **(A)** Outer and **(B)** inner morphology of a young barley stem/tiller around 5-6 weeks old. **(C)** Scheme of a young barley stem/tiller with the inner spike and a needle injected above the spike depicted. White arrow indicates leaf auricle of the inner leaf sheath. Yellow and red arrows indicate the two bottom nodes.

As a next step, a protocol for injection of chemical compounds *in planta* during the time cells undergo meiosis in a given spike/anther using EdU (5-Ethynyl-2'-deoxyuridine) as an example for chemical compounds was explored in cv. Barke as pilot material. To do so, plants in the greenhouse with less than 1 cm bottom internode distance and 2-4.5 cm between bottom nodes and leaf auricle were selected. First, the volume suitable for injection was explored by injecting 0.5, 1.0 or 1.5 mL of water within the space surrounding the spike within the stem (**Figure 7C**). Consistently an injection of 1.0 or 1.5 mL of water caused loss of water by squirting outside from the tiller, whereas an injection of 0.5

mL of water typically did not result in squirting of injected water from the tiller. Thus, all further injections were performed using a (compound) volume of 0.5 mL. Second, the uptake rate of the injected volume, i.e., for how long the injected volume persisted within the tiller, was assessed by opening the tiller with a razor blade after water injection. Two hours after injection, the water volume had disappeared while the interior of the tiller was still slightly wet. When performing two consecutive injections of water either within 5 mins or 1 hour, the injected water volume had disappeared while the interior of the tiller was wet consistently 4 or even 10-12 hours after injection, respectively. Despite a limited number of analyzed spikes (four per treatment), the data suggested that a second consecutive injection 1 hour after the first injection might increase the duration of the initial availability of the chemical compound within the tiller. Third, to monitor the uptake of the injected volume, i.e., whether the compound solution was absorbed from the spike/anthers, and whether the injected volume was sufficient to cover the whole spike, initially 0.5 mL of 1X PBS buffer containing a drop of food coloring (Dr. Oetker) were injected twice within a 1-hour interval. By cutting the spike vertically after 6 hours, staining across the whole spike was found, suggesting that the injected volume was sufficient to cover the whole spike. Moreover, while the outer spike parts were more or less uniformly stained, inner parts appeared unstained, suggesting that possibly the uptake/absorption of food color dye was limited, resulting only in staining of the outer parts with no strong plant uptake. To figure out if the uptake/absorption rate could be improved using the surfactant Silwet L-77, 0.5 mL of 1X PBS buffer with a drop of food coloring with or without 0.1% Silwet L-77 was injected twice within a 1-hour interval. Six hours after the treatment, typically, a more uniform food color staining of the spike injected with 0.1% Silwet L-77 compared to the spike injected without 0.1% Silwet L-77 was found. Dissected anthers also appeared to be more evenly stained with food coloring under the stereomicroscope in the presence of 0.1% Silwet L-77, suggesting improved uptake/absorption of the food color in presence of 0.1% Silwet L-77.

To identify whether a compound can be successfully delivered into meiotic cells, barley plants having less than 1 cm bottom internode distance and 2-4.5 cm between bottom nodes and leaf auricle were injected with 0.5 mL of 10 mM EdU together with 0.05% Silwet L-77. EdU was selected as an example for a chemical compound that enables to monitor the uptake into cells during S-phase including somatic and meiotic cells cytologically. Based on available data on barley meiosis duration (Bennett and Finch, 1971), successful uptake of EdU into meiocytes was found 43-72 hours after injection, suggesting that chemical compounds can be delivered *in planta* into barley meiocytes (**Figure 8**).

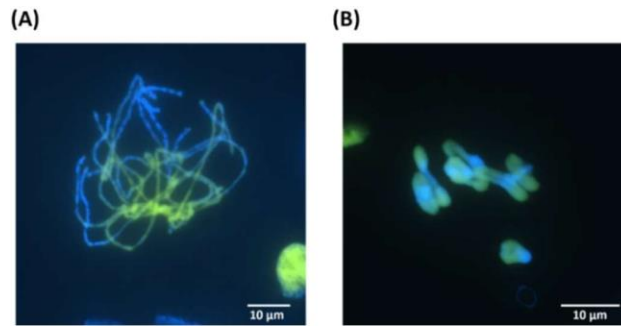
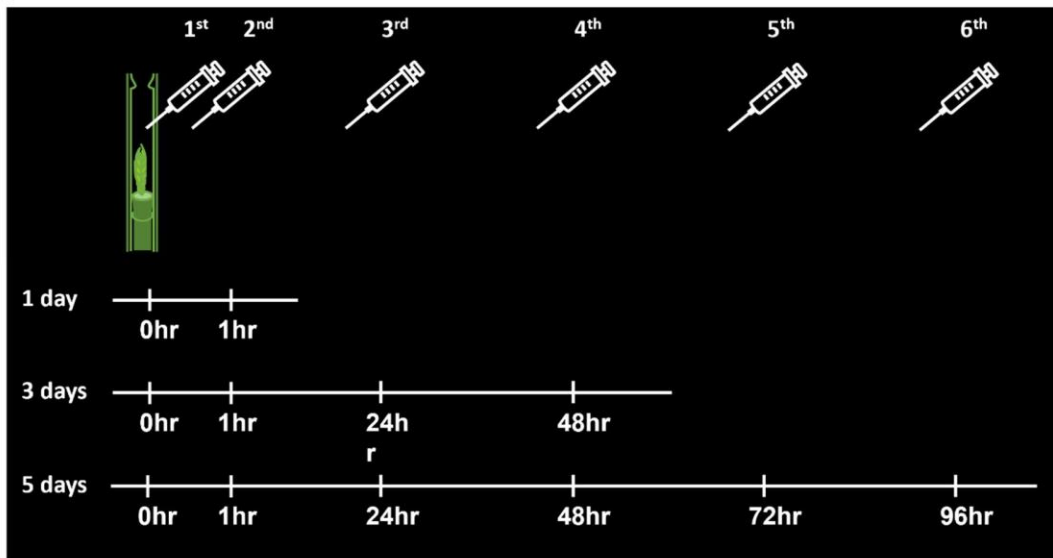


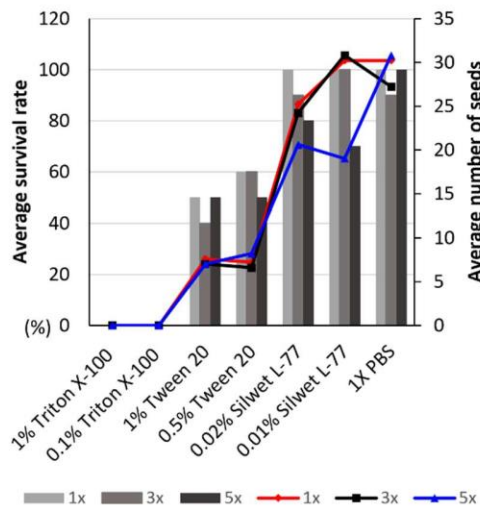
Figure 8. *In planta* EdU incorporation into barley male meiocytes visualized under a microscope 43-72 hours after injecting 0.5 mL of 10mM EdU with 0.05% Silwet L-77. Cells during (A) pachytene and (B) diakinesis with EdU-positive (yellow) chromosomes. DNA counterstained with DAPI in blue.

Finally, to assess whether the established injection protocols allow the generation of offspring plants as a requirement to dissect a heritable impact of a chemical compound on the barley recombination landscape. Therefore plant fertility (seed setting, spike survival rate) after different injection procedures was assessed. Given the observed improved uptake in the presence of Silwet L-77, the detergent Tween 20 or Triton X-100 at different concentrations were tested as well (**Figure 9**). The effect of detergents/surfactants on plant survival rate and seed development was studied by injecting Triton X-100 (1 and 0.1%), Tween 20 (1 and 0.5%) and Silwet L-77 (0.02 and 0.01%) into five spikes each for 1 day, 3 days or 5 days consecutively to boost delivery efficiency with 24 hr intervals with an additional injection on the 1st day 1 hr after the first injection (**Figure 9A** and **9B**).

(A)



(B)



(C)

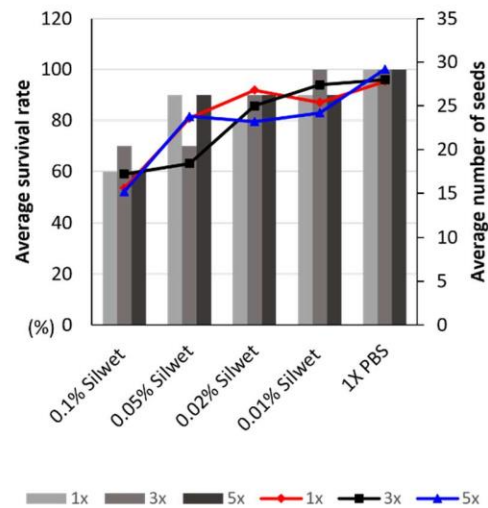


Figure 9. Injection scheme and impact of different concentrations of surfactants/detergents on barley spike survival rate and seed number. (A) Injections were conducted for 1 day, 3 days and 5 days consecutively with 24 hr intervals with an additional injection on the 1st day 1 hr after the first initial injection. The average survival rate of barley tillers (bar graphs) and the number of seeds (line graphs) after injection (B) of 1x PBS with/without detergents (Triton X-100, Tween 20) or surfactant Silwet L-77 (n=10, 5 spikes within 2 experiments) and (C) of different concentrations of Silwet L-77 (n=10, 5 spikes within 2 experiments). All detergents/surfactants were injected into 5 barley tillers for 1, 3 and 5 times consecutively with 24-hour intervals.

In case of injection of 1X PBS only (control), no impact on plant fertility independent of the number of consecutive injections was found, while in case of all injections of 1X PBS together with 1% and 0.1% Triton X-100 barley tillers wilted after injection and no single seed was recovered. 50% and 60% of injected tillers survived after 1X injection of 1% or 0.5% Tween 20, respectively. 100% of tillers survived after 1-day injection of 0.025% and 0.01% Silwet L-77, similar to the 1X PBS control. When 1% or 0.5%

of Tween 20 was injected for 3 days consecutively, 40% and 60% of tillers survived, respectively. 90% and 100% survived after 3 days injection of 0.025% and 0.01% Silwet L-77, respectively, similar to the control. After 5 days injection, the survival rate decreased compared to the respective 1 day and 3 days injections in all cases except for 1% Tween 20 and the control. Among surviving spikes, seed development after 1-day injection of 1% and 0.5% Tween 20 was 12.7 and 14.6, respectively. Seed development after 1-day injection of 0.01% of Silwet L-77 is similar (30.2 seeds) to 1-day injection of 1X PBS buffer, while 25.2 seeds developed after 1-day injection of 0.025% Silwet L-77. After 3 days injection, both 0.025% (27.1 seeds) and 0.01% (30.8 seeds) of Silwet L-77 were similar to 1X PBS buffer and both 1% (14.7 seeds) and 0.5% (16.5 seeds) Tween 20 resulted in nearly half the amount as with 1XPBS buffer. Seed development after 5 days injection of Tween 20 and Silwet L-77 with all concentrations were similar to that of 3 days of Silwet L-77 injection. In conclusion, all concentrations tested from Triton X-100 and Tween 20 were toxic to barley development, while Silwet L-77 (0.02 and 0.01%) did not harm the development and fertility of barley.

Silwet L-77 was the least harmful among tested detergents/surfactants to be added to the injection volume. Hence, four concentrations (0.5%, 0.1%, 0.025% and 0.01%) of Silwet L-77 were injected 1 day, 3 days and 5 days to analyze the effect on tiller survival rate and seed development in more detail (**Figure 9C**). Survival rate/seed development was reduced in a dosage-dependent manner in all cases compared to the control, while the number of injections for every tested concentration did not show a significant impact. In the case of low concentrations of Silwet L-77 only slightly reduced or similar numbers of seeds developed/spikes survived compared to the respective controls were found, suggesting that chemical compounds can be injected multiple times with low concentrations of Silwet L-77 for better uptake. Based on the acquired data, the following set-up was chosen for chemical compound injections: plant selection based on internode distance, 0.5 mL of injection volume with 0.05% Silwet L-77, 3 days injections with 24-hour intervals and one more injection after 1 hour after the first initial injection.

4.1.3. Chemical compound pre-screening

Three PTMs being implicated in shaping meiotic recombination landscapes were selected as targets for potential *in planta* application of chemicals compounds that possibly impact these marks (i.e., DNA methylation and histone acetylation/methylation) resulting in a putative change in the frequency and/or distribution of meiotic recombination events in barley (**Table 5**). The following compounds were selected: BIX-01294, Trichostatin A, Zebularine, 5-Azacytidine, and UNC0642 (**Table 5**). Except for UNC0642, compounds have been applied in plants before and some also in barley. However, a pre-screening assay for an *in planta* application of these compounds was established for barley (**Figure 10**),

to identify whether any impact is found at a given concentration enabling screening already tested and yet untested chemical compounds.

Table 5. Published post-translational modifications impacting meiotic recombination and selected compounds.

Post-translational modification	Impact on meiotic recombination	Chemical compound	Role of the chemical compound	Tested plant species
DNA methylation	Decreases CO rates in centromeric regions (Melamed-Bessudo and Levy, 2012; Mirouze <i>et al.</i> , 2012; Yelina <i>et al.</i> , 2015b; Underwood <i>et al.</i> , 2018)	5-Azacytidine	DNA methyltransferase inhibitor (Jones <i>et al.</i> , 1983)	Arabidopsis (Ogneva <i>et al.</i> , 2019), rice (Sano <i>et al.</i> , 1990), <i>Perilla frutescens</i> var. <i>crispa</i> (Kondo <i>et al.</i> , 2006), wheat (Vorontsova <i>et al.</i> , 2004), maize (Yang <i>et al.</i> , 2010), barley (Solís <i>et al.</i> , 2015)
		Zebularine	DNA methyltransferase inhibitor (Zhou <i>et al.</i> , 2002)	Arabidopsis (Liu <i>et al.</i> , 2015), wheat (Finnegan <i>et al.</i> , 2018), triticale (Ma <i>et al.</i> , 2016), barley (Han <i>et al.</i> , 2020)
Histone methylation	Regulates CO rates in (peri-)centromeric regions or CO distribution along chromosomes (Mirouze <i>et al.</i> , 2012; Choi <i>et al.</i> , 2013; Yelina <i>et al.</i> , 2015b; Underwood <i>et al.</i> , 2018)	BIX-01294	Histone (H3K9) methyltransferase inhibitor (Guo <i>et al.</i> , 2016)	Arabidopsis (Berenguer <i>et al.</i> , 2017), wheat (H., M., Wang <i>et al.</i> , 2019)
		UNC0642	Histone (H3K9) methyltransferase inhibitor (Cao <i>et al.</i> , 2019)	-
Histone acetylation	Global redistribution of CO events (Perrella <i>et al.</i> , 2010)	Trichostatin A	Histone deacetylase inhibitor (Li <i>et al.</i> , 2014)	Brassica (Li <i>et al.</i> , 2014), maize (Yang <i>et al.</i> , 2010), wheat (Vorontsova <i>et al.</i> , 2004), barley (Pandey <i>et al.</i> , 2017)

Selected chemical compounds at various concentrations were screened by treating germinated barley seedlings (cv. Barke) and analyzing root length and mitotic cell cycle values as a proxy for a potential impact in barley. The workflow (**Figure 10**) consisted of germinating seeds on Petri dishes with distilled water for three days and transferring them to a Petri dish with different concentrations of selected chemical compounds for three days. Pictures of Petri dishes were taken right after transfer and after three days of treatment and used to compare root length before and after treatment. Root meristems of chemical-treated seedlings were harvested and used for measuring relative cell cycle values.

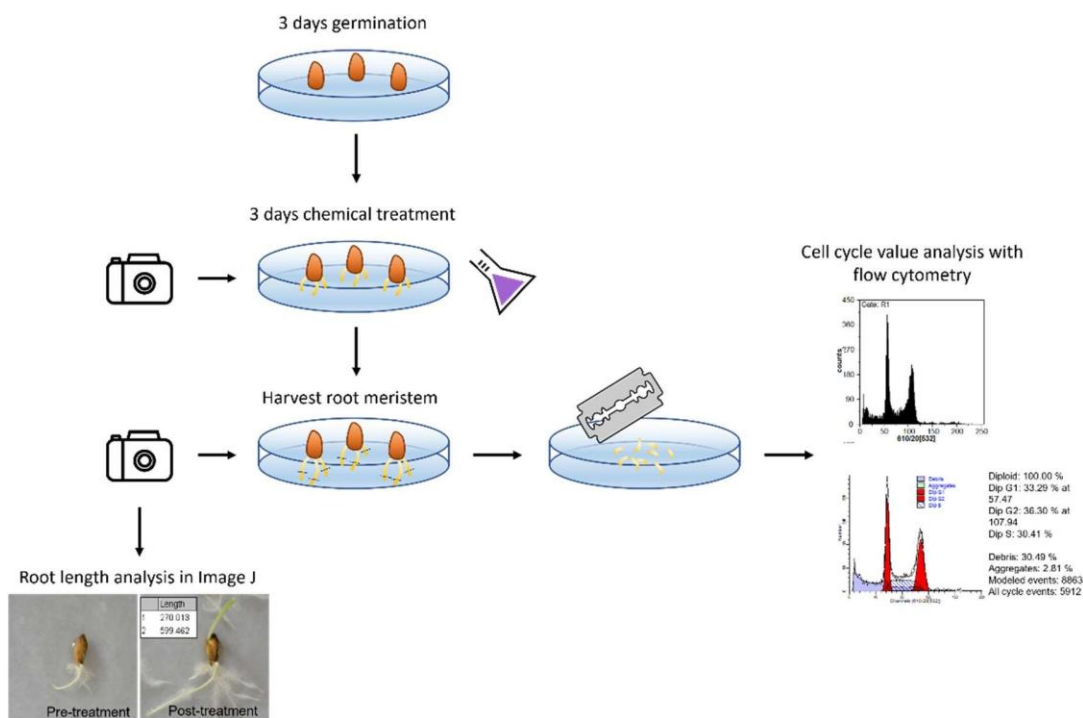


Figure 10. Scheme of chemical compound pre-screening using germinated barley seeds. Barely seeds were germinated on filter papers soaked in water for 3 days and transferred to new filter papers soaked with selected chemical compounds with different concentrations. Photos of seedlings were taken right after the transfer. After 3 days of compound treatment, photos of treated seedlings were taken again to compare root length between pre- and post-compound treatment. Nuclei from root meristems were isolated by chopping with a razor blade and the relative cell cycle values were determined flow cytometrically. All measurements of root length with Image J and of cell cycle values with flow-cytometry were performed in three independent experiments.

The relative percentages of cells in each phase of the mitotic cell cycle (G1-, S-, and G2-/M-phase) were measured by flow cytometry in nuclei suspensions isolated from root meristems of germinated barley seeds treated with selected chemical compounds: BIX-01294 (dissolved in distilled water and diluted to 40, 20, 10 and 5 μM), Trichostatin A (dissolved in DMSO and diluted to 1, 0.1, 0.01 and 0.001 μM), Zebularine (dissolved in DMSO and diluted to 100, 10, 1 and 0.1 μM), 5-Azacytidine (dissolved in DMSO and diluted to 100, 50, 25 and 12.5 μM) and UNC0642 (40, 20, 10 and 5 μM) (**Figures 10, 11** and **12A**). Additionally, a possible impact of 1% DMSO (used as a solvent for the highest concentration tested for Trichostatin A, Zebularine, 5-Azacytidine and UNC0642) and Silwet L-77 (0.05, 0.02, 0.01 and 0.001%; used as surfactant to improve compound uptake) was tested. To determine the potential impact of the selected chemical compounds on the cell cycle behavior the G2/G1 ratio and the amount of S-phase cells were compared. In case of 1% DMSO no severe difference in mitotic cell cycle values compared to the H₂O control was found, although the proportion of S-phase nuclei was slightly reduced. However, in case of in particular 0.05% but also 0.02% of Silwet L-77 the mitotic cell cycle was found to be severely disturbed indicated by an increased G2/G1 ratio and strongly decreased numbers of S phase nuclei. In addition, 10% and 3.3% of aneuploid seedlings were found (**Figure 11C**),

further supporting a strong impact on the mitotic cell cycle. At lower concentrations of Silwet L-77 (0.01% and 0.001%) the cell cycle values were similar to the control. Thus, the application of Silwet L-77 impacts relative mitotic cell cycle value in a dosage-dependent manner.

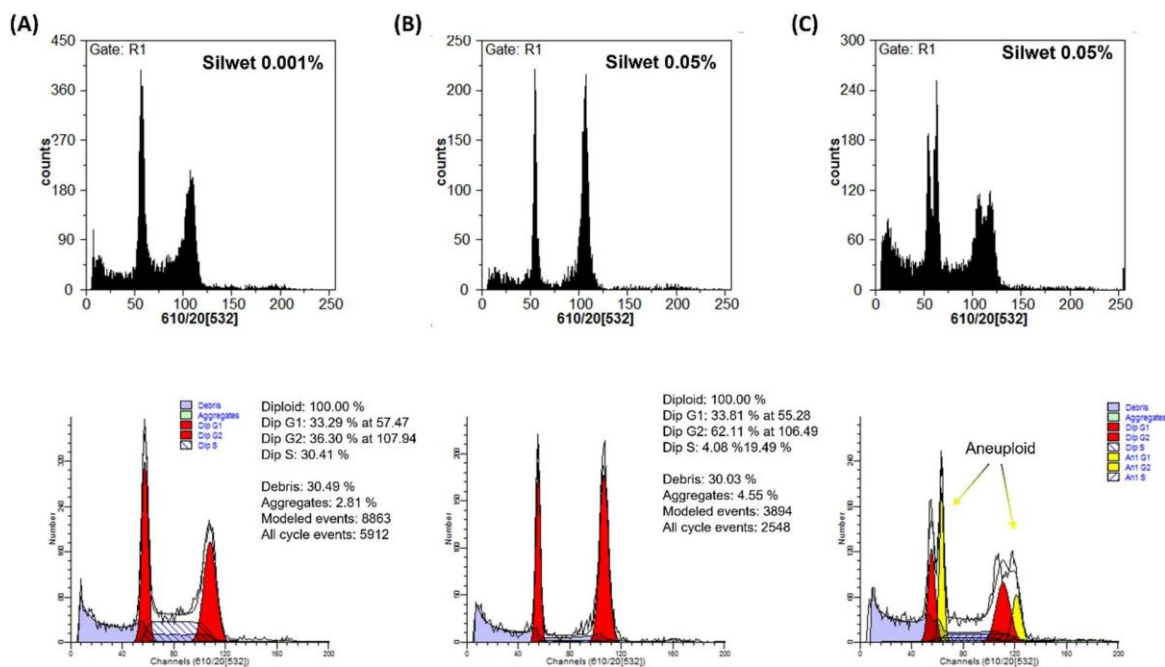


Figure 11. Example of the measured ratio of cells in each phase of the cell cycle from Silwet L-77 treated barley root meristem cells. **(A, B)** The relative percentage of cells in S phase lower in 0.05% of Silwet L-77 treated samples when compared with 0.001% of Silwet L-77 treated samples, while the relative percentage of cells in G2 phase in 0.05% of Silwet L-77 treated samples is higher than in 0.001% Silwet L-77 treated samples. **(C)** Aneuploidy in some of the 0.05% Silwet L-77 treated samples.

A clear dosage-dependent correlation for both parameters (G2/G1 ratio and S-phase proportion) was also found for Trichostatin A. A clear reduction of S-phase nuclei was also observed for higher concentrations of 5-Azacytidine and Zebularine. In the latter case 3.3% of aneuploidy was observed at the highest concentration (100 μ M). For BIX-01294 and UNC0642 no clear impact on the mitotic cell cycle behavior could be detected, neither with respect to the G2/G1 ratio nor to the S-phase proportion (**Figure 12A**).

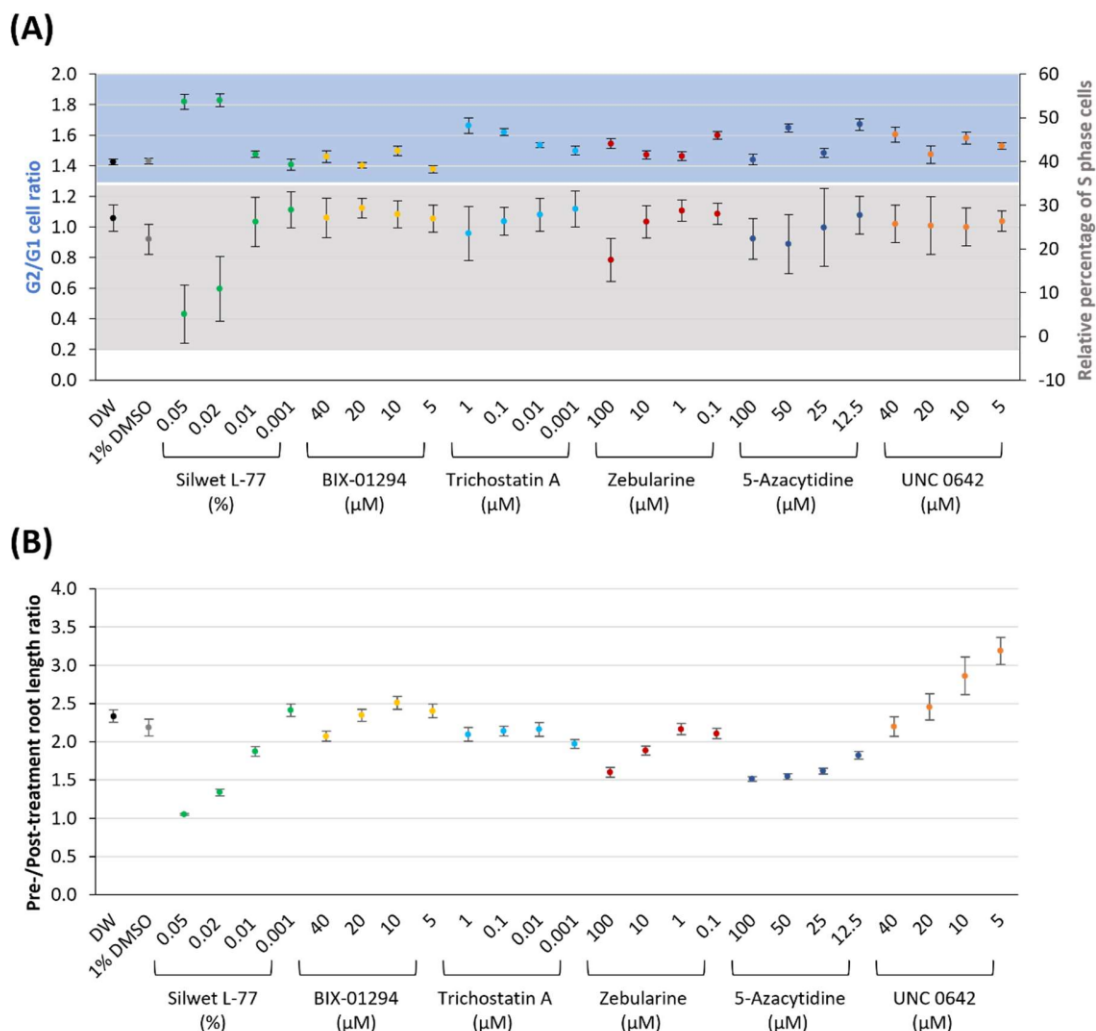


Figure 12. Impact of chemical compounds on barley seedlings. (A) G2/G1 ratio of the relative percentage of cells in each phase and the relative percentage of S phase cells. Blue block indicates values of G2/G1 cells ratio and grey block indicates values of S phase cells. **(B)** Root length ratio between pre- and post-treatment. Three independent experiments were performed except distilled water control (n=4).

As the second parameter for the detection of a possible *in planta* impact of tested chemical compounds, the root length pre- and post-treatment was measured (**Figures 10** and **12B**). After three days of treatment, for all chemical compound treated seedlings (including Silwet L-77) an increased root length with decreasing concentration of the compounds was found, except for Trichostatin A for which no variation was observed. The strongest effect on root development among all chemical compounds was observed for Silwet L-77 in accordance with the cell cycle analysis. Compared to the water control and the 1% DMSO treated seedlings with a root length increase from pre- to post-treated time point of $2.34X \pm 0.08$ (n=4) and $2.19X \pm 0.11$ (n=3), respectively, Silwet L-77 showed an increase of $1.05X \pm 0.01$ (n=3) for 0.05%, $1.34X \pm 0.05$ (n=3) for 0.02% and $1.88X \pm 0.06$ (n=3) for 0.01%. Only the lowest concentration (0.001%) revealed with $2.41X \pm 0.08$ a growth rate comparable to the control.

The difference in the growth rate between the highest and the lowest concentration of Silwet L-77 was $\Delta 1.36$. In all other cases, this difference was much lower: $\Delta 0.3$ for 5-Azacytidine, $\Delta 0.44$ for BIX-01294, $\Delta 0.57$ for Zebularine and 0.99 for UNC0642. In the case of Trichostatin A the root growth was rather stable independent of the concentration ($\Delta 0.07$). Thus, except for Trichostatin A, root growth was impacted by all compounds in a dosage-dependent manner. However, the extend varied severely between compounds.

In a nutshell, all tested compounds showed an effect on mitotic cells which could be detected by cell cycle analysis and/or root growth measurements. The applied range of concentrations allowed the selection of a starting concentration for injection experiments to impact meiosis.

4.2. PCR-based single pollen nucleus genotyping

To establish a protocol to efficiently genotype PCR-based single pollen nuclei without a prior Whole Genome Amplification (WGA) step enabling to measure meiotic recombination rates in defined chromosomal intervals, various approaches were explored: direct PCR-based genotyping (4.2.1) or targeted pre-amplification and subsequent PCR-based genotyping (4.2.2) of flow-sorted pollen nuclei, PCR-based genotyping employing (germinated) pollen grains (4.2.3), and Crystal dPCR-based genotyping of flow-sorted single pollen nuclei (4.2.4). A chromosomal interval Ic 1 defined by two InDels (6.7 cM, 344.7 Mbp; InDel1029 + InDel1076) between barley cultivars Barke and Morex on chromosome 1 was employed to test and compare the different approaches (**Figure 13**).

4.2.1. Direct PCR-based genotyping of flow-sorted single pollen nuclei

Single Barke x Morex F_1 hybrid pollen nuclei were flow-sorted into individual wells of a 384 well plate and directly used as a template for PCR-based genotyping employing InDel marker 1029 (144/137 bp) and/or 1076 (202/186 bp) (**Table 2**) without any pre-amplification or -treatment. Based on the analysis of 90 single pollen nucleus genotyping reactions, the success rate was 20% for InDel 1029 and 14.4% for InDel 1076 when employed separately. In the case of simultaneous genotyping using both InDel markers per reaction (in total 90 genotyping reactions), in 36.7% amplification of either InDel 1029 or InDel 1076 was found, while only in 5.5% of the reactions, both markers showed a simultaneous amplification. In sum, direct PCR-based single pollen nucleus genotyping to measure Ic 1 meiotic recombination rates was feasible; however, the efficiency, i.e., the number of successfully Ic1 genotyped nuclei, was low.

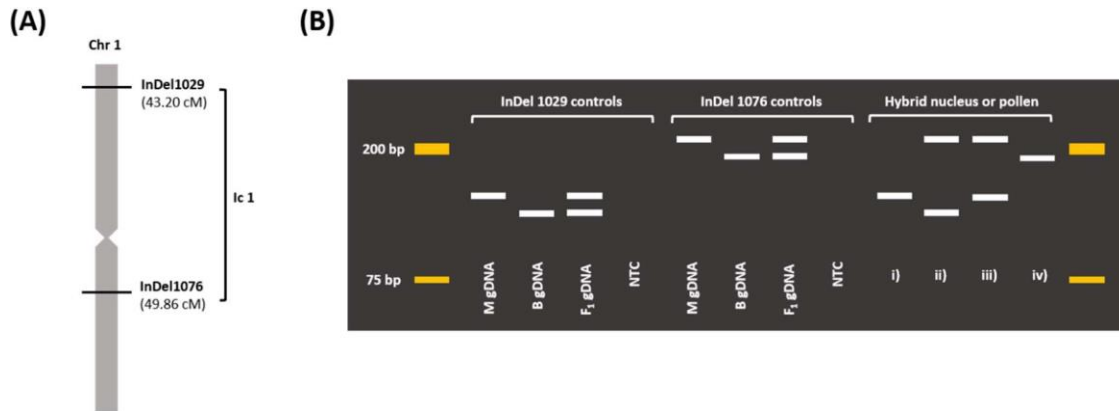


Figure 13. Scheme of PCR-based Ic 1 (InDel 1029+InDel 1076) genotyping of a single F₁ pollen grain or nucleus visualized by gel electrophoresis. (A) Chromosomal interval Ic 1 (InDel 1029 and InDel 1076). **(B)** Scheme of PCR-based genotyping using hybrid or parental genomic DNA (gDNA), pollen nucleus or pollen grain. Amplicon(s) after Ic 1 genotyping of a single hybrid pollen nucleus/grain sample: i) InDel 1029 only (M allele), ii) InDel 1029 (B allele) and InDel 1076 (M allele) simultaneously (recombinant), iii) InDel 1029 (M allele) and InDel 1076 (M allele) simultaneously (non-recombinant), and iv) InDel 1076 only (B) allele. M = Morex, B = Barke and F₁ = Barke x Morex. NTC=negative control.

4.2.2. Targeted pre-amplification and subsequent PCR-based genotyping of flow-sorted single pollen nuclei

Whether PCR-based targeted pre-amplification of genomic loci containing InDel 1029 or InDel 1076 could improve the subsequent InDel marker genotyping success rate, primer pairs were tested for targeted pre-amplification (974-1269 bp for InDel 1029, 917-1097 bp for InDel 1076) prior genotyping of InDel 1029 and InDel 1076 (**Table 4**). Pre-amplification primer pairs were verified individually on genomic DNA of Morex, Barke and F₁ hybrids (Barke x Morex) and subsequently, they were pooled and used for pre-amplification. Using individual primer pairs in each case, pre-amplified amplicons were detected; however, after pooling two pairs of pre-amplification primers not all former amplicons were detectable on a gel. Thus, InDel 1029_binding_2F+InDel 1029_binding_3R were used to pre-amplify InDel 1029 and InDel076_binding_1F+InDel1076_binding_1R to pre-amplify InDel 1076 due to higher efficiency. To pre-amplify both InDels in a single reaction, all four selected pre-amplification primers were pooled.

135 F₁ pollen nucleus PCR samples pre-amplified for either one or both genomic loci were used as subsequent templates for PCR-based genotyping of InDel marker 1029 and/or 1076 and analyzed as in **Figure 13B**. Genotyping success rate was 17.8% for InDel 1029 and 5.2% for InDel 1076 using their respective pre-amplified samples as templates. In the case of simultaneous genotyping of both InDel markers using as template pre-amplified samples simultaneously from both loci, in 23% of the reactions, either InDel 1029 or InDel 1076 were successfully genotyped while only in 7.4% of the reactions both markers showed successful amplification (**Table 6**). Despite the fact that the amplification of the individual loci was similar as in cases without preamplification for InDel 1029 or

even lesser for In Del 1076 (probably due to a partial failure of the PCR), the successful amplification of both markers simultaneously was increased in nested-PCR genotyping. In summary, pre-amplification and nested-PCR genotyping of a single pollen nucleus to measure Ic 1 meiotic recombination rate were slightly more efficient when compared with direct-PCR genotyping; however, considering the possible throughput, the efficiency was low.

4.2.3. PCR-based genotyping employing entire pollen grains

To explore whether an increased number of template copies could improve genotyping efficiency, the application of single pollen grains containing 3 haploid nuclei was explored. Therefore, intact and germinated pollen grains were tested as template. To germinate barley pollen grains, they were incubated in various concentrations of pollen germination media (PGM; 0.1X, 0.2X, 0.5X and 1X) or distilled water as control (**Figure 14A**) for 0, 15, 30, 45 and 60 mins. Compared with the other concentrations of PGM and the water control, in the case of 0.2X PGM already after 15 mins of incubation, consistent pollen germination was found (**Figure 14B**). Since the transfer of already germinated intact pollen grains was technically challenging, pollen grains were scattered on a Petri dish and individual pollen grains were transferred using a human hair into a microwell of a 384 well plate containing 2 μ L of 0.2X PGM. Successful transfer of individual pollen grains was confirmed using a stereomicroscope (**Figure 14C**).

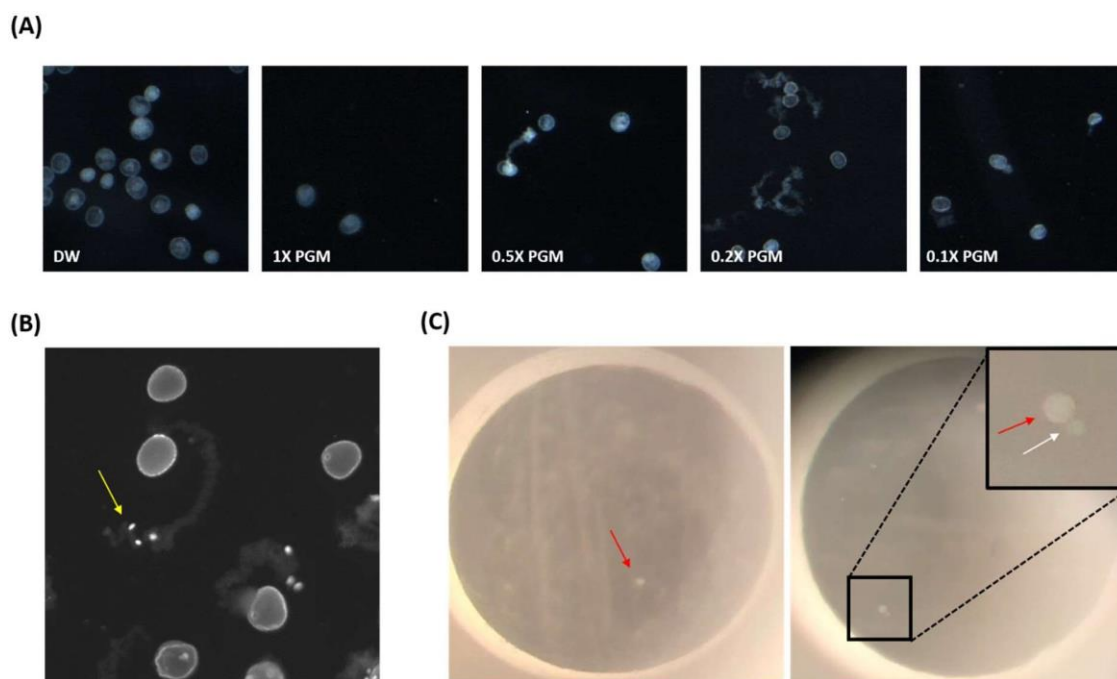


Figure 14. Germination of barley pollen *in vitro*. (A) Pollen incubated for 15 min in distilled water (DW) or 1X, 0.5X, 0.2X and 0.1X pollen germination media (PGM). (B) Germinated pollen in 0.2X PGM after 15 min. Grown pollen tube and pollen nuclei (DAPI stained) indicated with the yellow arrow. (C) Pollen grain transferred into 2 μ L of 0.2X PGM in a well of a 384 microwell plate (left, red arrow) and germinated after 15 min incubation (right, red arrow: pollen, white arrow: pollen tube).

Pollen grains were incubated for 15 min before performing PCR-based genotyping within Ic 1, i.e., InDel marker 1029 and/or 1076. Based on the analysis of 135 pollen grains in all cases, genotyping success rate was 30% and 18.3% for InDel 1029 and InDel 1076, respectively, when genotyped separately. In the case of simultaneous genotyping within one reaction, amplification success for either InDel 1029 or InDel 1076 was 15%, while only in 3.3% of the reactions amplification of both markers was found (**Table 6**). When using pollen grains directly without prior germination as templates for Ic 1 genotyping (135 pollen grains in all cases), the individual amplification success rate was 21.7% and 23.3% for InDel 1029 and InDel 1076, respectively. Simultaneous genotyping of both InDel markers resulted in 2.5% of reactions for either InDel 1029 or InDel 1076 and 0% of reactions for both InDel 1029 and InDel 1076 in successful amplification (**Table 6**). This result indicates that germination of pollen grains improved genotyping efficiency compared to un-germinated pollen grains, albeit less efficient than single nucleus genotyping. Employing germinated pollen grains for Ic 1 genotyping was feasible, while using pollen grains without prior germination was not. However, employing germinated pollen grains was less efficient and more laborious/technically challenging when compared to genotyping individual pollen nuclei and thus, it was not considered further as a high-throughput tool for measuring meiotic recombination rates.

Table 6. Average Ic 1 (InDel 1029+InDel 1076) genotyping efficiency employing different PCR methods. N=number of samples.

Target	Efficiency (%) of PCR-based genotyping			
	using flow-sorted single pollen nuclei		using single pollen grains	
	direct*	after targeted pre-amplification**	not germinated**	germinated**
InDel 1029	20.0	17.8	21.7	30.0
InDel 1076	14.4	5.2	23.3	18.3
InDel 1029 or InDel 1076	36.7	23.0	2.5	15.0
InDel 1029+InDel 1076	5.5	7.4	0	3.3
	*N = 90 **N = 135			

4.2.4. Crystal digital PCR: Encapsulation and genotyping of flow-sorted single haploid pollen nuclei

Considering the PCR-based genotyping efficiency and the number of pollen nuclei/grains that can be analyzed via the methods described above, a more efficient method, particularly in terms of throughput, was required to measure meiotic recombination rates in pollen nuclei within selected chromosomal intervals. To investigate the possible application of the Crystal digital PCR technology

(Naica®, Stilla Technologies®) (Jovelet *et al.*, 2017) for high-throughput single barley pollen nucleus genotyping (**Figure 15**), initially, it was explored whether the size of droplets formed is large enough to encapsulate a single barley pollen nucleus. After template partitioning, according to the manufacturer water-in-oil droplets formed with $\sim 100 \mu\text{m}$ \varnothing were theoretically big enough to encapsulate a single barley pollen nucleus (roughly $5 \mu\text{m}$ \varnothing). However, droplet size may differ based on the chemistry used or the type of PCR chips used. Using Perfecta qPCR Toughmix, the size of the formed droplets was on average $103.8 \mu\text{m}$ (\varnothing) corresponding to an average per droplet volume of 0.59 nL when using Sapphire chips (Stilla Technologies®) and thus being theoretically large enough to encapsulate a single barley pollen nucleus. Three individual Sapphire chips can be analyzed together in one dPCR run. Each chip contains four individual chambers, and each chamber generates roughly 25,000 water-in-oil droplets out of $25 \mu\text{L}$ reaction volume. Thus, per chip up to 100,000 water-in-oil droplets are generated and per PCR run up to around 300,000 water-in-oil droplets can be analyzed in parallel.

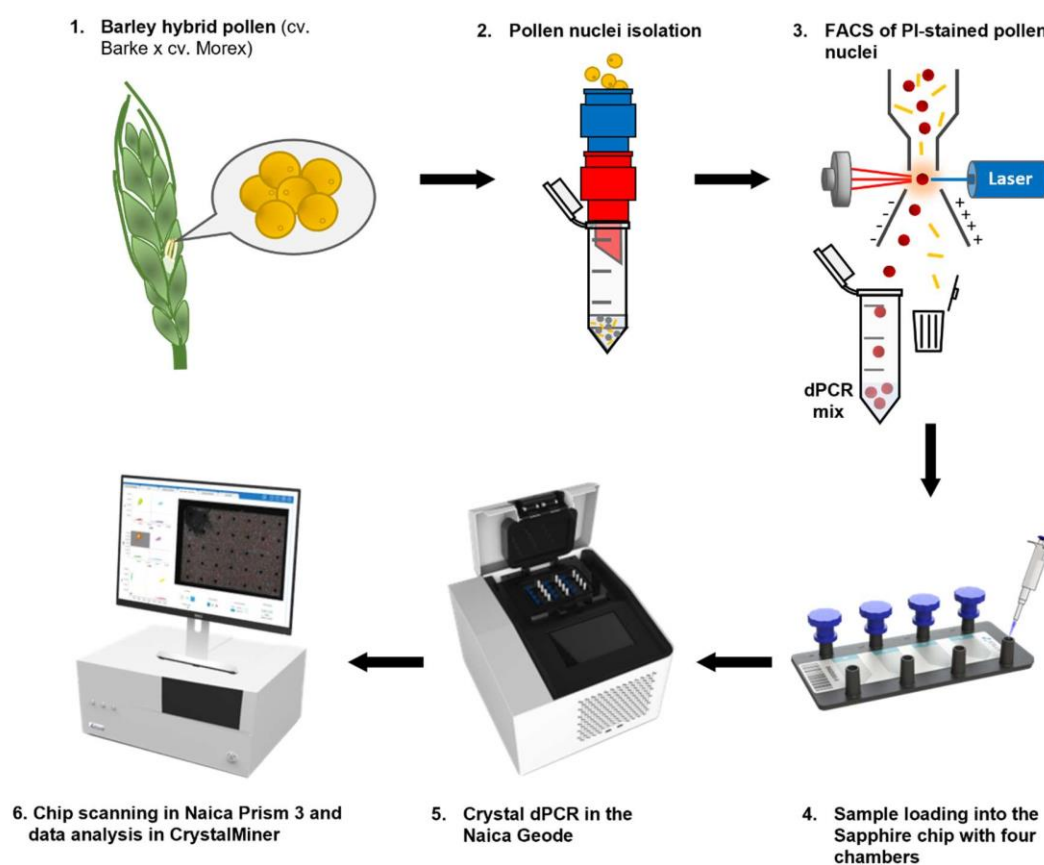


Figure 15. Workflow of single pollen nucleus genotyping using Crystal digital PCR. Modified from Ahn *et al.* (2021) and Stilla Technologies®. 1. Anthers from cv. Barke x cv. Morex barley hybrid plants are collected. 2. Pollen and pollen nuclei are isolated in suspensions by using filters of different mesh sizes ($100 \mu\text{m}$ and $20 \mu\text{m}$). 3. Pollen nuclei are stained with propidium iodide (PI) and flow-sorted into the Crystal dPCR mix. 4. $25 \mu\text{L}$ of Crystal dPCR mix including sorted pollen nuclei are loaded into one of the four chambers of a Sapphire chip. 5. Up to three Sapphire chips can be employed for droplet generation and thermocycling on a Naica® Geode. 6. Sapphire chips are scanned in a Naica® Prism 3 (or Prism 6) after thermocycling, followed by data analysis in Crystal Miner software.

Even though the original Crystal dPCR set-up with the Naica® Prism 3 enables detection of up to three colors simultaneously (FAM, HEX and Cy5), initially single pollen nucleus genotyping assays using only two colors, i.e., FAM and HEX, were tested. In addition to Ic 1 (6.7 cM, 344.7 Mbp; InDel1029 + InDel1076), three more chromosomal intervals located on chromosome 3 were chosen to measure meiotic recombination rates. To do so, pairs of SNP or InDel markers between cv. Barke and cv. Morex spanning a genetic distance between 6.7 and 11.7 cM were selected (Zhou *et al.*, 2015) (**Figure 16A** and **Tables 2** and **3**) and their genotype-specificity was confirmed (**Figure 17**): Ic 1 – Interval at centromeric region of chromosome 1 (6.7 cM, 344.7 Mbp; InDel1029 + InDel1076), Ic 3 – Interval at centromeric region of chromosome 3 (8.5 cM, 333.0 Mbp; InDel3039 + SNP6), Id 3-1 – Interval at distal region of chromosome 3 (11.7 cM, 18.5 Mbp; InDel3118 + InDel3135) and Id 3-2 – Interval at distal region of chromosome 3 (11.1 cM, 12.2 Mbp, InDel3135 + InDel3152). The presence of possible polymorphisms between Barke and Morex within primer/probe binding regions was analyzed by Sanger sequencing (**Figure 18**). Polymorphisms were absent in all cases except for InDel 1029 in cv. Morex (primer binding region), InDel 1076 in cv. Morex (primer and probe binding region) and InDel 3135 in cv. Barke (probe binding region). However, none of these polymorphisms did impact genotyping-specificity (**Figure 17**).

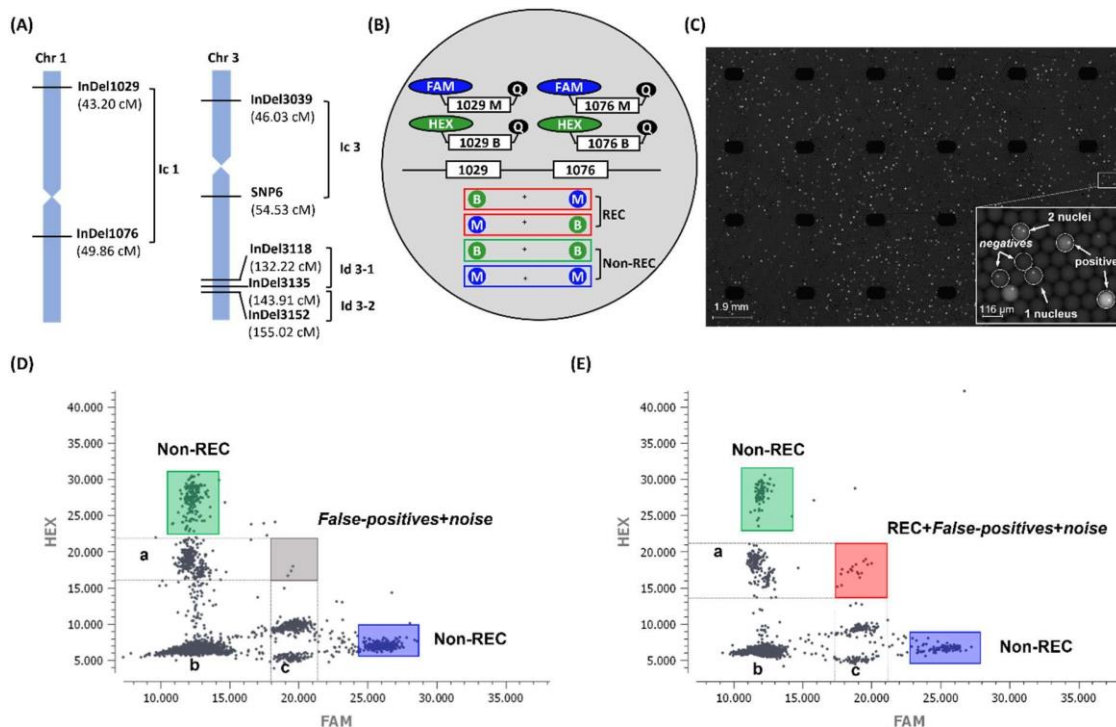


Figure 16. Selected chromosomal intervals and working principle of Crystal dPCR-based single pollen nucleus genotyping. (A) Selected InDel or SNP markers defining four chromosomal intervals on chromosomes 1 and 3. (B) Crystal digital PCR-based pollen nucleus genotyping assay exemplified for Ic 1: possible combinations of two fluorescence probes enable to distinguish between recombinant and non-recombinant pollen nuclei. (C) A complete view of a scanned Sapphire chip chamber. Each chamber typically contains around 25,000 individual droplets. Droplets with successful amplification in any channel (FAM or HEX) are light-grey compared to negative droplets in dark-grey. Note, black semi-circles on the scanned image represent the 24 stabilizing pillars within each chamber. (D, E) Crystal digital PCR-based single pollen nucleus genotyping data from a

scanned chamber displayed as dot plot in Crystal Miner software of pollen nuclei from **(D)** the parental genotypes mixed in a 1:1 ratio and **I** from a hybrid plant being heterozygous for *Ic 1*. The two non-recombinant parental populations are detected as droplets with successful genotyping calls by the two HEX-labeled (green box) or FAM-labeled allelic probes (blue box). The recombinant population including *false-positives+noise* indicated in a gray and red box (recombinants, *false-positives* and *noise*) are detected as droplets positive for both HEX and FAM. Clusters a and c represent droplets reflecting the successful amplification of only one of the markers. Cluster b indicates droplets without any successful genotyping call (either no nuclei encapsulation or no amplification from the encapsulated nucleus).

To set up dPCR-based genotyping of single barley pollen nuclei, initial genotyping assays of InDel1029 and InDel1076 defining the interval *Ic 1* were performed. Barke (B) allele-specific probes for InDel1029 and for InDel1076 were both labeled with HEX fluorophore (green) and Morex (M) allele-specific probes for InDel1029 and for InDel1076 were both labeled with FAM fluorophore (blue) (**Figure 16B**). 3,000 barley pollen nuclei were flow-sorted either from both parental plants mixed in a 1:1 ratio or from a plant heterozygous for *Ic 1* and subjected to Crystal dPCR-based genotyping. Droplets with successful marker amplification are detected based on emitting brighter fluorescence than droplets with no amplification (either droplets containing an encapsulated nucleus with no PCR amplification or droplets that did not encapsulate any nucleus during the partitioning step) by scanning the chip after PCR in the Prism3 and analyzing the data using Crystal Miner software (**Figure 16C**). In case of no recombination within *Ic 1*, the droplets with successful amplification from both markers (either both FAM allelic probes or both HEX allelic probes) were expected to be located at the highest point of each axis in a dot plot displaying FAM and HEX intensity. In the case of an encapsulated pollen nucleus with a recombination event within *Ic 1*, the droplets with successful amplification from both markers were expected to be located at the center of the dot plot intermediate between FAM and HEX, i.e., FAM for InDel1029 and HEX for InDel1076 or HEX for InDel1029 and FAM for InDel1076. In both cases, roughly equal numbers of droplets were detected positive for either FAM or HEX, representing parental genotypes or non-recombinants (**Figures 16D** and **16E**). However, in the case of flow-sorted pollen nuclei from a plant heterozygous for *Ic 1*, an enrichment of droplets with amplification of both FAM and HEX, representing recombinants, was found. In addition, droplets reflecting the successful amplification of only one of the markers (**Figures 16D** and **16E**, clusters a and c) and droplets without any amplification (**Figure 16D** and **16E**, clusters b) can be differentiated. Thus, encapsulation and genotyping of flow-sorted single barley pollen nuclei using Crystal dPCR seemed feasible. Notably, PI-stained nuclei were visible in the HEX channel even after thermocycling due to the similar wavelength between PI and HEX.

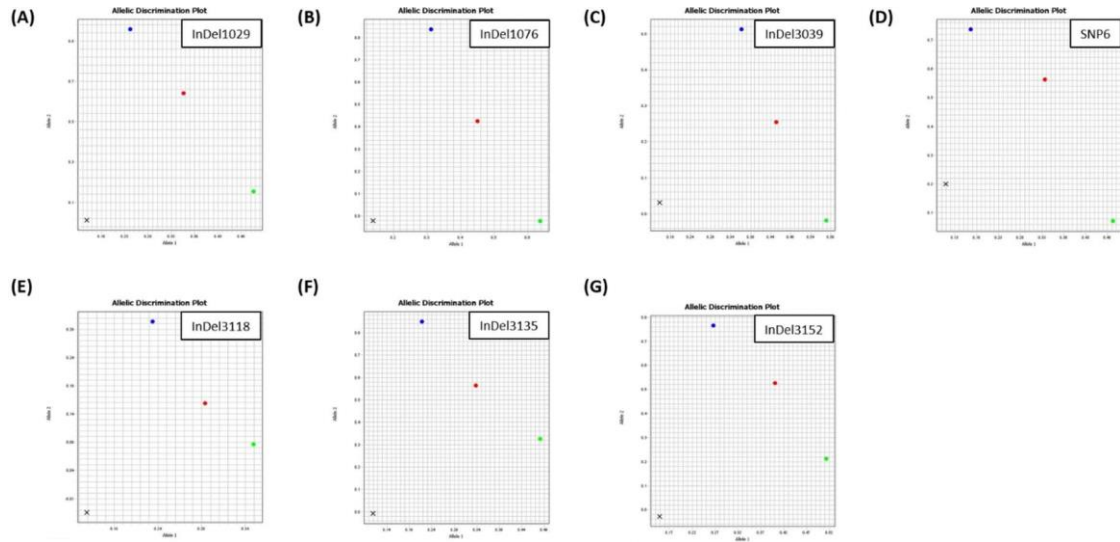


Figure 17. Genotype-specificity of employed markers. (A) InDel1029, (B) InDel1076, (C) InDel3039, (D) SNP6, (E) InDel3118, (F) InDel3135 and (G) InDel3152. Blue dot: Morex genomic DNA (FAM), green dot: Barke genomic DNA (HEX), red dot: hybrid (Barke x Morex) genomic DNA and black cross: negative control.

4.2.4.1. Refining a Crystal dPCR-based single pollen nucleus genotyping approach

The fact that PI-stained nuclei were visible in the HEX channel even after thermocycling enabled assessing the nuclei encapsulation rate and amplification efficiency in detail (**Figure 16C**). The total number of encapsulated nuclei and the number of successfully amplified droplets thereof as well as the number of droplets with more than a single encapsulated nucleus with and without any amplification, were manually counted (**Figure 16C**) and used as a benchmark for further improvements of the method.

efficiency was found. Thus *MseI* was not considered further. Compared to an untreated nuclei control, in the case of Proteinase K and *TaqI* an increase in the number of positive parental genotype droplets (successful amplification in either FAM or HEX) was observed; an increase of 164% (n=6) for *TaqI* and of 31% (n=5) for Proteinase K compared to untreated pollen nuclei (n=6) (**Figure 19**). Hence, likely by increasing the accessibility of the DNA for PCR amplification, a positive impact on the PCR efficiency is found after a destructive nuclei treatment. Since the Proteinase K treatment was less efficient and more laborious (see Materials and Methods) only the *TaqI* treatment was applied for all subsequent experiments.

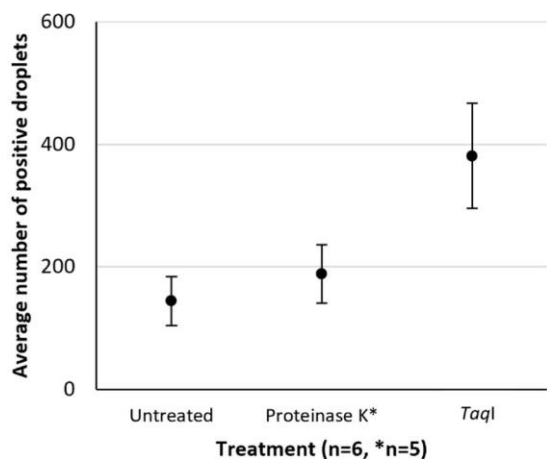


Figure 19. Crystal dPCR efficiency for Id 3-1 genotyping employing 3,000 (1:1 ratio of Barke and Morex) treated (Proteinase K or *TaqI* restriction enzyme) and untreated pollen nuclei. The average total number of droplets with one encapsulated nucleus showing successful genotyping calls in FAM or HEX shown for untreated, Proteinase K treated and *TaqI* treated nuclei samples (n=6 for *TaqI* treated and non-treated pollen nuclei, n=5 for Proteinase K treated pollen nuclei).

Considering the different nucleus structures and condensation of vegetative and sperm pollen nuclei (Twell, 2011), it was of interest whether the type of nucleus employed impacted the genotyping efficiency of the Crystal dPCR. 3,000 vegetative and sperm nuclei were either separately or pooled together flow-sorted and used for Crystal dPCR-based genotyping in Id 3-1 (**Figure 20**). Both vegetative and sperm nuclei samples did not show differences in terms of the average number of encapsulated nuclei compared with pooled nuclei samples (**Figure 20C**). The average amplification rate in the FAM channel was the highest in sperm nuclei (23.0%, n=4), followed by pooled nuclei (18.3%, n=8) and vegetative nuclei (16.1%, n=4). The average amplification rate in the HEX channel was the highest in sperm nuclei (17.9%, n=3), followed by vegetative nuclei (10.4%, n=3) and pooled nuclei (7.9%, n=6) (**Figure 20D**). The average fluorescence value in both FAM and HEX channel was the highest in sperm nuclei (FAM: 30,314.0 (n=4), HEX: 31,262.2 (n=3)), followed by similar values found in both pooled and vegetative nuclei samples (**Figure 20E**).

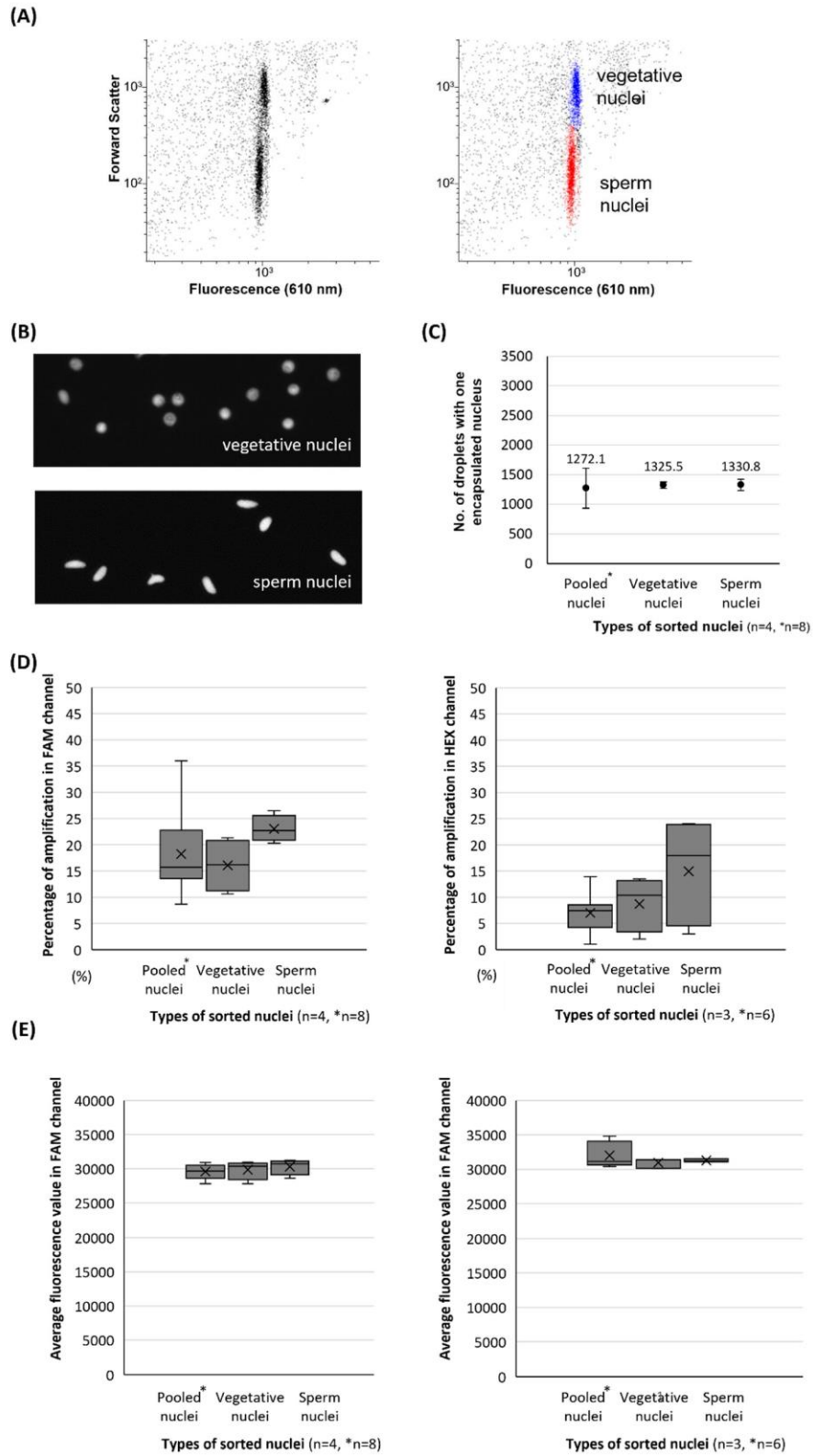


Figure 20. Crystal dPCR-based Id 3-1 genotyping efficiency employing flow-sorted pooled, vegetative or sperm nuclei samples. (A) Distinctive population clusters of vegetative and sperm nuclei during flow sorting. (B) Morphology of vegetative and sperm nuclei under the fluorescence microscope. (C) The average number of encapsulated nuclei. (D) Percentage of

amplification in FAM and HEX channel **(E)** Average fluorescence value in FAM and HEX channel. All chambers with 3,000 flow-sorted nuclei.

In a second experiment employing Ic 1, 1,241 droplets encapsulated a single vegetative nucleus (n=1) and 1339 droplets encapsulated a single sperm nucleus (n=1), while 1,143 droplets encapsulated a single nucleus using pooled nuclei samples (n=2) (**Figure 21A**). The average amplification rate in the FAM channel was the highest using sperm nuclei (9.9%, n=1), followed by vegetative nuclei (8.2%, n=1) and pooled nuclei samples (8.0%, n=2) (**Figure 21B**). In the HEX channel, pooled nuclei samples showed the highest average amplification rate (16.3%, n=2), followed by sperm (14.6%, n=1) and vegetative (12.8 %, n=1) nuclei samples. The average FAM and HEX fluorescence values in pooled, vegetative and sperm nuclei samples were similar for Id 3-1 (**Figure 21C**). Considering the results from both intervals the use of only sperm nuclei seems to be promising. However, the different quality of the individual pollen nuclei isolations did not necessarily allow a clear separation of the two nuclei types in each case. Furthermore, due to the limited number of available pollen nuclei per spike, in further experiments, both nuclei types were sorted together into the genotyping assay.

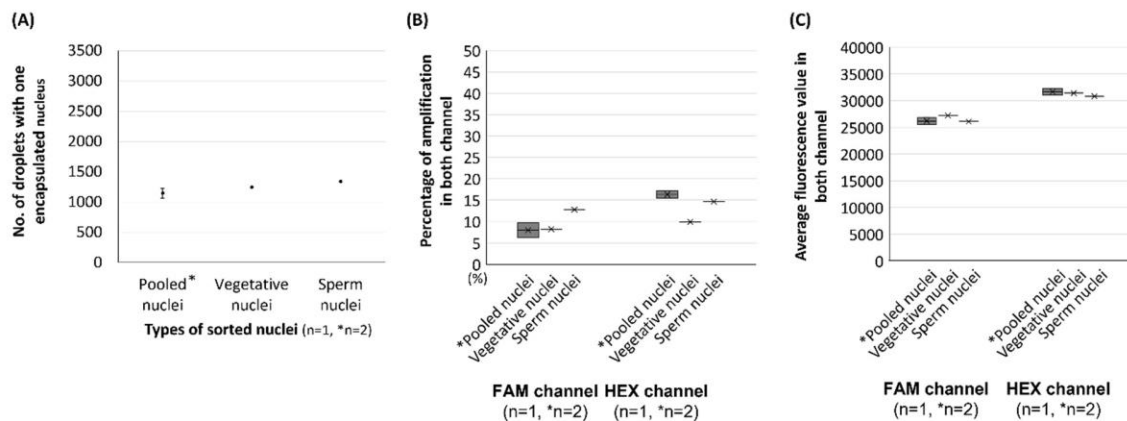


Figure 21. Comparison of Crystal dPCR-based Ic 1 genotyping efficiency employing flow-sorted pooled, vegetative or sperm nuclei samples. (A) Average number of encapsulated nuclei. **(B)** Percentage of amplification in FAM and HEX channel. **(C)** Average fluorescence value in FAM and HEX channel. All chambers with 3,000 flow sorted nuclei.

Next, 2,000-6,000 flow-sorted pollen nuclei were employed, and the nuclei encapsulation rate across different chambers for Id 3-1 was assessed by manual counts. A positive correlation between the number of flow-sorted pollen nuclei and the number of droplets encapsulating a single nucleus was observed (**Figure 22A**). Regardless of the amount of flow-sorted pollen nuclei, roughly half of them were encapsulated (39.9-42.4%) close to the encapsulation rate predicted based on the Poisson distribution. The observed number of droplets containing HEX more than a single nucleus, i.e., two nuclei (droplets with more than two were not observed), also positively correlated with the number of employed sorted nuclei but was much lower than expected from the calculated Poisson distribution,

too (**Figure 22B**). Since these droplets could result in possible *false-positive* genotyping calls in case of encapsulation of nuclei from both parental genotypes, they should be avoided. In further experiments, all droplets containing more than a single nucleus were excluded from the calculations.

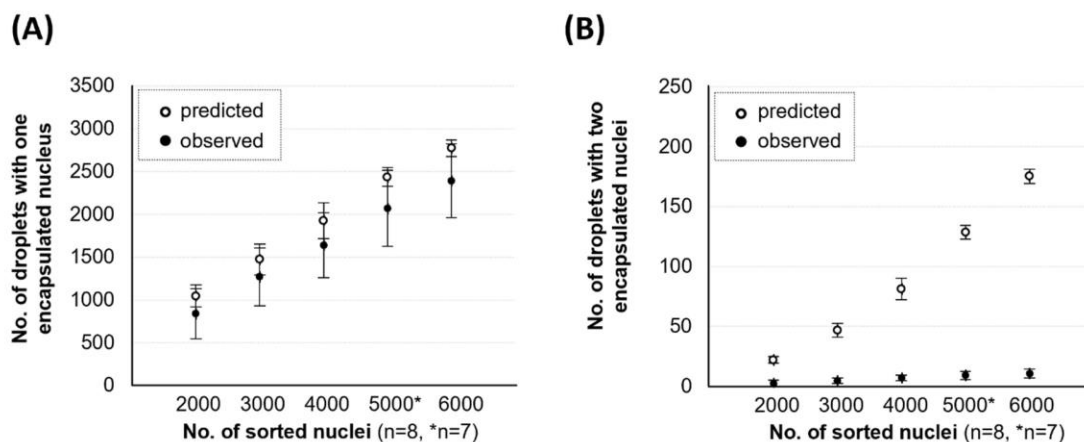


Figure 22. Comparison of nucleus/nuclei encapsulation frequencies based on manual counts or Poisson-predicted distribution in relation to the number of employed flow-sorted pollen nuclei using Id 3-1. The average number of droplets encapsulating one nucleus (**A**) or two nuclei (**B**) is predicted by a Poisson distribution (white dots) or based on manual counts (black dots) in relation to the number of employed flow-sorted pollen nuclei.

To address whether different numbers of encapsulated nuclei might impact Crystal dPCR amplification efficiency, 1:1 mixtures of both parental pollen nuclei (2,000-6,000) were flow-sorted and used for evaluation of the dPCR efficiency for Id 3-1 by determining the average number of positive parental genotype droplets and the average fluorescence intensities for both, FAM and HEX. A positive correlation between the number of flow-sorted pollen nuclei and the number of droplets with positive PCR amplification was found. Independent on the number of flow-sorted nuclei, a similar percentage of dPCR-positive droplets for both, FAM and HEX, was found (**Figures 23A** and **23B**). Notably, the fluorescence intensity of dPCR-positive droplets slightly decreased with an increasing number of flow-sorted nuclei in both channels, FAM and HEX (**Figures 23C** and **23D**).

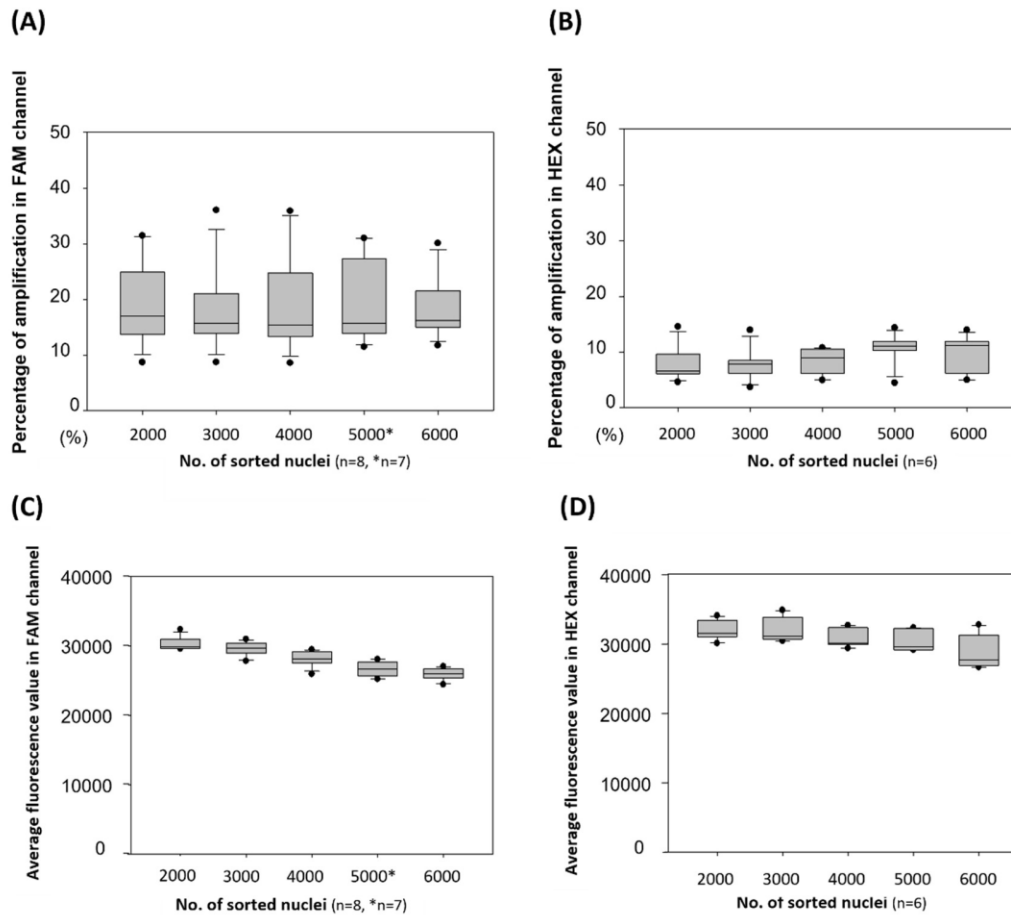


Figure 23. Crystal dPCR efficiency for Id 3-1 in relation to the total number of employed flow-sorted nuclei. (A, B) Percentage of the total number and (C, D) average fluorescence value of droplets with encapsulated nucleus showing successful genotyping calls in FAM (A, C) or HEX (B, D) in relation to the number of employed flow-sorted pollen nuclei.

Since the increasing amount of PBS buffer (sheath fluid used during the flow-sorting procedure) when sorting higher numbers of pollen nuclei could negatively impact the dPCR efficiency (Zhu *et al.*, 2015), fluorescence values of FAM and HEX were measured across different concentrations of PBS buffer within the Crystal dPCR mix using isolated genomic DNA as template (**Figure 24**). Fluorescence values in both FAM and HEX decreased as the concentration of PBS buffer within Crystal dPCR mix increased, indicating a negative impact of PBS buffer on PCR efficiency.

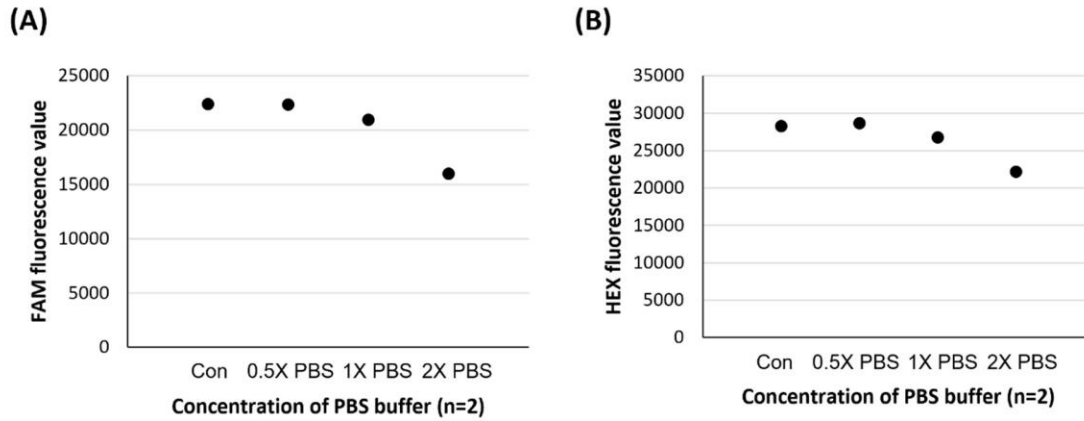


Figure 24. Inhibiting effect of PBS buffer (sheath fluid for flow sorting) on the efficiency of Crystal dPCR employing Ic 1. (A) Average fluorescence value in FAM channel. (B) Average fluorescence value in HEX channel.

Considering the encapsulation rate, the percentage of droplets encapsulating more than one nucleus and the dPCR efficiency employing different numbers of flow-sorted pollen nuclei and the average number of pollen nuclei available from an individual barley spike (generally 30,000~50,000 flow-sorted pollen nuclei from a single spike), 3,000 pollen nuclei were flow-sorted into each chamber as a benchmark for all further genotyping assays aiming to establish the approach.

To test if this approach is suitable for other (crop) plant species with different DNA contents and nuclear sizes, 3,000 leaf nuclei from five different plant species were flow-sorted for encapsulation experiments: *A. thaliana* (0.32 pg/2C; 2.9 μm), *G. max* (2.26 pg/2C; 4.2 μm), *P. crispum* (4.50 pg/2C; 5.3 μm), *C. annuum* (6.32 pg/2C; 6.4 μm), *H. vulgare* (10.92 pg/2C; 6.1 μm) and *V. faba* (26.70 pg/2C; 10.4 μm) (**Figure 25**). In all cases, the encapsulation rate was similar to that of barley pollen nuclei (**Figure 22**) and close to predicted encapsulation rates calculated by the Poisson distribution (**Figure 25A**). The number of droplets encapsulating more than one nucleus was much lower than predicted by the Poisson distribution, similar to what was found for barley pollen nuclei (**Figures 22 and 25B**).

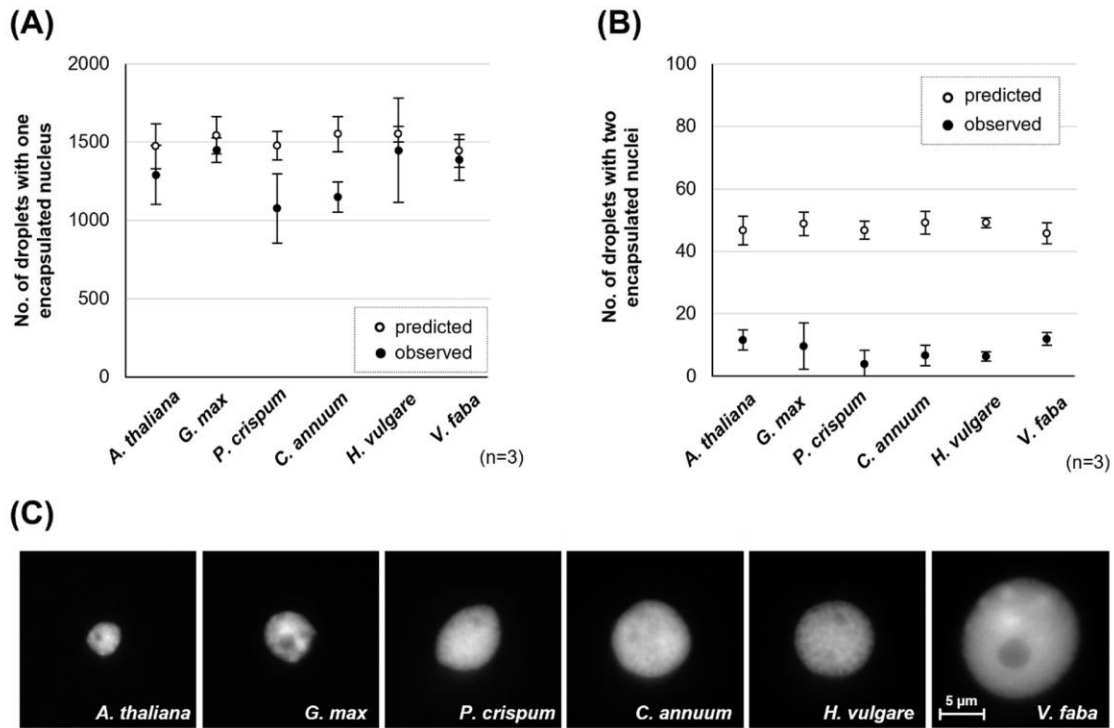


Figure 25. Comparison of nuclei encapsulation frequencies based on manual counts or Poisson-predicted distribution in relation to the number of employed flow-sorted leaf nuclei from plant species differing in DNA content and nuclear size. (A, B) *Arabidopsis thaliana* (0.32 pg/2C; 2.9 μm), *Glycine max* (2.26 pg/2C; 4.2 μm), *Petroselinum crispum* (4.50 pg/2C; 5.3 μm), *Capsicum annuum* (6.32 pg/2C; 6.4 μm), *Hordeum vulgare* (10.92 pg/2C; 6.1 μm) and *Vicia faba* (26.70 pg/2C; 10.4 μm). The given DNA content values correspond to the prime estimates according to Pellicer and Leitch (2020) and nuclear sizes were measured based on 50 2C nuclei of each species; a representative nucleus for each species is shown in (C).

4.2.4.2. Crystal dPCR-based single pollen nucleus genotyping: Measuring meiotic recombination rates within four defined chromosomal intervals

To measure meiotic recombination rates within four selected chromosomal intervals, for every interval, a potential *false-positive* or *noise* rate was established (**Figure 16A**). Using a 1:1 mixture of flow-sorted pollen nuclei (1,500 of each parent), a population of droplets with amplification from both parental genotypes was found (**Figure 16D**, gray rectangle), although at a lower frequency compared to hybrid pollen nuclei samples (**Figure 16E**, red rectangle). Droplets with both, FAM and HEX amplification, encapsulating zero or more than one nucleus (*false-positives*) were counted manually and deducted from all droplets with amplification of both genotypes. After their deduction, an interval-specific *noise* rate (frequency of droplets with one encapsulated nucleus showing amplification of both genotypes among all droplets that show amplification from both markers normalized for marker imbalances) of $1.5 \pm 1.3\%$ for Ic 1 (n=6,188 nuclei with amplification from both markers from 6 plants based on 28 chambers), $2.8 \pm 1.8\%$ for Ic 3 (n=6,450 nuclei with amplification from both markers from 6 plants based on 28 chambers), $0.6 \pm 1.0\%$ for Id 3-1 (n=13,667 nuclei with amplification from both markers

from 9 plants based on 43 chambers) and $0.8 \pm 0.6\%$ for Id 3-2 (n=1,403 nuclei with amplification from both markers from 3 plants based on 6 chambers) remained (Appendix 1). The *noise* droplets could have derived e.g. from allelic markers calling infrequent the opposite genotype and/or the presence of fragmented DNA in these droplets. To identify if the *noise* is derived from fragmented DNA (due to the mechanical disruption of the pollen grains and/or the *TaqI* treatment) accidentally encapsulated together with an intact nucleus of the other genotype, fluorescent calibration beads were added to the pollen nuclei suspension and mixed. After flow-sorting 3,000 fluorescent calibration beads from the mixture into the dPCR mix, droplet generation, including encapsulation, was performed. If the disruption of the pollen grains and/or the *TaqI* treatment were the origin of fragmented DNA and consequently caused the *noise* droplets, the flow-sorted calibration beads from the mixture with pollen nuclei should also result in *noise* droplets. Successful bead encapsulation was found (**Figure 26**). However, no amplification in any of the bead-containing droplets was observed.

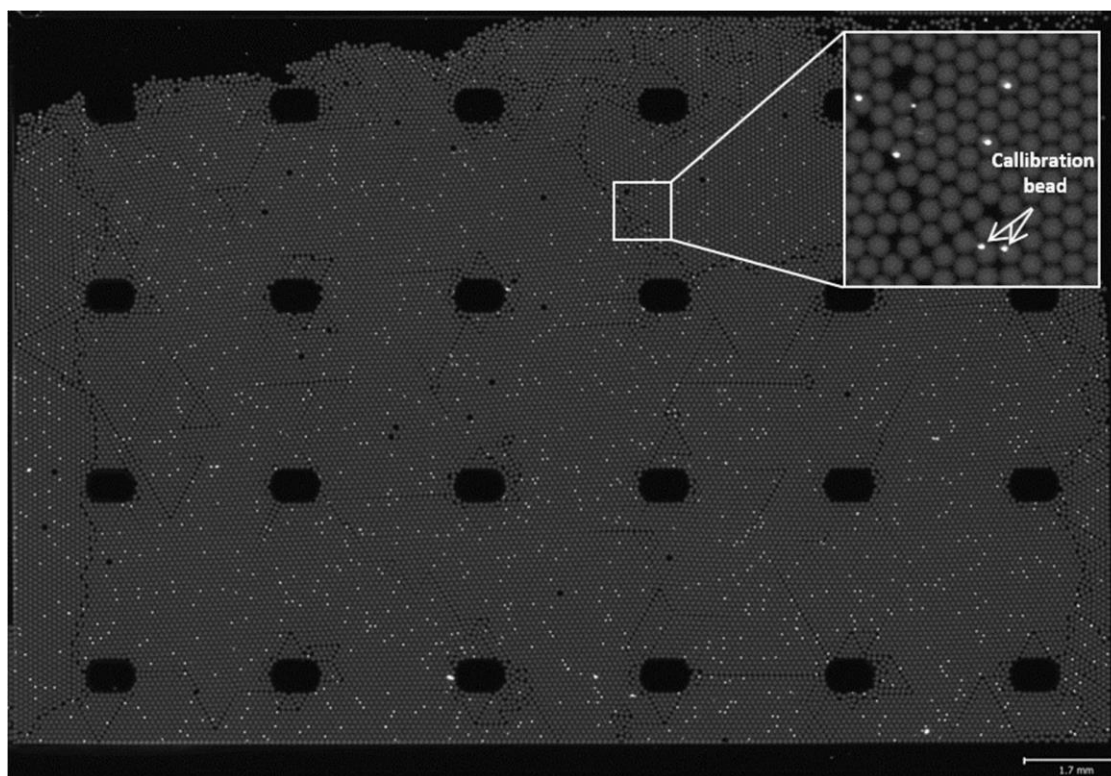


Figure 26. Crystal dPCR-based Id 3-1 genotyping employing 3,000 fluorescent calibration beads sorted from a suspension of pollen nuclei. Despite successful encapsulation of beads, no amplification in any of the bead-containing droplets was found.

A similar result, i.e., no amplification in any bead-containing droplet, was found even when *TaqI* was added to the dPCR mix (**Figure 27**). Hence, possible contamination by fragmented DNA originating from the pollen nuclei isolation/sorting step and/or the *TaqI* treatment leading to *noise* (*false-positive* recombination calls) was excluded. Accordingly, since the *noise* rate per interval was consistent across

samples/experiments, to measure meiotic recombination rates within the four selected chromosomal intervals, the established interval-specific *noise* rate was subtracted in further genotyping assays.

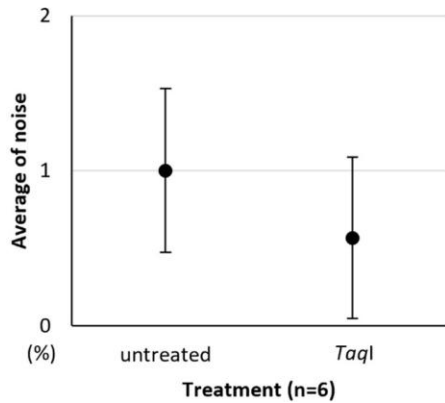


Figure 27. The average frequency of *noise* between untreated and *TaqI* treated pollen nuclei genotyping assays (n=6).

Next, Crystal dPCR-based genotyping of single pollen nuclei from six to nine independent plants heterozygous for the four chromosomal intervals were performed to measure meiotic recombination rates within the four selected intervals. The number of droplets corresponding to successful amplification of both parental alleles, i.e., either non-recombinants (either B+B or M+M) or recombinants (B+M and M+B), was determined according to the manufacturer's instruction as illustrated in **Figure 16D**. Manual counts of droplets that encapsulated zero or more than one nucleus were deducted from the total of normalized (the non-recombinant population with the lower number of positive genotyping calls was considered half of the entire non-recombinants) before calculating the resulting recombination rates per plant/interval as follows:

$$\frac{\text{number of recombinants}}{\text{sum of two non recombinants} + \text{number of recombinants}} \times 100$$

Finally, the established interval-specific *noise* rate was subtracted from the calculated interval-specific meiotic recombination rate. Accordingly, average recombination rates in pollen nuclei across different plants of $7.1 \pm 0.9\%$ for Ic 1 (n=7,687 nuclei with amplification from both markers from 6 plants based on 28 chambers), $6.0 \pm 3.1\%$ for Ic 3 (n=6,827 nuclei with amplification from both markers from 6 plants based on 30 chambers), $12.0 \pm 2.2\%$ for Id 3-1 (20,821 nuclei with amplification from both markers from 9 plants based on 48 chambers) and $10.9 \pm 1.7\%$ for Id 3-2 (n=7,000 nuclei with amplification from both markers from 6 plants based on 27 chambers) were measured (**Figure 28**). For any given plant, 551-4,906 pollen nuclei split into 2-10 chambers were genotyped. While the measured recombination rates for Ic 1 showed the least variation across plants, the variation between plants was higher for Ic 3 and Id 3-1 and intermediate for Id 3-2.

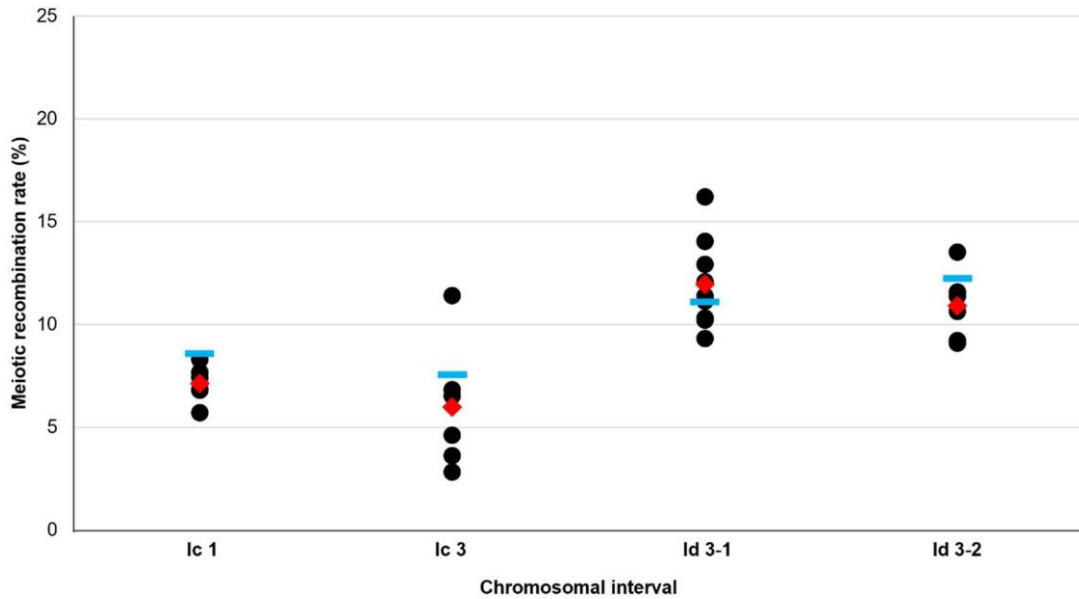


Figure 28. Meiotic recombination rates were measured in pollen nuclei and segregating barley offspring populations. Black dots indicate the meiotic recombination rate for each plant. Red diamonds indicate the average meiotic recombination rate among analyzed plants within each interval (Ic 1, Ic 3 and Id 3-2: 6 plants analyzed, Id 3-1: 9 plants analyzed; data available in Appendix 1). Blue lines indicate the average meiotic recombination rate in segregating offspring populations (Ic 1 and Ic 3: 99 offspring plants analyzed), Id 3-1 (54 offspring plants analyzed) and Id 3-2 (98 offspring plants analyzed).

To evaluate whether measured male meiotic recombination rates in pollen nuclei reflect recombination rates *in planta*, offspring plants in segregating populations for all four intervals were genotyped. In all cases, assuming an equal contribution from both male and female gametes, recombination frequencies were similar to the frequencies measured in pollen nuclei samples: 8.6 % for Ic 1 (n=99 offspring plants), 7.6 % for Ic 3 (n=99 offspring plants), 11.1 % for Id 3-1 (n=54 offspring plants) and 12.2 % for Id 3-2 (n=98 offspring plants) (**Figure 28**).

The percentage of 9.7 % successful Ic 1 genotyping calls using Crystal dPCR was higher than all other explored PCR-based genotyping methods (**Table 7**). Also, the number of employed pollen nuclei was 84,000 from 6 individual plants with 7,687 nuclei being successfully genotyped for Ic 1 and thus by far exceeded the number of nuclei/germinated grains that could be analyzed by all other PCR-based genotyping methods tested (**Tables 6 and 7**). Hence, the established protocol for Crystal dPCR-based single pollen nucleus genotyping to measure meiotic recombination rates in defined chromosomal intervals enables high-throughput measurements compared to PCR-based genotyping methods.

Table 7. Comparison of the average Ic 1 (InDel 1029+InDel 1076) genotyping efficiencies achieved in this study.

PCR-based genotyping approach	Target	Efficiency (%)	Number of analyzed pollen nuclei/grains
Targeted pre-amplification and subsequent PCR-based genotyping of flow-sorted single pollen nuclei	InDel 1029+InDel 1076	7.4	135
Crystal digital PCR-based genotyping of flow-sorted pollen nuclei	InDel 1029+InDel 1076	9.7	84,000

4.2.4.3. Reliable meiotic recombination rate measurements in pollen nuclei samples

Offspring plants recombinant for Ic 1 were selected to evaluate the reliability of the single pollen nucleus genotyping set-up. Pollen nuclei from these plants were mixed in various defined ratios (0, 10, 20 and 100 % recombinant pollen) with a 1:1 ratio mixture of both parental pollen nuclei (cv. Barke and cv. Morex; 100, 90, 80 and 0 %) (**Figure 29**). Measured recombination rates in employed samples with pre-defined numbers of recombinant versus non-recombinant pollen nuclei did not deviate from the expected recombination rates confirming the robustness of our approach. Predefined recombination rates were also successfully measured for Ic 3 and Id 3-1 (**Figure 29**).

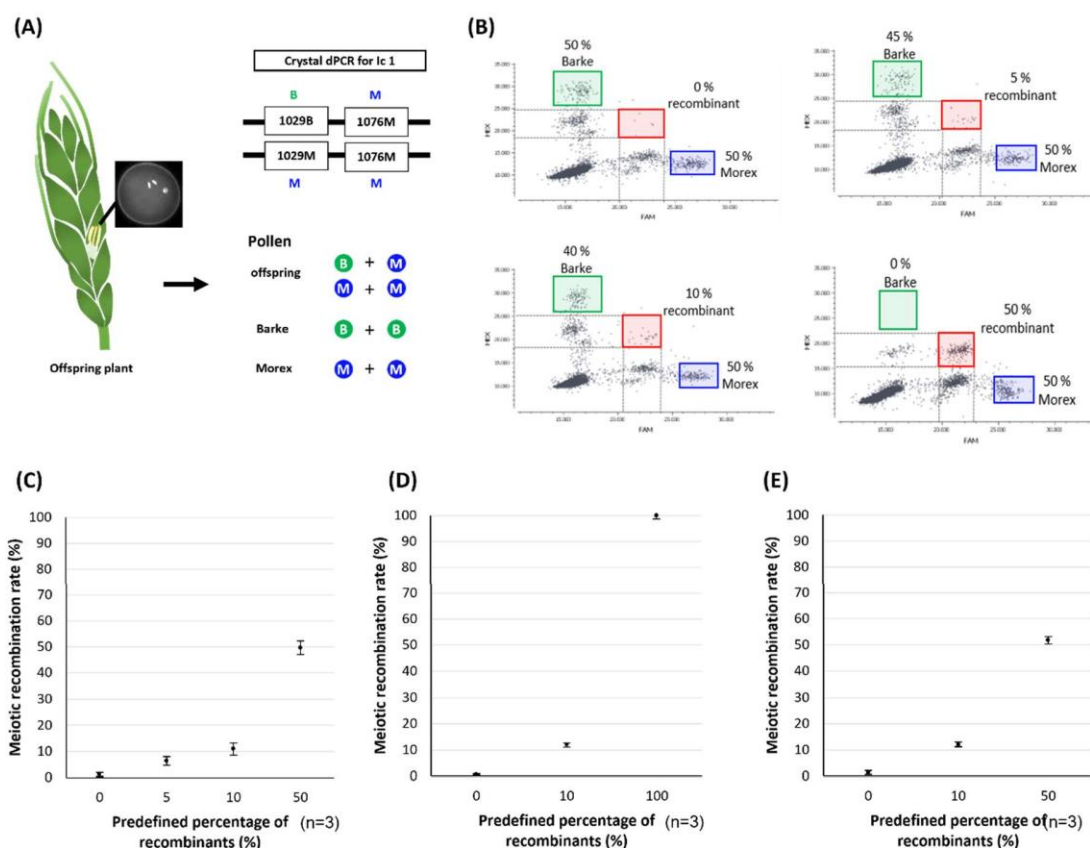


Figure 29. Reliable meiotic recombination rate measurements in pollen nuclei samples. (A) Pollen nuclei of offspring plant recombinant for Ic 1 mixed with parental pollen nuclei (1:1 Barke and Morex) in defined ratios (0, 10, 20 or 100% offspring

pollen) as predefined recombination suspensions (0, 5, 10 or 50% of recombinants). Crystal dPCR-based pollen nucleus genotyping of predefined recombination suspensions (0, 5, 10 or 50% of recombinants): **(B)** the two non-recombinant parental droplet populations with successful genotyping calls by the two HEX-labeled (green box) or FAM-labeled allelic probes (blue box) and the recombinant droplet population positive for both HEX and FAM (red box). **(C)** the average measured meiotic recombination frequency for Ic 1 in predefined recombination suspensions (n=3). The average measured meiotic recombination frequency for **(D)** Id 3-1Id for **(E)** Ic 3 in predefined recombination suspensions (n=3).

4.2.5. Measuring meiotic recombination rates for plants grown under different environmental conditions, in different spikes of single plants as well as chemical-treated and untreated plants

To utilize the established protocols, (4.3.1.1.) for plants grown under different conditions (greenhouse or phytochamber), (4.3.1.2.) in different tillers from the same plant and (4.3.1.3.) in plants treated with selected chemical compounds and untreated plants meiotic recombination rates were studied.

4.2.5.1. Meiotic recombination rates in plants grown under different environmental conditions

To identify whether differences in Ic 1 and/or Id 3-1 recombination rates exist between plants grown in the greenhouse or phytochamber, recombination rates in plants grown in either environment were assessed using Crystal dPCR-based single pollen nucleus genotyping (**Figure 30**). The average Ic 1 recombination rate of $5.9 \pm 1.8\%$ (5,219 nuclei with amplification from both markers from 4 plants; 876-1,897 nuclei per plant) in plants grown in the phytochamber was lower than that of plants grown in the greenhouse ($7.1 \pm 0.9\%$; 7,687 nuclei with amplification from both markers from 6 plants; 768-1,562 nuclei per plant), while for Id 3-1 the recombination rate measured was higher in plants grown in the phytochamber ($15.1 \pm 1.4\%$; 4,746 nuclei with amplification from both markers from 3 plants; 1,343-1,874 nuclei per plant) when compared to plants grown in the greenhouse ($12.0 \pm 2.2\%$; 20,821 nuclei with amplification from both markers from 9 plants; 647-4,906 nuclei per plant). Despite lower numbers of plants/nuclei analyzed from the phytochamber condition compared with the greenhouse condition, Ic 1 meiotic recombination rates under phytochamber condition showed higher variation compared with greenhouse condition, while for Id 3-1 recombination rates, the opposite was found.

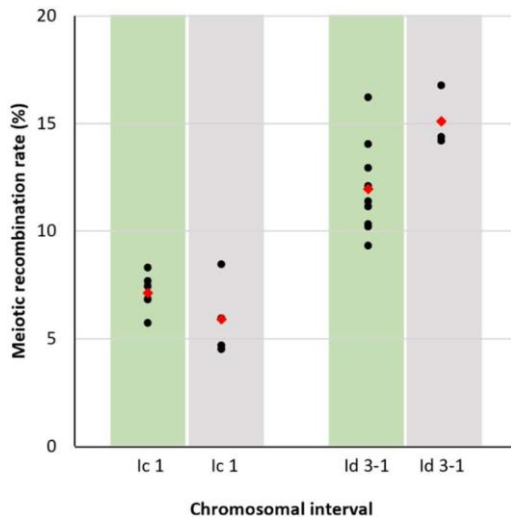


Figure 30. Average lc 1 and ld 3-1 meiotic recombination rates measured in plants grown in the greenhouse or in the phytochamber. Black dots indicate the meiotic recombination rate for each plant. Red diamonds indicate the average meiotic recombination rate among analyzed plants within each interval (lc 1 and ld 3-1). Green blocks indicate measurements from plants grown in the greenhouse and grey blocks indicate measurements from plants grown in the phytochamber.

4.2.5.2. Measuring meiotic recombination rates in different spikes of single plants

To identify whether variation in meiotic recombination rate within individual plants is found, lc 1, lc 3, ld 3-1 and ld 3-2 recombination rates were measured from primary (1st), secondary (2nd) and tertiary (3rd) tillers from five plants grown in the phytochamber (**Figure 31**). For lc 1, meiotic recombination rates were $7.1 \pm 2.0\%$ (750-1,507 nuclei per plant genotyped) in the 1st tiller, $11.1 \pm 4.0\%$ (150-1,430 nuclei per plant genotyped) in the 2nd tiller and $10.1 \pm 4.0\%$ (98-1,611 nuclei per plant genotyped) in the 3rd tiller. For lc 3, $7.2 \pm 2.3\%$ (661-1,360 nuclei per plant genotyped) in the 1st tiller, $8.9 \pm 4.2\%$ (245-1,301 nuclei per plant genotyped) in the 2nd tiller and $10.4 \pm 1.7\%$ (399-1,374 nuclei per plant genotyped) in the 3rd tiller was measured. For ld 3-1, $14.5 \pm 3.7\%$ (390-1,694 nuclei per plant genotyped) in the 1st tiller, $15.0 \pm 1.7\%$ (70-2,243 nuclei per plant genotyped) in the 2nd tiller and $15.1 \pm 4.0\%$ (118-2,625 nuclei per plant genotyped) in the 3rd tiller was measured. Finally, for ld 3-2, $12.0 \pm 1.7\%$ (207-1,695 nuclei per plant genotyped) in the 1st tiller, $16.3 \pm 5.3\%$ (111-1,088 nuclei per plant genotyped) in the 2nd tiller and $14.4 \pm 1.6\%$ (135-1,270 nuclei per plant genotyped) in the 3rd tiller was measured. Considering all measurements within the 1st tiller, in particular for lc 1, lc 3 and ld 3-2, consistently the lowest average recombination rates were found compared to that of the 2nd and 3rd tillers. However, for ld 3-1 difference in average recombination rates measured in 1st tillers among plants was high and within the 2nd and 3rd tiller either higher (in case of a rather low recombination within the 1st tiller) or lower (in case of plants with a rather high recombination rate within the 1st tiller) recombination rates when compared to the 1st tillers were found. In conclusion, substantial variation in recombination rates within and between 1st, 2nd and 3rd tillers was found across tested intervals among individual plants.

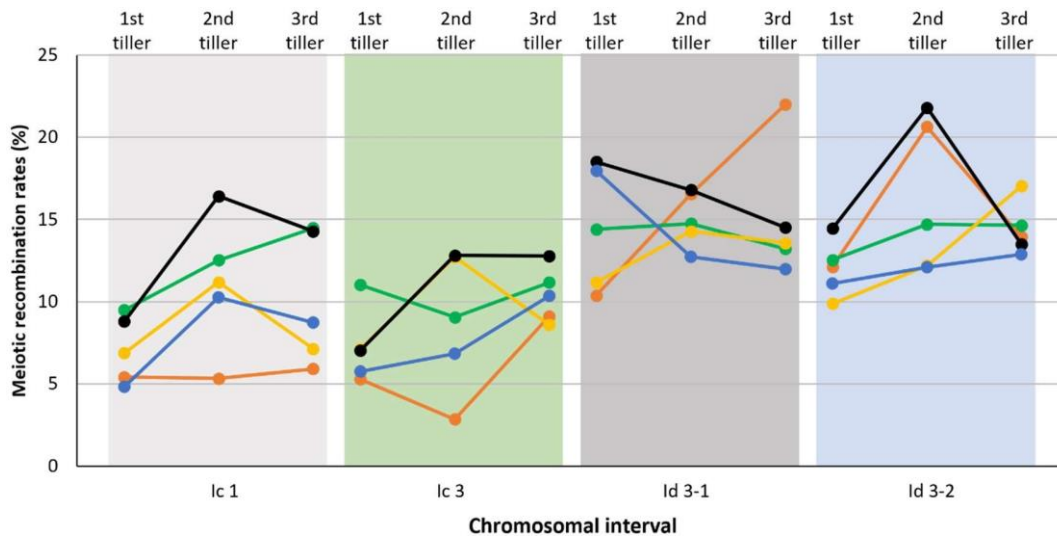


Figure 31. Average meiotic recombination rates within 1st, 2nd and 3rd tillers from five individual plants in four chromosomal intervals. Black line: plant 1. Green line: plant 2. Blue line: plant 3. Yellow line: plant 4. Orange line: plant 5.

4.2.5.3. Measuring meiotic recombination rates simultaneously within two chromosomal intervals after *in planta* chemical compound injections

To further improve the throughput of Crystal digital PCR-based genotyping of single pollen nuclei, also enabling the simultaneous measurement of recombination rates within two chromosomal intervals in a single pollen nucleus, two chromosomal intervals were multiplexed at the same time using four different colors (fluorescence-labeled allelic probes) and employing increasing numbers of pollen nuclei as templates in a given chamber (*Figure 32*).

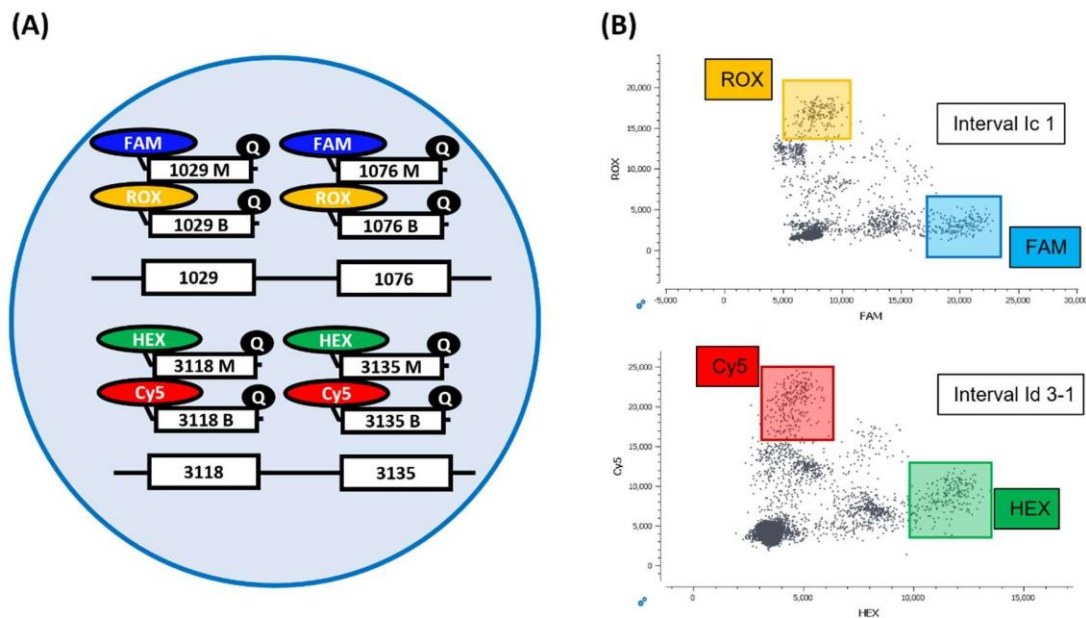


Figure 32. Selected chromosomal intervals for multiplexing of single pollen nucleus genotyping assays. (A) Crystal digital PCR-based pollen nucleus genotyping assay exemplified for lc 1 and ld 3-1: possible combinations of four fluorescence probes

enable to distinguish between recombinant and non-recombinant pollen nuclei within two chromosomal intervals in parallel. **(B)** Crystal digital PCR-based pollen nucleus lc 1 and ld 3-1 genotyping data from a scanned chamber displayed as dot plot in Crystal Miner software of pollen nuclei from the hybrid genotypes.

First, higher numbers of pollen nuclei than 3,000, i.e., 4,000, 5,000 and 6,000 were flow-sorted to improve the genotyping throughput per chamber. During flow-sorting a smaller nozzle size (70 μm) and lower concentrated 0.5X PBS buffer were tested and compared with the original bigger nozzle (86 μm) and the higher concentrated 1X PBS buffer (**Figure 33**). 0.5X PBS buffer was tested to minimize the negative impact of the increasing amount of PBS as increased numbers of nuclei were flow-sorted. (**Figure 24**). Therefore, employing 0.5X PBS as sheath fluid was expected to limit the inhibitory PBS impact even when a higher volume of PBS buffer together with pollen nuclei were sorted and used for Crystal dPCR-based genotyping. Flow-sorting 3,000 nuclei using an 86 μm nozzle resulted in roughly 5 μL of volume, while a 70 μm nozzle resulted only in roughly 2.5 μL of volume, suggesting that potentially up to the double number of nuclei (i.e., up to 6,000) could be implemented in genotyping assays. Surprisingly, in the case of 3,000 nuclei, the average FAM fluorescence value was the highest when 1X PBS buffer+86 μm nozzle was used compared with tested variants which were expected to be more efficient due to the lower amount of PBS in the Crystal dPCR mix (**Figure 33**). While 1X PBS buffer+86 μm nozzle variant and 0.5X PBS buffer+70 μm nozzle variant showed decreasing FAM fluorescence values as the number of flow-sorted nuclei increased especially between 4,000 and 5,000 nuclei, FAM fluorescence values from 0.5X PBS buffer+86 μm nozzle variant and 1X PBS buffer+70 μm nozzle variant remained consistent. In all variants, 6,000 nuclei showed the lowest FAM fluorescence value. However, sorting using the 70 μm nozzle was less consistent and frequently required a new alignment of the sorting set-up regardless of the PBS buffer concentration. Thus, considering acquired data and sorting conditions, 0.5X PBS buffer+86 μm nozzle was used to sort up to 5,000 pollen nuclei per chamber (depending on the number of nuclei available from a given spike) to measure meiotic recombination rates from plants injected with chemical compounds in the phytochamber.

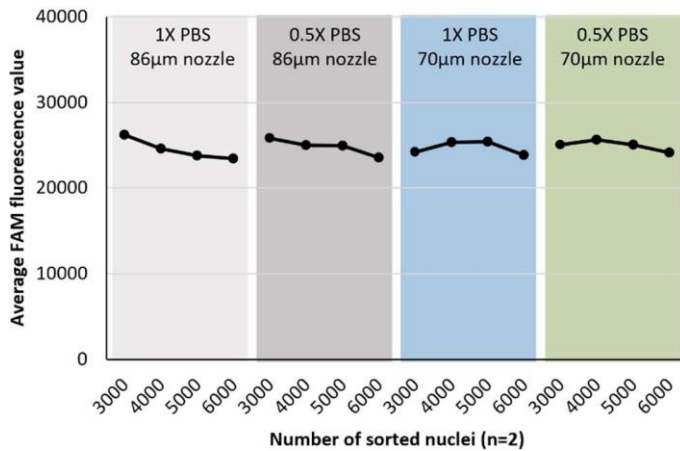


Figure 33. Impact of different concentrations of PBS sheath fluid and the nozzle size used during flow-sorting on the average FAM fluorescence values for Ic 1 employing different numbers of nuclei. Average FAM fluorescence value for Ic 1 with four tested variants (1X/0.5X PBS buffer and 86/70 µm nozzle) with different numbers of nuclei.

Next, Ic 1 and Id 3-1 meiotic recombination rates in chemical compound-injected hybrid plants were measured using multiplex Crystal dPCR-based single pollen nucleus genotyping. Based on the pre-screening test on barley seedlings (see 4.1.3.), Zebularine, TSA and BIX-01294 were selected and injected into hybrid plants grown in the phytochamber at concentrations that showed the lowest effect on mitotic tissue, 0.1 µM, 0.001 µM and 5 µM, respectively. However, plants injected with TSA and BIX-01294 did not survive when these concentrations were applied. Therefore, the applied concentration of TSA and BIX-01294 was drastically reduced to 0.5 nM and 0.5 µM, respectively (**Figure 34**). All three injected chemical compounds included 0.05% of Silwet L-77. Meiotic recombination rates measured in *uninjected* plants in the phytochamber were $5.9 \pm 1.8\%$ for Ic 1 (n=876-1,897 nuclei per plant genotyped from 4 plants) and $15.1 \pm 1.4\%$ for Id 3-1 (n=1,343-1,874 nuclei per plant genotyped from 3 plants) (**Appendix 2**). Plants injected with distilled water showed $9.1 \pm 0.6\%$ (n=851-1,056 nuclei per plant genotyped from 2 plants) for Ic 1 and $13.6 \pm 1.7\%$ (n=1,052-1,268 nuclei per plant genotyped from 2 plants) for Id 3-1. 0.05% Silwet L-77 injected plants showed $7.0 \pm 2.7\%$ (n=358-3,547 nuclei per plant genotyped from 2 plants) for Ic 1 and 11.6% (n=4,622 nuclei per plant genotyped from 1 plant) for Id 3-1. Unfortunately, measurements from 1% DMSO injected plants failed due to poor pollen quality. Recombination rate from 0.05% Silwet L-77+1% DMSO showed 6.9% (n=7,635 nuclei per plant genotyped from 1 plant) for Ic 1 while data for Id 3-1 is not available. Three plants among 0.5 µM Zebularine injected plants showed $14.4 \pm 1.6\%$ (n=727-2,827 nuclei per plant genotyped from 3 plants) and other four plants showed $8.2 \pm 1.0\%$ (n=641-1,673 nuclei per plant genotyped from 4 plants) for Ic 1. Recombination rate for Id 3-1 from 0.5 µM Zebularine injected plants showed $11.9 \pm 1.3\%$ (n=1,277-2,054 nuclei per plant genotyped from 3 plants). Recombination rate in 0.5 nM Trichostatin A injected plants was $6.8 \pm 1.5\%$ (n=380-3,248 nuclei per plant genotyped from 4 plants) for Ic 1 and $12.6 \pm 1.4\%$ (n=490-2,763 nuclei per plant genotyped from 4 plants) for Id 3-1. BIX-10294 (0.5 µM) injected plants showed $7.9 \pm 1.5\%$ (n=677-2,879 nuclei per plant genotyped from 3 plants) for Ic 1 and 14.1% (n=2,783

nuclei per plant genotyped from 1 plant) for Id 3-1. Except for the increased meiotic recombination rate in Ic 1 from distilled water injected plants compared to *uninjected* plants, other control groups, e.g. 0.05% Silwet L-77 injection and 0.05% Silwet L-77+1% DMSO injection showed a similar recombination rate range in Ic 1 compared to *uninjected* plants (**Figure 34A**). On the other hand, meiotic recombination rates in Id 3-1 from control groups were lower than that of *uninjected* plants (**Figure 34B**). In total, simultaneous measurements of meiotic recombination rates within Ic 1 and Id 3-1 were performed in 14 plants, except when measurements failed in Id 3-1 (9 plants) and three plants out of seven Zebularine-injected plants showed twofold increase in recombination rates than *uninjected* plants.

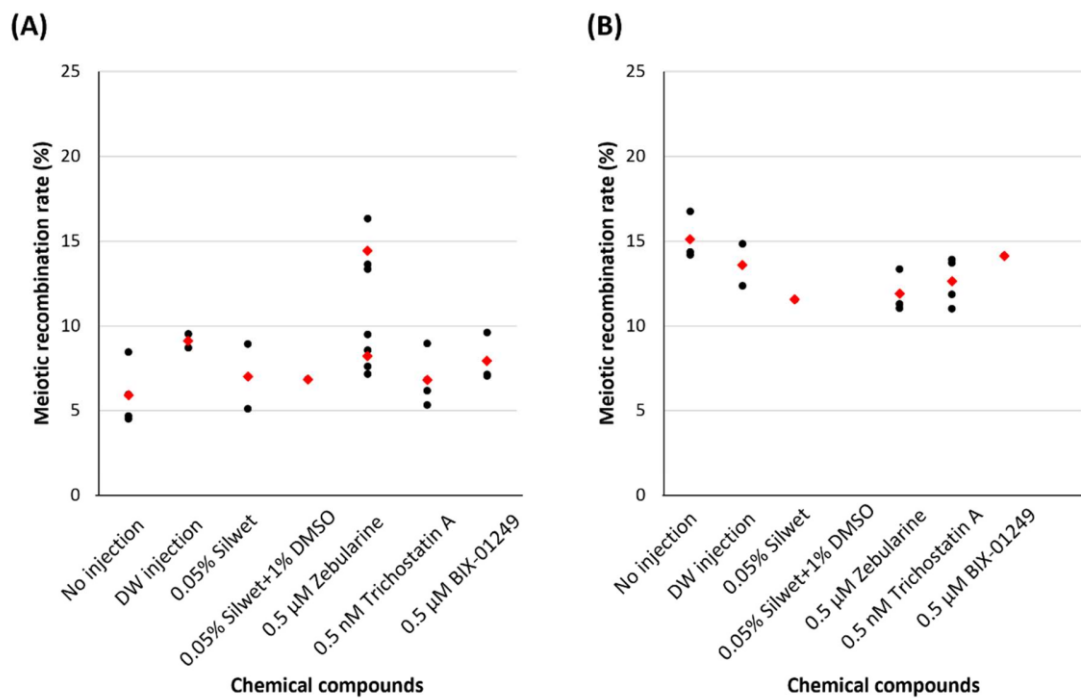


Figure 34. Meiotic recombination rates within Ic 1 and Id 3-1 from uninjected and chemical injected plants. (A) Ic 1 and (B) Id 3-1. Black dots indicate the meiotic recombination rate for each plant. Red diamonds indicate the average meiotic recombination rate among analyzed plants. Data available in Appendix 2.

5. Discussion

5.1. When and how to deliver chemical compounds *in planta*

5.1.1. Phenotype analysis of barley hybrids

In cereals such as barley, the developmental stage when cells within spikelets undergo meiosis occurs when the spike is wrapped in layers of leaf sheaths and thus is not visible without destructive methods. Hence, it is challenging to identify a given plant/tiller in which spikelets contain cells undergoing meiosis. Typically, tillers are cut for destructive analysis and accordingly, no offspring can be acquired from these tillers. Even once a spike in a given tiller is identified to contain cells undergoing meiosis, independent tillers from the same plant cannot be used simultaneously for meiotic studies due to different development timing of individual tillers, i.e., tillers undergoing meiosis at different time points in the life cycle of a given plant.

To tackle this issue, developmental scales for cereals were established (Zadoks or Waddington scale). However, a correlation between plant developmental characteristics and the meiotic stage was not established for diverse genotypes (Zadoks *et al.*, 1974; Waddington *et al.*, 1983; Tottman, 1987). Non-destructive methods to correlate spike development and plant developmental features are either restricted to developmental stages after meiosis or require sophisticated equipment (Gómez and Wilson, 2012; Tracy *et al.*, 2017). Arrieta *et al.* established a modular tray system enabling to grow a high number of barley plants producing single tillers more or less synchronously in a controlled environment and establishing a correlation between plant development and meiotic progression (Arrieta *et al.*, 2020). While this system could possibly also be applied to other barley genotypes or even other cereals, it needs to be thoroughly established for other barley genotypes grown under different conditions. Moreover, it only enables acquiring single tillers per plant, and thus the gametes or offspring are limited per individual, representing a bottleneck in studies aiming e.g. to compare meiotic recombination rates within different tillers from the same plant or in plants treated with selected chemical compounds compared with untreated plants.

In this study, initially, various developmental parameters of primary tillers from barley plants grown in a greenhouse or in a phytochamber were dissected and cytologically studied for the meiotic stages within anthers to figure out when to deliver selected chemical compounds *in planta* to assure delivery of the compound during or prior cells undergo meiosis. While external phenotypic plant features e.g. plant height or plant age, do enable a rough estimate of the underlying spike size and thus whether meiotic cells are present in plants grown under greenhouse conditions or in a phytochamber with more controlled conditions, the phenotyping results revealed that the plant height or plant age was not a reliable estimate for spike development. The most reliable criteria identified were the distance

between the leaf ear and the two bottom nodes (2-4.5 cm) and the distance between the two bottom nodes (less than 1 cm) showing a rather good fit with the spike development and meiotic cells likely undergoing early meiosis (**Figure 7**). Additional features such as the number of leaves could be considered to increase possibly further the fit, however likely for any given growth environment and likely also for every plant material, a set-up needs to be tested thoroughly.

Methods to deliver compounds into meiocytes are available such as dipping in or spraying the stem/reproductive tissue with the compound solution or incubating dissected inflorescences or cut stems/tillers in solution (Griffing and Langridge, 1963; Perrella *et al.*, 2010). However, in this study, plant survival after compound delivery was required to measure meiotic recombination rates in pollen nuclei and to acquire offspring plants as a prerequisite for a potential application in breeding. Selected compounds were delivered through injection using a needle and syringe (Sinha and Helgason, 1969; Higgins *et al.*, 2012; Colas *et al.*, 2016; Osman *et al.*, 2021). Considering potential costs of a given chemical compound, an injection volume of 0.5 mL per injection was determined to be sufficient. Larger injection volumes caused loss of the delivered compound by squirting outside from the tip of the tiller, and thus were not required. In the future, even lower injection volumes could be explored. However, in the current study, an injection volume of 0.5 mL was considered to maximize the potential impact. To assess for how long the injected volume persisted within the tiller, tillers were opened 2-12 hours after single or multiple consecutive injections. Based on acquired data, two initial injections (a second injection 1 hour after the first injection) improved soaking of the young spike with the injected compound solution compared to a single injection and were accordingly used for the experiments. Whether the uptake could be further improved by increased numbers of injections and/or reducing the duration between injections should be explored in the future. The uptake of injected compounds into the spike was monitored initially by adding a drop of food coloring, showing that the compound was soaked up from the outside of the inflorescences and that the addition of a surfactant (possibly by reducing surface tension) could improve its uptake.

A successful *in planta* delivery of injected compounds based on EdU incorporation into meiotic cells confirmed that the established injection procedure is suitable to deliver a compound into meiotic cells (**Figure 8**). Given the uptake improvement upon inclusion of a surfactant in the injected solution as well as after multiple injections, the impact of the number of injections with/without further detergents/surfactants on plant survival rate and fertility was assessed based on 1-day, 3-days and 5-days of consecutive injections within 24 hours intervals (**Figure 9**). Based on obtained data, despite impacting plant survival rate and fertility, an injection protocol for 3-days with 24 hours intervals together with the surfactant Silwet L-77 was chosen based on improved uptake of the injected fluid. In the future, different concentrations and additional surfactants/detergents could be explored for *in*

planta injection that are less harmful while still improving the uptake rate when compared to the established and employed set-up.

5.1.2. Selected chemical compounds and pre-screening of their impact

Chemical compounds previously described to impact DNA methylation and histone acetylation/methylation were selected (**Table 5**). These modifications are implicated in shaping meiotic recombination in plants and thus were selected as potential targets to possibly alter the frequency and/or distribution of meiotic recombination events in barley (Melamed-Bessudo and Levy, 2012; Mirouze *et al.*, 2012; Choi *et al.*, 2013; Yelina *et al.*, 2015a; 2015b; Kianian *et al.*, 2018; Underwood *et al.*, 2018). Initially, it was essential to identify whether in barley any *in planta* effect after application of a selected compound was found and at which concentration. To do so, a pre-screening assay based on seedlings for an *in planta* application of these compounds was established. To test the impact of chemical compounds was tested on plant development (root length) and mitotic cell cycles values (**Figures 10, 11 and 12**). While seeds/grains can be soaked/germinated in a compound solution or uptake of the compound solution can occur through the root system of germinated seedlings (Cho *et al.*, 2012; Ma *et al.*, 2016), in the established setup barley grain-soaking was hazardous and thus seedlings were exposed to the compound solutions (uptake via the root system).

Zebularine is a DNA methyltransferase inhibitor with increased stability and lower toxicity compared with other DNA methyltransferase inhibitors (Zhou *et al.*, 2002; Ben-Kasus *et al.*, 2005). Similar to Arabidopsis and wheat (Baubec *et al.*, 2009; Cho *et al.*, 2012), barley root development was inhibited by all tested Zebularine concentrations (100, 10, 1 and 0.1 μM) (**Figure 12**). While mitotic barley chromosomes after Zebularine treatment were not cytologically analyzed, the negative correlation between the relative percentage of cells in S phase and the Zebularine concentration may reflect cell cycle arrest caused by chromosome breakage or other aberrations (**Figure 12**) (You and Park, 2012).

The DNA methyltransferase inhibitor 5-Azacytidine induces chromatin decondensation, microspore reprogramming and embryogenesis induction in rapeseed and barley by reducing DNA methylation levels (Solís *et al.*, 2015). Genome-wide demethylation caused by 5-Azacytidine also caused growth retardation and changes in flowering time or flower sexuality (Fieldes *et al.*, 2005; Brown *et al.*, 2008; Marfil *et al.*, 2012). Similar to reports on root development in Arabidopsis and *V. faba* (Fučík *et al.*, 1965; Zhu *et al.*, 2020), the barley root growth was inhibited in a dosage-dependent manner (**Figure 12**). Possibly, similar like observed in *Aegilops sharonensis* (De Las Heras *et al.*, 2001), 5-Azacytidine in barley may cause chromosome breakage resulting from the observed mitotic cell cycle arrest (**Figure 12**).

Trichostatin A (TSA) is used as a histone deacetylation inhibitor in mammals and plants (Yoshida *et al.*, 1990; Perrella *et al.*, 2010). Activities of HDACs (see 1.3.2.) are associated with several developmental processes in plants such as root formation and development or flowering time (Xu *et al.*, 2005; Fukaki *et al.*, 2006; Wu *et al.*, 2000). In this study, inhibitory effect on barley root growth induced by Trichostatin A was not as obvious (**Figure 12**). In contrast an effect on rice root growth was induced by the HDACs inhibitor sodium butyrate (Chung *et al.*, 2009). Considering impact in rice, sodium butyrate can be tested in barley to screen its HDACs inhibitory effect in the future. On the other hand, TSA had a strong impact on mitotic cell cycle values (**Figure 12**), with a decreasing G2/G1 cell ratio and increasing S cell percentage as the applied TSA concentration decreased. These results are similar to human cells where TSA induced G2 cell cycle arrest and a delayed transition from G2 to M phase resulting in chromosome missegregation and multi-nucleation and thus causing mitotic cell cycle interruption (Noh *et al.*, 2009).

In Brassica and barley, the H3K9 histone methyltransferase inhibitor BIX-01294 promotes microspore totipotency and embryogenesis by decondensing chromatin (Kubicek *et al.*, 2007; Guo *et al.*, 2016; Berenguer *et al.*, 2017). Considering a correlation between histone methylation (H3K4) and root development (Yao *et al.*, 2013), both BIX-01294 and UNC0642 (another H3 methylation inhibitor) were expected to inhibit root growth in a dosage-dependent manner. However, the inhibitory effect of BIX-01294 on root growth was not as clear as that of UNC0642 (**Figure 12**). BIX-01294 was reported to interrupt the cell cycle acting as a H3 methylation inhibitor in human cells (Yang *et al.*, 2012). However, at concentrations applied here, this impact was not found in barley root meristem cells (**Figure 12**). UNC0642 did not show an impact on the cell cycle as well, possibly due to different sensitivity to compounds based on different species.

Silwet L-77 (used as surfactant to improve compound uptake) had a negative impact on root development and mitotic cell cycle values in a dosage-dependent manner (**Figure 12**). However, given the improved uptake in meiotic cells, Silwet L-77 was still considered for injection experiments.

In conclusion, the application of germinated barley seedlings enabled a pre-screening for a potential impact of chemical compounds on plant development and mitotic cell cycle values. It allows to pre-select chemical compounds and their concentrations for further analysis, including their application during meiosis through *in planta* injection. Moreover, the set-up offers the possibility to expand the pre-screening to additional compounds, likely even in other crops.

5.2. Comparison of different PCR-based single pollen nucleus genotyping methods

5.2.1. Gel-based genotyping of a single pollen nuclei with or without pre-amplification

Methods to measure meiotic recombination rates in haploid gametes are available, yet the number of analyzed samples is typically relatively low (Higgins *et al.*, 2012; Dreissig *et al.*, 2015). However, FTLs enable meiotic recombination rate measurements in defined chromosomal intervals in tetrads in high numbers both in an inbred and hybrid background. However, their use is restricted to Arabidopsis with FTLs being not available in crops including barley (Melamed-Bessudo *et al.*, 2005; Berchowitz and Copenhaver, 2008; Wu *et al.*, 2015). In addition, PCR-based methods exist to detect CO molecules within selected short (bp-kbp) chromosomal intervals from haploid gametes, e.g. using human sperm (Jeffreys *et al.*, 1998) or Arabidopsis pollen nuclei for 'pollen typing' (Drouaud and Mézard, 2011; Yelina *et al.*, 2012; Drouaud *et al.*, 2013; Yelina *et al.*, 2015b). Pollen typing omits the need for large progeny populations. However, it is limited to a few selected short chromosomal regions. In barley and citrus FACS-mediated, flow-sorted pollen nuclei were used for KASP marker genotyping. However, in both cases, a rather expensive-WGA step of every single pollen nucleus is required for efficient genotyping and thus strongly limits the number of analyzed samples (Dreissig *et al.*, 2015; Garavello *et al.*, 2020). To overcome some of these limitations, several PCR-based barley pollen (nucleus) genotyping methods without WGA were explored and compared in this study with regards to their genotyping efficiency and throughput using as a benchmark the chromosomal interval Ic 1.

Using flow-sorted single pollen nuclei without WGA as templates for Ic 1 genotyping and subsequent gel-based analysis resulted in 5.5 % and 7.4 % genotyping efficiency when used directly or after a pre-amplification PCR, respectively (**Table 6**). Considering the frequency of successfully analyzed pollen nuclei, KASP-based multi locus genotyping of single barley pollen nuclei after WGA (26.0%, 50 out of 192 flow-sorted pollen nuclei (Dreissig *et al.*, 2015)) outperforms both the direct PCR or the pre-amplification genotyping approach of flow-sorted barley pollen nuclei. However, considering the rather costly and time-consuming procedure of WGA limiting the number of samples that can be analyzed, direct PCR or pre-amplification PCR-based genotyping of flow-sorted pollen nuclei without WGA represents a valid alternative and it could also easily be adopted in diverse crops. Despite a slight tendency for higher Ic 1 genotyping rates using pre-amplified PCR products, the rather limited number of analyzed samples as well as Ic 1 being the only tested interval hinders a solid conclusion as to whether a pre-amplification PCR outperforms direct PCR. Altogether, employing single pollen nuclei without WGA for genotyping is feasible, however, considering the genotyping success rate and the number of samples that can be analyzed, its application as a high throughput procedure is limited.

5.2.2. Gel-based genotyping of single pollen grains with or without prior germination

To assess whether genotyping rates could be improved by increasing the number of available templates from one to three, single pollen grains (two sperm nuclei and one vegetative nucleus) were either used directly or after germination in pollen germination media for Ic 1 genotyping (**Table 6**). Single pollen grain genotyping was used in several crop species (Matsuki *et al.*, 2007; Mase *et al.*, 2014; Honsho *et al.*, 2016); however, a WGA step was commonly used and it was technically challenging to isolate single pollen grains and therefore limiting the number of samples analyzed. Pollen grain genotyping in this study was performed similarly to the method developed by Honsho *et al.*, including pollen grain transfer using a human hair (Honsho *et al.*, 2016). Only considering the number of successful genotyping reactions using a pollen grain, in citrus a genotyping rate of 14.6% after pollen germination for 6 hours was achieved, while in barley a genotyping rate of only 3.3% within Ic 1 was achieved (**Table 6**). This discrepancy could be derived from the different pollen donor species, genomic context, germination media or germination conditions and could be explored in the future. Overall, the rather low number of analyzed samples as well as Ic 1 being the only tested interval, hinders a solid comparison of both approaches. In any case, both citrus and barley pollen grains showed 0% genotyping efficiency without any germination. This indicates that pollen germination is required for successful genotyping (**Table 6**) (Honsho *et al.*, 2016). In addition, Honsho *et al.* showed that single pollen grain genotyping efficiency can be improved significantly when DNA was extracted from a germinated pollen grain (47.9% of successful amplification), which can also be tested in barley in future studies. A major drawback of PCR-based pollen grain genotyping was the technically challenging and time-consuming manual transfer of single pollen grains into individual PCR reaction wells. In the future, a large particle flow-sorter could enable automatic sorting of single pollen grains in high numbers and/or diverse pollen germination media not inhibiting the actual genotyping PCR could be explored. In any case, pollen nuclei with/without a prior pre-amplification PCR or germinated pollen grains can be employed for PCR-based genotyping. Unfortunately, these approaches are rather laborious and time-consuming given the limited number of samples that can be analyzed and are dependent on the presence of rather (large) InDels for gel-based amplicon length distinction and thus were not further explored in more detail.

5.2.3. Crystal Digital PCR-based genotyping of single pollen nuclei

In comparison with the rather low number of samples that could be gel-based analyzed, the established Crystal dPCR-based set-up enables to analyze by far higher numbers of pollen nuclei at once. It thus increases the throughput largely while decreasing the workload and time required. In addition, not only the number of Ic 1 genotyping calls but also the efficiency of Crystal dPCR-based Ic 1 genotyping was slightly higher (9.7%, **Table 7**) than direct or pre-amplification PCR genotyping of a

single pollen nuclei. However, the addition of a restriction enzyme to digest the pollen nucleus template (see 3.12.3.) might have additionally contributed to the higher efficiency of the Crystal dPCR-based genotyping assay compared with gel-based approaches where no enzyme was used. Also, the genomic context (genetic location of markers) and the rather low number of analyzed samples from gel-based genotyping methods may explain a higher or lower genotyping efficiency, and thus, it is difficult to draw a solid conclusion whether the improvement in efficiency was only based on the Crystal dPCR approach.

5.3. Establishment and optimization of Crystal dPCR-based genotyping of single pollen nuclei

Initially, the set-up (Naica®, Stilla Technologies®) was chosen based on the droplet size being large enough to encapsulate a single pollen nucleus of barley (roughly 5 µm) and the possibility to detect up to three or even six colors simultaneously (FAM, HEX and Cy5 for Prism3 and FAM, Yakima Yellow, Cy3, ROX, Cy5 and Atto700 for Prism6). In addition to Ic 1, also the intervals Ic 3, Id 3-1 and Id 3-2 were selected based on the available polymorphic markers (Zhou *et al.*, 2015) and genotype-specific fluorescent TaqMan probes were designed. Although KASP markers can result in slightly higher genotyping efficiencies at a lower cost per reaction than TaqMan probes (Broccanello *et al.*, 2018; Ayalew *et al.*, 2019), KASP marker chemistry was not compatible with Crystal dPCR and thus TaqMan probes were used. Surprisingly, Sanger sequencing of the amplicons of selected InDel or SNP markers revealed a number of polymorphisms at primer/probe binding regions. However, the numbers were rather limited, and they did not impact the genotyping outcome in the setup. The Crystal dPCR-based single pollen nucleus genotyping set-up greatly improves throughput by allowing 12 individual chambers (4 chambers × 3 chips) forming in total roughly 300,000 (25,000 droplets per chamber × 12 chambers) droplets to be analyzed at once.

5.3.1. Improving sample throughput

Encapsulation rates of single nuclei of barley and other crops with different nuclear (2.9-10.4 µm) and genome sizes (0.32-26.70 pg/2C) were similar, indicating that the set-up can be applied to a broad range of plant species in the future and is not only limited to pollen nuclei (**Figures 22** and **25**). Detection of encapsulated pollen nuclei was possible after thermocycling due to the fact that PI used for staining of the nuclei for flow-sorting shares a similar absorption/emission spectrum with the HEX channel in the Crystal dPCR. Regardless of flow-sorted pollen nuclei numbers (2,000-6,000 tested), slightly less than half of them were successfully encapsulated in single droplets with encapsulation rates being close to the prediction from the Poisson distribution. Initially, 3,000 flow-sorted pollen nuclei were used to limit the number of droplets encapsulating more than a single nucleus that might induce errors in data analysis and to limit the volume and thus the inhibitory effect of the sheath fluid

used for FACS (1X PBS buffer was initially used) (**Figure 24**) (Zhu *et al.*, 2015). To minimize either concentration or volume of PBS in the flow-sorted nuclei suspension, a smaller nozzle (70 μm) compared to the original nozzle (86 μm) and a lower concentration (0.5X PBS) compared to the original concentration (1X PBS) were tested. However, the combination of the 70 μm nozzle and 0.5 x PBS as sheath fluid resulted in repeated experiments in an unstable droplet formation what made the sorting unreliable. Therefore, 5,000 pollen nuclei per chamber were finally flow-sorted using 0.5X PBS buffer and the 86 μm nozzle to measure meiotic recombination rates in higher throughput than the initial set-up.

During this work, it was noted that the quality of the pollen plays a key role in successful flow-sorting. Isolation and flow-sorting of pollen nuclei from aged or “unhealthy” plants led to strongly decreased numbers of isolated pollen nuclei. Consistent availability of fresh pollen/anther material can be a limiting factor. Hence, several approaches to store anther or pollen material such as air-drying, organic solvent storage, freezing, etc. (Barnabas *et al.*, 1988; Volk, 2011; Sidhu, 2019) were tested. Unfortunately none of them led to sufficient numbers of isolated pollen nuclei afterwards when compared to the numbers obtained with fresh pollen. Acetone-washed and air-dried barley pollen remained intact for at least two weeks (based on a microscopic evaluation). However, pollen nuclei isolation from acetone-washed pollen by mechanical disruption was not as efficient as from fresh pollen (see 3.7.). In the future, it will be of interest to explore different pollen nuclei isolation procedures and different approaches to store harvested anther/pollen material or even pollen nuclei in suspension.

5.3.2. Increasing efficiency of Crystal Digital PCR

The accessibility of the target DNA is a crucial factor for Crystal dPCR-based genotyping assays. Since an intact pollen nucleus structure when compared to fragmented genomic DNA can hinder to some extent successful PCR amplification, an enzymatic pre-treatment of nuclei using Proteinase K or the thermostable restriction enzyme *TaqI* was applied to improve dPCR efficiency. Proteinase K pre-treatment improved dPCR efficiency by 31% compared with untreated control (**Figure 19**). However, pre-treatment of pollen nuclei with Proteinase K and their flow-cytometric isolation were technically challenging, resulting in rather limited numbers of isolated nuclei that could be used for dPCR-based genotyping, and thus it was not routinely used for the current set-up. A modified pre-treatment of pollen nuclei using e.g. different Proteinase K concentrations or treatment durations could possibly improve nuclei yield and thus improve Crystal dPCR efficiency in the future. Crystal dPCR efficiency with *TaqI* pre-treated pollen nuclei increased by 164% when compared with untreated pollen nuclei (**Figure 19**). The thermostable restriction enzyme *MseI* was also tested. However, it did not improve dPCR efficiency. Considering the easy addition of a restriction enzyme into the Crystal dPCR mix by

pipetting, usage of a thermostable restriction enzyme during dPCR is a simple way to improve genotyping efficiency. The selected thermostable restriction enzyme should neither cut the desired amplicon nor be (strongly) active at temperatures below 40°C (the temperature for droplet generation of pollen nucleus in the Crystal dPCR).

Accessibility of chromatin can differ also based on the level of chromatin condensation. The different condensation degrees and structures of vegetative and sperm nuclei could provide different dPCR efficiencies. Based on their different sizes, vegetative and sperm nuclei were flow-cytometrically sorted into the dPCR mix (**Figure 20**). Surprisingly, the fluorescence value in both FAM and HEX channel was higher in sperm nuclei than in vegetative nuclei, which are more densely packed (**Figure 20**). However, despite possible differences in genotyping efficiency between the two pollen nuclei types, both types of nuclei were pooled together for Crystal dPCR genotyping since not all nuclei isolations offered a reliable separation of the two nucleus types and since the yield of isolated pollen nuclei per plant was limited.

5.3.3. Data quality and analysis

The encapsulation rate per chamber of a single pollen nucleus was between 39.9 and 42.4% across the range of flow-sorted pollen nuclei (2,000-6,000 pollen nuclei per chamber). Hence, nearly half of the flow-sorted pollen nuclei were successfully encapsulated (**Figure 22**) close to the encapsulation rate predicted by the Poisson distribution.

Notably, the number of droplets encapsulating more than a single nucleus was much lower than predicted by the Poisson distribution (**Figure 22**). Although it was assumed that the 'small' size of pollen or leaf nuclei would not interfere with encapsulation rates (see above), possibly their rather large size when compared with fragmented or plasmid DNA generally used as the template for digital PCR (Madic *et al.*, 2016) may have contributed to the slightly lower number of droplets with two nuclei than predicted.

To analyze Crystal dPCR-based single pollen nucleus genotyping data, two factors were critical: *false-positives* and *noise*. By performing Crystal dPCR using both parental pollen nuclei (cv. Barke and cv. Morex) mixed in a 1:1 ratio, droplets being genotyped as *hybrid* were defined as *false-positives* (**Figures 16D** and **16E**). These *false-positives* were interval-specific while consistent across samples and experiments for a given interval. Droplets encapsulating more than one nucleus or no nucleus within the *false-positives* were easily detected in the HEX channel and subtracted. However, between 0.6-2.8% (Interval Ic 1, Ic 3, Id 3-1 and Id 3-2, Appendix 1) of *hybrid* droplets remained even after the subtraction having a single nucleus encapsulated and were defined as *noise*. Employing flow-sorted beads from a suspension of beads and pollen nuclei for Crystal dPCR suggested the *false-positives* were likely not

caused by fragmented DNA derived during the pollen nuclei isolation step (**Figure 26**). Due to the limited resolution of the scanner, these *false-positives* identified as encapsulating a single nucleus might have possibly also encapsulated two or even more nuclei (e.g. above each other). However, considering the range of *noise* among different chromosomal intervals (0.6-2.8%), neither DNA contaminations nor the presence of more than a single nucleus are considered as the major origin of *false-positives*. In theory, a total maximum of 0.6% (lowest *noise* rate for a tested interval) of successfully genotyped droplets containing a single visible nucleus could be *false-positives* due to the presence of more than a single nucleus and/or due to DNA contaminations. Nevertheless, the *noise* rate was consistent across experiments and samples for a given interval, possibly due to allelic markers calling the opposite genotype infrequently. Therefore, the established *noise* for a given interval can be subtracted from acquired hybrid pollen data. Due to the *noise* being consistent for a given interval, two independent samples (e.g. wild type and *mutants*) could also be compared relative to each other without correction for *noise*.

5.3.4. Reliable measurements of meiotic recombination rates in pollen nuclei using Crystal Digital PCR

Next, meiotic recombination rates in pollen nuclei within four selected chromosomal intervals, either in distal or centromeric locations on chromosomes 1 and 3 were measured based on Crystal dPCR (**Figure 16A**). After subtraction of *noise*, meiotic recombination rates of 7.1 ± 0.9 % for Ic 1, 6.0 ± 3.1 % for Ic 3, 12.0 ± 2.2 % for Id 3-1 and 10.9 ± 1.7 % for Id 3-2 were found (**Figure 28** and **Appendix 1**). These measurements were similar to reported values (male and female meiotic recombination) for Barke \times Morex with 6.7 cM for Ic 1, 8.5 cM for Ic 3, 11.7 cM for Id 3-1 and 11.1 cM for Id 3-2 (Zhou *et al.*, 2015) and similar to independent measurements in segregation offspring populations (blue lines in **Figure 28**). Slight deviations across measurements, such as 6.0 ± 3.1 % versus 8.5 cM for Ic 3, might be based on different plant cultivation conditions known to impact the rate of meiotic recombination (Higgins *et al.*, 2012; Modliszewski *et al.*, 2018; Dreissig *et al.*, 2019). Also, sex-specific differences in meiotic recombination rates (Phillips *et al.*, 2015) may have contributed to the slight differences found; in pollen only male while in offspring plants, both male and female meiotic recombination rates are assessed. While measurements were consistent within the interval Ic 1 across plants, Ic 3 and Id3-1 showed some variation in recombination rates among plants (**Figure 28** and **Appendix 1**). Likely, some genetic intervals are more *variable* in terms of meiotic recombination than others possibly due to different genetic locations. Nevertheless, meiotic recombination rate measurements in predefined recombination suspensions, i.e., pollen nuclei from offspring plants being recombinant for the tested intervals mixed with the two parental pollen nuclei types in defined ratios, assured the reliability of the approach to measure recombination frequencies within defined chromosomal regions (**Figure 29**).

In a nutshell, Crystal dPCR-based single pollen nucleus genotyping allows to measure meiotic recombination rates reliably and in high throughput within defined chromosomal intervals. Successful encapsulation of leaf nuclei from other (crop) plants with different DNA content and nuclear sizes suggests that the set-up can be used for diverse plant species in future studies.

5.4. Meiotic recombination rates in plants grown under different environmental conditions

Although meiotic HR is tightly regulated, the plasticity of the meiotic recombination landscapes towards environmental conditions is found (Lambing *et al.*, 2017; Wang and Copenhaver, 2018). In barley, natural variation in meiotic recombination rates among different barley populations correlates with different environmental conditions (Dreissig *et al.*, 2019). To test whether meiotic recombination rates within chromosomal intervals Ic 1 (centromeric) and/or Id 3-1 (distal) are impacted by plant growth conditions, plants were either grown in a greenhouse or a phytochamber to compare their meiotic recombination rates (**Figure 30**). Meiotic recombination rates within Ic 1 were higher under greenhouse conditions when compared to the phytochamber while the opposite was found for Id 3-1. These differences in meiotic recombination rates could be based on several variables differing between the greenhouse and the phytochamber. For example, plants in the greenhouse perceived $\sim 600 \mu\text{mol}/\text{m}^2\text{s}$ of artificial light for 16 hours together with natural light that varied depending on the day (length, weather) whereas plants grown in the phytochamber perceived for 16 hours daily a specific ratio of warm white and cold white LED light (see materials and methods). Moreover, plants perceived slightly different growing temperatures (17°C day/ 13°C night for the greenhouse and 19°C day/ 17°C night for the phytochamber). Soil composition, fertilizer application and watering were conducted in a similar manner in both growing conditions. Thus, the exact underlying cause of observed differences in meiotic recombination rates could not be identified. However, despite the fact that only two growing conditions were tested for their impact on meiotic recombination rates within just two chromosomal intervals, the results suggest that changes in meiotic recombination rates both in centromeric and distal chromosome regions can be achieved by simply growing plants under different growing conditions and that the developed Crystal dPCR-based pollen nucleus genotyping set-up enabled efficient measurements of CO frequencies.

5.5. Measuring meiotic recombination rates in different spikes of single plants

Within flowers developed from different bolts in *Arabidopsis*, differences in CO frequencies in pollen were found (Francis *et al.*, 2007). Also in five individual barley plants grown in the phytochamber variations in meiotic recombination rates among different tillers (primary, secondary and tertiary) in a single barley plants across the four tested intervals (Ic 1, Ic 3, Id 3-1 and Id 3-2) were found (**Figure 31**). Based on the acquired data from a limited number of plants and genetic intervals studied, it seems

feasible that differences between different tillers in a given plant exist (at least across the four tested chromosomal intervals on two independent chromosomes and being located within centromeric as well as distal regions). Hence, it is tempting to speculate that, the frequency of recombinant offspring plants in a given genetic interval in an offspring population could be increased/decreased by simply collecting seeds from specific tillers, and pre-screening by single pollen nucleus genotyping could help the identify of such polymorphisms.

5.6. Impact of chemical compounds on meiotic recombination rates in barley

The formation and localization of meiotic COs are influenced by epigenetic marks such as DNA methylation and histone modifications or additional PTMs of (meiotic) proteins (Choi *et al.*, 2017). Based on the pre-screening using germinated barley seedlings, three compounds known to impact DNA methylation (Zebularine), histone methylation (BIX-01294) and histone acetylation (Trichostatin A) were selected and delivered via *in planta* injections. All three targeted DNA/histone modifications are known to impact meiotic recombination landscapes. Thus, it was explored whether an *in planta* application of chemical compounds impacts meiotic recombination rates in selected chromosomal regions, i.e., within a centromeric interval on chromosome 1 (Ic 1) and a subtelomeric interval on chromosome 3 (Id 3-1). The concentrations of compounds to be injected had to be lowered compared with the ones used during the pre-screening procedure in seedlings, since tillers aborted upon delivery of chemical compounds with the concentrations explored during the pre-screening procedure. However, the pre-screening of chemical compounds using seedlings offered a platform to identify potential *in planta* activity of any given compound.

Meiotic recombination rates in injected and *uninjected* plants were measured within the intervals Ic 1 and Id 3-1 simultaneously via the multiplexed Crystal dPCR-based single pollen nucleus genotyping set-up (**Figure 34**). Measurements from control groups (358-7,635 and 1,052-4,622 pollen nuclei per plant for Ic 1 and Id 3-1, respectively) were: $5.9 \pm 1.8\%$ for Ic 1 and $15.1 \pm 1.4\%$ for Id 3-1 in *uninjected* plants, $9.1 \pm 0.6\%$ for Ic 1 and $13.6 \pm 1.7\%$ for Id 3-1 in distilled water injected plants, $7.0 \pm 2.7\%$ for Ic 1 and 11.6% for Id 3-1 in 0.05% Silwet L-77 injected plants, and 6.9% for Ic 1 while data for Id 3-1 could not be obtained due to poor pollen quality in 0.05% Silwet L-77+1% DMSO injected plants. Overall, higher meiotic recombination rates were found within Ic 1 while the opposite was found within Id 3-1 in plants injected with fluids (water, 0.05% Silwet L-77 and/or 1% DMSO) compared to *uninjected* plants.

Among seven plants injected with $0.5 \mu\text{M}$ Zebularine, three plants showed an almost twofold increase in Ic 1 meiotic recombination rates compared with control groups, while the remaining four plants showed Ic 1 meiotic recombination rates similar to the control. The data may suggest either differences between plant responses and/or that possibly in three out of the seven injected plants Zebularine

showed an impact on meiotic recombination rates. Possibly in these cases Zebularine was injected in plants with cells prior/during meiosis while in the remaining either the injection failed or Zebularine was delivered too early or too late to have an impact on meiosis. In the case of Id 3-1, recombination rates were slightly lower than control groups, suggesting possibly a different response depending on the genetic interval. While the number of plants as well as the number of genetic intervals analyzed is limited, future further experiments are required. Injection of Zebularine might be a promising approach to alter recombination frequencies via reduction of DNA methylation, at least in selected chromosomal regions. Interestingly, in *Arabidopsis* plants defective for DNA methylation, a redistribution of COs towards centromeric areas or increased CO rates within centromeric and subtelomeric regions was found (Melamed-Bessudo and Levy, 2012; Mirouze *et al.*, 2012; Underwood *et al.*, 2018). While the observed increase in centromeric recombination rates in some of the barley plants is in agreement with results from *Arabidopsis*, decreased recombination rates within Id 3-1 (subtelomeric interval on chromosome 3) are not. Thus, further data are needed to confirm these observations and to draw solid conclusions as to whether Zebularine impacts meiotic recombination rates in barley depending on the genetic context/interval. Furthermore, additional chemical compounds impacting DNA methylation, such as 5-Azacytidine (Griffin *et al.*, 2016), could be explored in barley for a putative impact on meiotic recombination rates.

In *Arabidopsis*, histone hyperacetylation caused redistribution of COs (Perrella *et al.*, 2010). Therefore, Trichostatin A as a histone deacetylation inhibitor was expected to induce changes in CO landscapes in barley as well. Measurements from 0.5 nM Trichostatin A injected plants showed $6.8 \pm 1.5\%$ for Ic 1 and $12.6 \pm 1.4\%$ for Id 3-1 (**Figure 34**). Although lacking measurements from plants injected with 0.05% Silwet L-77 and 1% DMSO within Id 3-1 hinders a comparison between control groups and Trichostatin A injected plants, the measurements within Ic 1 and Id 3-1 were similar to what was found in control groups when injected with only 0.05% Silwet L-77 and 0.05% Silwet L-77 and 1% DMSO with increased rates in the centromeric interval and decreased rates in the distal interval compared to *uninjected* plants. Therefore, it can be concluded that an effect of Trichostatin A on the CO landscape in barley was not detected in the current set-up. Higher numbers of Trichostatin A (or other histone deacetylase inhibitors) injected barley plants and possibly additional chromosomal intervals need to be tested to confirm whether histone acetylation can alter CO landscapes in barley in future studies.

Lastly, BIX-01294 (0.5 μ M), an H3K9 methyltransferase inhibitor (Berenguer *et al.*, 2017) was injected into barley. Plants injected with BIX-01294 showed $7.9 \pm 1.5\%$ for Ic 1 and 14.1% for Id 3-1 (**Figure 34**). Meiotic recombination rates within Ic 1 from this variant were in the range of the control injection groups ($7.0 \pm 2.7\%$ - $9.1 \pm 0.6\%$), which were higher than *uninjected* plants ($5.9 \pm 1.8\%$). While rates within Id 3-1 were higher than injection groups (11.6-13.6 \pm 1.7%) yet lower than *uninjected* groups

(15.1 ± 1.4%). Increased rates within Ic 1 correspond to a previous report in Arabidopsis about increased meiotic recombination rates within centromeric chromosome regions when the level of H3K9 is reduced (Underwood *et al.*, 2018). BIX-01294 injected plants appear to have similar meiotic recombination rates to that of uninjected plants, which is higher than control injection groups with Silwet L-77 and DMSO. However, further data are needed to assure whether BIX-01294 (or other histone methyltransferase inhibitors) can alter meiotic recombination rates within centromeric and/or distal regions of chromosomes in barley.

In addition to these widely known chemical compounds also further chemical compounds impacting epigenetic marks or PTMs such as phosphorylation, ubiquitination or SUMOylation implicated in regulating meiotic recombination landscapes across species could be explored using the establishing set-up.

In a nutshell, meiotic recombination rates within the chromosomal intervals Ic 1 and Id 3-1 after *in planta* injection of chemical compounds were measured simultaneously through Crystal dPCR single pollen genotyping and scanned with the Naica® Prism6 using four colors: FAM, HEX, ROX and Cy5 (**Figure 34**). Together with the increased number of employed flow-sorted pollen nuclei per chamber (5,000 nuclei), the genotyping throughput of single pollen nuclei could be significantly improved. High-throughput measurements of meiotic recombination rates via Crystal dPCR-based single pollen nucleus using hybrid plants grown in different conditions, different tillers from one plant and chemical compound injected plants indicate that the set-up can be applied to screen for an impact of a wide range of “factors” or “stresses” such as various chemical compounds, abiotic/biotic factors or environmental stresses. Moreover, the established single pollen nucleus genotyping set-up can likely also be used in diverse (crop) species in the context of basic and applied research or breeding.

6. Outlook

In future, the following points should be addressed:

- i) To further improve Crystal Digital PCR-based single pollen nucleus genotyping throughput, efficiency and applicability, the following aspects should be explored:
 - increased number of employed fluorochromes (up to 6 colors) for Crystal dPCR,
 - different thermostable restriction enzyme or Proteinase K pre-treatments (and combinations thereof) of pollen nuclei prior/during genotyping,
 - improved pollen nuclei isolation method and flow-sorting of only sperm nuclei,
 - and storage of pollen grains and/or flow-sorted pollen nuclei suspensions.
- ii) Harness the established approaches to increase the number of treated plants and to explore further chemical compounds and various “stresses” or factors for their impact on the meiotic recombination landscape in barley.
- iii) Transfer the developed approaches and knowledge gained in barley to other (crop) plant species.

7. Summary

In this study, a high-throughput Crystal Digital PCR-based single pollen nucleus genotyping approach was established to measure meiotic recombination rates in barley (*Hordeum vulgare*).

- i) A combination of flow sorting of pollen nuclei and Crystal Digital PCR allows reliable measurements of meiotic recombination rates in male gametes of barley (Barke x Morex) in a high-throughput manner for up to two chromosomal intervals in parallel. Enzymatic pre-treatment of the isolated pollen nuclei with a thermostable restriction enzyme increased the genotyping efficiency. The described approach was proven to be applicable to various (crop) species independent of their nuclear and genome size.
- ii) Alternatively, successful pollen genotyping was performed on individual pollen nuclei with and without target-specific pre-amplification and on pollen grains with and without prior germination using gel-based genotyping approaches, however, with a slightly lower efficiency and with a by far lower throughput.
- iii) Altogether the meiotic recombination rates were determined for four defined chromosomal intervals in the centromeric (Ic) and distal region (Id) of chromosomes 1 and 3. Depending on the chromosomal position the interval-specific recombination rates were $7.1 \pm 0.9\%$ for Ic 1, $6.0 \pm 3.1\%$ for Ic 3, $12.0 \pm 2.2\%$ for Id 3-1 and $10.9 \pm 1.7\%$ for Id 3-2. The obtained values were similar to reported data (male and female meiotic recombination) for Barke x Morex and similar to independent measurements in segregating offspring populations, indicating the reliability of the method.
- iv) Applying the established method on barley plants cultivated in different growth conditions (greenhouse versus phytochamber) detected for both centromeric and distal chromosome regions, changes in meiotic recombination rates. Similarly, differences in the meiotic recombination rates were found when different tillers (primary, secondary and tertiary) of single barley plants were compared. These results suggest that changes in meiotic recombination rates can be achieved by simply growing plants under different growing conditions and/or by collecting seeds from different tillers of the same plant.
- v) A protocol for *in planta* delivery of chemical compounds into barley meiocytes to potentially impact meiotic recombination was developed. Phenotypic characteristics e.g. plant height, age of barley, internode distances, the distance between the two nodes and the leaf auricle (2-4.5 cm), etc. were recorded, and their indicative values for distinct meiotic stages of young barley spikes were analyzed from plants grown either in greenhouse or phytochamber. The impact of injection together with 0.05% Silwet L-77 on survival and seed set rates were studied. Plants were selected for injection based on internode distance. Injections were performed for 3 days

with 24-hour intervals and one additional injection after 1 hour after the first initial injection using an injection volume of 0.5 mL with 0.05% Silwet L-77. The successful delivery of compounds was confirmed with EdU microscopically.

- vi) Chemical compounds Zebularine, Trichostatin A and BIX-01294 impacting DNA methylation, histone acetylation and histone methylation, were screened for their potential impact on the meiotic recombination landscape in barley. Prior to injection, a set-up enabling a pre-screening of chemical compounds for their potential impact on root development and mitotic cell cycle values was developed. This pre-screening of compounds enabled to determine concentrations for following injections and provided a platform to screen various compound candidates in future studies. After a pre-screening, compounds were injected *in planta* and meiotic recombination rates within Ic 1 and Id 3-1 were measured in parallel.

8. Zusammenfassung

In dieser Studie wurde eine Hochdurchsatz Crystal Digital-PCR-basierende Einzelpollenkern-Genotypisierung zur Messung der meiotischen Rekombinationsraten in Gerste (*Hordeum vulgare*) etabliert.

- i) Eine Kombination aus Flow Sorting von Pollenkernen und Crystal Digital PCR ermöglicht eine zuverlässige Hochdurchsatzmessung der meiotischen Rekombinationsraten in männlichen Gameten der Gerste (Barke x Morex) für bis zu zwei chromosomale Intervalle parallel. Eine enzymatische Vorbehandlung der isolierten Pollenkerne mit einem thermostabilen Restriktionsenzym erhöhte die Genotypisierungseffizienz. Der beschriebene Ansatz erwies sich unabhängig von der Kern- und Genomgröße als anwendbar für verschiedene Pflanzenarten.
- ii) Alternativ wurde eine Pollengenotypisierung an einzelnen Pollenkernen mit und ohne Zielsequenz-spezifischer Voramplifikation und an Pollenkörnern mit und ohne vorheriger Keimung mittels gelbasierten Genotypisierungsansätzen erfolgreich durchgeführt, jedoch mit etwas geringerer Effizienz und mit einem weitaus geringeren Durchsatz.
- iii) Insgesamt wurden die meiotischen Rekombinationsraten für vier definierte chromosomale Intervalle in zentromerischen (Ic) und distalen Bereichen (Id) der Chromosomen 1 und 3 bestimmt. Abhängig von der Chromosomenregion lagen die intervallspezifischen Rekombinationsraten bei $7,1 \pm 0,9$ % für Ic 1, $6,0 \pm 3,1$ % für Ic 3-1, $12,0 \pm 2,2$ % für Id 3-1 und $10,9 \pm 1,7$ % für Id 3-2. Die ermittelten Werte sind vergleichbar mit bereits vorliegenden Daten (männliche und weibliche meiotische Rekombination) für Barke × Morex und ähnelten unabhängigen Messungen in segregierenden Nachkommenpopulationen, was die Zuverlässigkeit der Methode verdeutlicht.
- iv) Die Anwendung der etablierten Methode zeigte, dass Gerstenpflanzen, die unter verschiedenen Wachstumsbedingungen (Gewächshaus versus Phytokammer) kultiviert wurden, sich in der meiotischen Rekombinationsrate unterscheiden. Zentromerische als auch distale Chromosomenregionen zeigten Veränderungen in der Rekombinationsrate. Ebenso wurden Unterschiede in den meiotischen Rekombinationsraten gefunden, wenn verschiedene Ähren (primär, sekundär und tertiär) einzelner Gerstenpflanzen verglichen wurden. Diese Ergebnisse legen nahe, dass Änderungen der meiotischen Rekombinationsraten durch eine Kultivierung der Pflanzen unter verschiedenen Wachstumsbedingungen erreicht werden kann. Weiterhin können unterschiedliche Ähren einer Pflanze genutzt werden, um Pflanzen mit unterschiedlichen Rekombinationsfrequenzen zu gewinnen.

- v) Es wurde ein Protokoll für die *in planta* Zufuhr chemischer Verbindungen in die Meiozyten der Gerste entwickelt, um die meiotische Rekombination potenziell zu beeinflussen. Phänotypische Merkmale junger Gersteähren wie z.B. Pflanzenhöhe, Alter der Pflanze, Internodienabstände, Abstand zwischen den beiden Knoten und dem Blattöhrchen (2-4,5 cm) wurden aufgezeichnet und ihre Aussagekraft bezüglich der Identifizierung verschiedener meiotischer Stadien analysiert. Dafür wurden die Pflanzen entweder im Gewächshaus oder in einer Phytokammer angebaut. Der Einfluss der Injektion zusammen mit 0,05% Silwet L-77 auf die Überlebensrate der Pflanze und dem Samenansatz wurde untersucht. Die Pflanzen wurden anhand des Internodienabstands für die Injektion ausgewählt. Injektionen über 3 Tage im Abstand von 24 Stunden und eine zusätzliche Injektion 1 Stunde nach der Erstinjektion wurde mit 0,5 ml Injektionsvolumen mit 0,05% Silwet L-77 durchgeführt. Die erfolgreiche Aufnahme chemischer Verbindungen durch Injektion wurde mit EdU mikroskopisch bestätigt.
- vi) Die chemischen Verbindungen Zebularin, Trichostatin A und BIX-01294, die die DNA-Methylierung, Histonazetylierung und Histonmethylierung beeinflussen, wurden auf ihren möglichen Einfluss auf die meiotische Rekombinationslandschaft in der Gerste untersucht. Vor der Injektion wurde eine experimentelle Strategie entwickelt, die ein Vor-Screening chemischer Verbindungen auf ihren möglichen Einfluss auf die Wurzelentwicklung und mitotischen Zellzyklus ermöglicht. Dieses Vor-screening ermöglichte die Bestimmung von potentiellen Wirkkonzentrationen und bietet eine Plattform zum Screenen unterschiedlichster Wirkstoffkandidaten in zukünftigen Studien. Die Verbindungen wurden *in planta* nach dem Vor-Screening injiziert und die meiotischen Rekombinationsraten innerhalb von Ic 1 und Id 3-1 wurden parallel gemessen.

9. References

- Abdullah, M.F.F. and Borts, R.H.** (2001) Meiotic recombination frequencies are affected by nutritional states in *Saccharomyces cerevisiae*. *Proc. Natl. Acad. Sci. U. S. A.*, **98**, 14524–14529.
- Ahn, Y.J., Fuchs, J., Houben, A. and Heckmann, S.** (2021) High-throughput measuring of meiotic recombination rates in barley pollen nuclei using Crystal Digital PCR TM. *Plant J.*, **102**, 649–661.
- Ahn, Y.J., Cuacos, M., Ayoub, M.A., Kappermann, J., Houben, A. and Heckmann, S.** (2020) In Planta Delivery of Chemical Compounds into Barley Meiocytes: EdU as Compound Example. In *Methods in Molecular Biology*. Springer. 381–402.
- Andronic, L.** (2012) Viruses as triggers of DNA rearrangements in host plants. *Can. J. Plant Sci.*, **92**, 1083–1091.
- Arrieta, M., Colas, I., Macaulay, M., Waugh, R. and Ramsay, L.** (2020) A Modular Tray Growth System for Barley. In *Methods in Molecular Biology*. 367–379.
- Asensi-Fabado, M.A., Amtmann, A. and Perrella, G.** (2017) Plant responses to abiotic stress: The chromatin context of transcriptional regulation. *Biochim. Biophys. Acta - Gene Regul. Mech.*, **1860**, 106–122.
- Ayalew, H., Tsang, P.W., Chu, C., Wang, J., Liu, S., Chen, C. and Ma, X.F.** (2019) Comparison of TaqMan, KASP and rhAmp SNP genotyping platforms in hexaploid wheat. *PLoS One*, **14**.
- Barakate, A., Higgins, J.D., Vivera, S., et al.** (2014) The synaptonemal complex protein ZYP1 is required for imposition of meiotic crossovers in barley. *Plant Cell*, **26**, 729–740.
- Barnabas, B., Kovacs, G., Abranyi, A. and Pfahler, P.** (1988) Effect of pollen storage by drying and deep-freezing on the expression of different agronomic traits in maize (*Zea mays* L.). *Euphytica*, **39**, 221–225.
- Bastien, M., Boudhrioua, C., Fortin, G., Belzile, F. and Phillips, D.W.** (2018) Exploring the potential and limitations of genotyping-by-sequencing for SNP discovery and genotyping in tetraploid potato. *Genome*, **61**, 449–456.
- Baubec, T., Pecinka, A., Rozhon, W. and Mittelsten Scheid, O.** (2009) Effective, homogeneous and transient interference with cytosine methylation in plant genomic DNA by zebularine. *Plant J.*, **57**, 542–554.
- Baudat, F., Buard, J., Grey, C., Fledel-Alon, A., Ober, C., Przeworski, M., Coop, G. and Massy, B. De** (2010) PRDM9 is a major determinant of meiotic recombination hotspots in humans and mice. *Science (80-.)*, **327**, 836–840.
- Ben-Kasus, T., Ben-Zvi, Z., Marquez, V.E., Kelley, J.A. and Agbaria, R.** (2005) Metabolic activation of zebularine, a novel DNA methylation inhibitor, in human bladder carcinoma cells. *Biochem. Pharmacol.*, **70**, 121–133.
- Bennett, M.D. and Finch, R.A.** (1971) Duration of meiosis in barley. *Genet. Res. (Camb.)*, **17**, 209–214.
- Bennett, M.D., Leitch, I.J., Price, H.J. and Johnston, J.S.** (2003) Comparisons with *Caenorhabditis* (~100 Mb) and *Drosophila* (~175 Mb) using flow cytometry show genome size in *Arabidopsis* to be ~157 Mb and thus ~25% larger than the *Arabidopsis* genome initiative estimate of ~125 Mb. *Ann. Bot.*, **91**, 547–557.
- Bennett, M.D. and Rees, H.** (1970) Induced variation in chiasma frequency in Rye in response to phosphate treatments. *Genet. Res.*, **16**, 325–331.

- Berchowitz, L.E. and Copenhaver, G.P.** (2008) Fluorescent Arabidopsis tetrads: A visual assay for quickly developing large crossover and crossover interference data sets. *Nat. Protoc.*, **3**, 41–50.
- Berchowitz, L.E., Hanlon, S.E., Lieb, J.D. and Copenhaver, G.P.** (2009) A positive but complex association between meiotic double-strand break hotspots and open chromatin in *Saccharomyces cerevisiae*. *Genome Res.*, **19**, 2245–2257.
- Berenguer, E., Bárány, I., Solís, M.T., Pérez-Pérez, Y., Risueño, M.C. and Testillano, P.S.** (2017) Inhibition of histone H3K9 methylation by BIX-01294 promotes stress-induced microspore totipotency and enhances embryogenesis initiation. *Front. Plant Sci.*, **8**.
- Berg, I.L., Neumann, R., Lam, K.W.G., Sarbajna, S., Odenthal-Hesse, L., May, C.A. and Jeffreys, A.J.** (2010) PRDM9 variation strongly influences recombination hot-spot activity and meiotic instability in humans. *Nat. Genet.*, **42**, 859–863.
- Blackwell, A.R., Dluzewska, J., Szymanska-Lejman, M., et al.** (2020) MSH 2 shapes the meiotic crossover landscape in relation to interhomolog polymorphism in Arabidopsis. *EMBO J.*, **39**.
- Blary, A., Gonzalo, A., Eber, F., et al.** (2018) FANCM limits meiotic crossovers in Brassica crops. *Front. Plant Sci.*, **9**.
- Blary, A. and Jenczewski, E.** (2019) Manipulation of crossover frequency and distribution for plant breeding. *Theor. Appl. Genet.*, **132**, 575–592.
- Blat, Y., Protacio, R.U., Hunter, N. and Kleckner, N.** (2002) Physical and functional interactions among basic chromosome organizational features govern early steps of meiotic chiasma formation. *Cell*, **111**, 791–802.
- Bombles, K., Higgins, J.D. and Yant, L.** (2015) Meiosis evolves: Adaptation to external and internal environments. *New Phytol.*, **208**, 306–323.
- Borde, V., Robine, N., Lin, W., Bonfils, S., Géli, V. and Nicolas, A.** (2009) Histone H3 lysine 4 trimethylation marks meiotic recombination initiation sites. *EMBO J.*, **28**, 99–111.
- Boyko, A., Kathiria, P., Zemp, F.J., Yao, Y., Pogribny, I. and Kovalchuk, I.** (2007) Transgenerational changes in the genome stability and methylation in pathogen-infected plants: (Virus-induced plant genome instability). *Nucleic Acids Res.*, **35**, 1714–1725.
- Broccanello, C., Chiodi, C., Funk, A., McGrath, J.M., Panella, L. and Stevanato, P.** (2018) Comparison of three PCR-based assays for SNP genotyping in plants. *Plant Methods*, **14**, 28.
- Brown, J.C.L., Decker, M.M. De and Fieldes, M.A.** (2008) A comparative analysis of developmental profiles for DNA methylation in 5-azacytidine-induced early-flowering flax lines and their control. *Plant Sci.*, **175**, 217–225.
- Burke, J.J., Velten, J. and Oliver, M.J.** (2004) In vitro analysis of cotton pollen germination. *Agron. J.*, **96**, 359–368.
- Cao, Y. peng, Sun, J. ya, Li, M. qian, Dong, Y., Zhang, Y. heng, Yan, J., Huang, R. min and Yan, X.** (2019) Inhibition of G9a by a small molecule inhibitor, UNC0642, induces apoptosis of human bladder cancer cells. *Acta Pharmacol. Sin.*, **40**, 1076–1084.
- Capilla-Pérez, L., Durand, S., Hurel, A., Lian, Q., Chambon, A., Taochy, C., Solier, V., Grelon, M. and Mercier, R.** (2021) The synaptonemal complex imposes crossover interference and heterochiasmy in Arabidopsis. *Proc. Natl. Acad. Sci.*, **118**.
- Caryl, A.P., Armstrong, S.J., Jones, G.H. and Franklin, F.C.H.** (2000) A homologue of the yeast HOP1 gene is inactivated in the Arabidopsis meiotic mutant asy1. *Chromosoma*, **109**, 62–71.

- Chambon, A., West, A., Vezon, D., et al.** (2018) Identification of ASYNAPTIC4, a component of the meiotic chromosome axis. *Plant Physiol.*, **178**, 233-246.
- Chelysheva, L., Vezon, D., Chambon, A., et al.** (2012) The Arabidopsis HEI10 is a new ZMM protein related to Zip3. *PLoS Genet.*, **8**.
- Cheng, C.H., Lo, Y.H., Liang, S.S., Ti, S.C., Lin, F.M., Yeh, C.H., Huang, H.Y. and Wang, T.F.** (2006) SUMO modifications control assembly of synaptonemal complex and polycomplex in meiosis of *Saccharomyces cerevisiae*. *Genes Dev.*, **20**, 2067–2081.
- Chiriac, G.I., Andronic, L.I., Bujoreanu, V. V. and Marii, L.I.** (2006) Features of crossing-over in virus-infected tomato. *Cent. Eur. J. Biol.*, **1**, 386–398.
- Cho, S.-W., Ishii, T., Matsumoto, N., Tanaka, H., Eltayeb, A. and Tsujimoto, H.** (2012) Effects of the cytidine analogue zebularine on wheat mitotic chromosomes. *Chromosom. Sci.*, **14**, 23–28.
- Choi, K., Reinhard, C., Serra, H., et al.** (2016) Recombination Rate Heterogeneity within Arabidopsis Disease Resistance Genes. *PLoS Genet.*, **12**.
- Choi, K., Yelina, N.E., Serra, H. and Henderson, I.R.** (2017) Quantification and sequencing of crossover recombinant molecules from Arabidopsis pollen DNA. In *Methods in Molecular Biology*. 23–57.
- Choi, K., Zhao, X., Kelly, K.A., et al.** (2013) Arabidopsis meiotic crossover hot spots overlap with H2A.Z nucleosomes at gene promoters. *Nat. Genet.*, **45**, 1327–1338.
- Choi, K., Zhao, X., Tock, A.J., et al.** (2018) Nucleosomes and DNA methylation shape meiotic DSB frequency in Arabidopsis thaliana transposons and gene regulatory regions. *Genome Res.*, **28**, 532–546.
- Choudhary, S.S. and Sajid, S.M.** (1986) The Behaviour of Meiotic Chromosomes as Revealed through the Use of Bavistin on Pea. *Cytologia (Tokyo)*, **51**, 279-288.
- Chung, P.J., Kim, Y.S., Jeong, J.S., Park, S.H., Nahm, B.H. and Kim, J.K.** (2009) The histone deacetylase OsHDAC1 epigenetically regulates the OsNAC6 gene that controls seedling root growth in rice. *Plant J.*, **59**, 764–776.
- Colas, I., Darrier, B., Arrieta, M., Mittmann, S.U., Ramsay, L., Sourdille, P. and Waugh, R.** (2017) Observation of extensive chromosome axis remodeling during the “Diffuse-phase” of Meiosis in large genome cereals. *Front. Plant Sci.*, **8**.
- Colas, I., Macaulay, M., Higgins, J.D., et al.** (2016) A spontaneous mutation in MutL-Homolog 3 (HvMLH3) affects synapsis and crossover resolution in the barley desynaptic mutant des10. *New Phytol.*, **212**, 693–707.
- Colomé-Tatché, M., Cortijo, S., Wardenaar, R., et al.** (2012) Features of the Arabidopsis recombination landscape resulting from the combined loss of sequence variation and DNA methylation. *Proc. Natl. Acad. Sci. U. S. A.*, **109**, 16240–16245.
- Copenhaver, G.P., Keith, K.C. and Preuss, D.** (2000) Tetrad analysis in higher plants. A budding technology. *Plant Physiol.*, **124**, 7–15.
- Coulton, A., BurrIDGE, A.J. and Edwards, K.J.** (2020) Examining the Effects of Temperature on Recombination in Wheat. *Front. Plant Sci.*, **11**.
- Crismani, W., Girard, C., Froger, N., Pradillo, M., Santos, J.L., Chelysheva, L., Copenhaver, G.P., Horlow, C. and Mercier, R.** (2012) FANCM limits meiotic crossovers. *Science (80-.)*, **336**, 1588–1590.

- Desjardins, S.D., Ogle, D.E., Ayoub, M.A., Heckmann, S., Henderson, I.R., Edwards, K.J. and Higgins, J.D.** (2020) MutS homologue 4 and MutS homologue 5 maintain the obligate crossover in wheat despite stepwise gene loss following polyploidization. *Plant Physiol.*, **183**, 1545–1558.
- Dong, X.** (2004) Pathogen-induced systemic DNA rearrangement in plants. *Trends Plant Sci.*, **9**, 60–61.
- Doležel, J., Binarová, P. and Lucretti, S.** (1989) Analysis of Nuclear DNA content in plant cells by Flow cytometry. *Biol. Plant.*, **31**, 113–120.
- Dreissig, S., Fuchs, J., Cápál, P., Kettles, N., Byrne, E. and Houben, A.** (2015) Measuring meiotic crossovers via multi-locus genotyping of single pollen grains in barley. *PLoS One*, **10**.
- Dreissig, S., Fuchs, J., Himmelbach, A., Mascher, M. and Houben, A.** (2017) Sequencing of single pollen nuclei reveals meiotic recombination events at megabase resolution and circumvents segregation distortion caused by postmeiotic processes. *Front. Plant Sci.*, **8**, 1620.
- Dreissig, S., Mascher, M., Heckmann, S. and Purugganan, M.** (2019) Variation in Recombination Rate Is Shaped by Domestication and Environmental Conditions in Barley. *Mol. Biol. Evol.*, **36**, 2029–2039.
- Drouaud, J., Khademian, H., Giraut, L., Zanni, V., Bellalou, S., Henderson, I.R., Falque, M. and Mézard, C.** (2013) Contrasted Patterns of Crossover and Non-crossover at Arabidopsis thaliana Meiotic Recombination Hotspots. *PLoS Genet.*, **9**.
- Drouaud, J. and Mézard, C.** (2011) Characterization of meiotic crossovers in pollen from Arabidopsis thaliana. *Methods Mol. Biol.*, **745**, 223–249.
- Eichinger, C.S. and Jentsch, S.** (2010) Synaptonemal complex formation and meiotic checkpoint signaling are linked to the lateral element protein red1. *Proc. Natl. Acad. Sci. U. S. A.*, **107**, 11370–11375.
- Eversole, R.A. and Tatum, E.L.** (1956) CHEMICAL ALTERATION OF CROSSING-OVER FREQUENCY IN CHLAMYDOMONAS. *Proc. Natl. Acad. Sci.*, **42**, 68–73.
- Fedak, G.** (1973) Increased chiasma frequency in desynaptic barley in response to phosphate treatments. *Can. J. Genet. Cytol.*, **15**, 647–649.
- Ferdous, M., Higgins, J.D., Osman, K., et al.** (2012) Inter-homolog crossing-over and synapsis in arabidopsis meiosis are dependent on the chromosome axis protein atasy3. *PLoS Genet.*, **8**.
- Fieldes, M.A., Schaeffer, S.M., Krech, M.J. and Brown, J.C.L.** (2005) DNA hypomethylation in 5-azacytidine-induced early-flowering lines of flax. *Theor. Appl. Genet.*, **111**, 136–149.
- Filkowski, J., Yeoman, A., Kovalchuk, O. and Kovalchuk, I.** (2004) Systemic plant signal triggers genome instability. *Plant J.*, **38**, 1–11.
- Finnegan, E.J., Ford, B., Wallace, X., et al.** (2018) Zebularine treatment is associated with deletion of FT-B1 leading to an increase in spikelet number in bread wheat. *Plant Cell Environ.*, **41**, 1346–1360.
- France, M.G., Enderle, J., Röhrig, S., Puchta, H., Franklin, F.C.H. and Higgins, J.D.** (2021) ZYP1 is required for obligate cross-over formation and cross-over interference in Arabidopsis. *Proc. Natl. Acad. Sci. U. S. A.*, **118**.
- Francis, K.E., Lam, S.Y., Harrison, B.D., Bey, A.L., Berchowitz, L.E. and Copenhaver, G.P.** (2007) Pollen tetrad-based visual assay for meiotic recombination in Arabidopsis. *Proc. Natl. Acad. Sci. U. S. A.*, **104**, 3913–3918.
- Fučík, V., Šormová, Z. and Šorm, F.** (1965) Effyekt 5-azatsitidina na kornyevuyu myeristyemuVicia

faba. *Biol. Plant.*, **7**, 58–64.

- Fukaki, H., Taniguchi, N. and Tasaka, M.** (2006) PICKLE is required for SOLITARY-ROOT/IAA14-mediated repression of ARF7 and ARF19 activity during Arabidopsis lateral root initiation. *Plant J.*, **48**, 380–389.
- Galbraith, D.W., Harkins, K.R., Maddox, J.M., Ayres, N.M., Sharma, D.P. and Firoozabady, E.** (1983) Rapid flow cytometric analysis of the cell cycle in intact plant tissues. *Science (80-.)*, **220**, 1049–1051.
- Garavello, M., Cuenca, J., Dreissig, S., Fuchs, J., Navarro, L., Houben, A. and Aleza, P.** (2020) Analysis of Crossover Events and Allele Segregation Distortion in Interspecific Citrus Hybrids by Single Pollen Genotyping. *Front. Plant Sci.*, **11**.
- Girard, C., Chelysheva, L., Choinard, S., Froger, N., Macaisne, N. and Lemhemdi, A.** (2015) Correction To: AAA-ATPase FIDGETIN-LIKE 1 and Helicase FANCM Antagonize Meiotic Crossovers by Distinct Mechanisms (PLoS Genet, 11, 9). *PLoS Genet.*, **11**.
- Girard, C., Crismani, W., Froger, N., Mazel, J., Lemhemdi, A., Horlow, C. and Mercier, R.** (2014) FANCM-associated proteins MHF1 and MHF2, but not the other Fanconi anemia factors, limit meiotic crossovers. *Nucleic Acids Res.*, **42**, 9087–9095.
- Giraut, L., Falque, M., Drouaud, J., Pereira, L., Martin, O.C. and Mézard, C.** (2011) Genome-wide crossover distribution in Arabidopsis thaliana meiosis reveals sex-specific patterns along chromosomes. *PLoS Genet.*, **7**.
- Golubovskaya, I.N., Wang, C.J.R., Timofejeva, L. and Cande, W.Z.** (2011) Maize meiotic mutants with improper or non-homologous synapsis due to problems in pairing or synaptonemal complex formation. *J. Exp. Bot.*, **62**, 1533–1544.
- Gómez, J.F. and Wilson, Z.A.** (2012) Non-destructive staging of barley reproductive development for molecular analysis based upon external morphology. *J. Exp. Bot.*, **63**, 4085–4094.
- Griffin, P.T., Niederhuth, C.E. and Schmitz, R.J.** (2016) A comparative analysis of 5-azacytidine- and zebularine-induced DNA demethylation. *G3 Genes, Genomes, Genet.*, **6**, 2773–2780.
- Griffing, B. and Langridge, J.** (1963) Factors Affecting Crossing Over in the Tomato. *Aust. J. Biol. Sci.*, **16**, 826.
- Guo, A.S., Huang, Y.Q., Ma, X.D. and Lin, R.S.** (2016) Mechanism of G9a inhibitor BIX-01294 acting on U251 glioma cells. *Mol. Med. Rep.*, **14**, 4613–4621.
- Han, J.-Y., Kang, S.-W., Chun, J., Kim, Y.-K., Yoon, Y.-M. and Cho, S.-W.** (2020) Effect of Zebularine Soaking on the Early Growth Stage and Mitotic Chromosomes of Barley (*Hordeum vulgare* L.). *KOREAN J. Crop Sci.*, **65**, 399–405.
- He, Y., Wang, M., Dukowic-Schulze, S., et al.** (2017) Genomic features shaping the landscape of meiotic double-strand-break hotspots in maize. *Proc. Natl. Acad. Sci. U. S. A.*, **114**, 12231–12236.
- Higgins, J.D., Osman, K., Jones, G.H. and Franklin, F.C.H.** (2014) Factors underlying restricted crossover localization in barley meiosis. *Annu. Rev. Genet.*, **48**, 29–47.
- Higgins, J.D., Perry, R.M., Barakate, A., Ramsay, L., Waugh, R., Halpin, C., Armstrong, S.J. and Franklin, F.C.H.** (2012) Spatiotemporal asymmetry of the meiotic program underlies the predominantly distal distribution of meiotic crossovers in barley. *Plant Cell*, **24**, 4096–4109.
- Higgins, J.D., Sanchez-Moran, E., Armstrong, S.J., Jones, G.H. and Franklin, F.C.H.** (2005) The Arabidopsis synaptonemal complex protein ZYP1 is required for chromosome synapsis and

normal fidelity of crossing over. *Genes Dev.*, **19**, 2488–2500.

Honsho, C., Sakata, A., Tanaka, H., Ishimura, S. and Tetsumura, T. (2016) Single-pollen genotyping to estimate mode of unreduced pollen formation in Citrus tamurana cv. Nishiuchi Konatsu. *Plant Reprod.*, **29**, 189–197.

Jeffreys, A.J., Murray, J. and Neumann, R. (1998) High-resolution mapping of crossovers in human sperm defines a minisatellite-associated recombination hotspot. *Mol. Cell*, **2**, 267–273.

Jones, P.A., Taylor, S.M. and Wilson, V.L. (1983) Inhibition of DNA methylation by 5-azacytidine. *Recent Results Cancer Res.*, **84**, 202–211.

Jovelet, C., Madic, J., Remon, J., et al. (2017) Crystal digital droplet PCR for detection and quantification of circulating EGFR sensitizing and resistance mutations in advanced non-small cell lung cancer. *PLoS One*, **12**.

Khademian, H., Giraut, L., Drouaud, J. and Mézard, C. (2013) Characterization of meiotic non-crossover molecules from arabidopsis thaliana pollen. *Methods Mol. Biol.*, **990**, 177–190.

Khoo, K.H.P., Able, A.J. and Able, J.A. (2012) The isolation and characterisation of the wheat molecular ZIPper i homologue, TaZYP1. *BMC Res. Notes*, **5**.

Kianian, P.M.A., Wang, M., Simons, K., et al. (2018) High-resolution crossover mapping reveals similarities and differences of male and female recombination in maize. *Nat. Commun.*, **9**.

Kim, J.M., Sasaki, T., Ueda, M., Sako, K. and Seki, M. (2015) Chromatin changes in response to drought, salinity, heat, and cold stresses in plants. *Front. Plant Sci.*, **6**.

Kim, Y., Lee, H.M., Xiong, Y., et al. (2017) Targeting the histone methyltransferase G9a activates imprinted genes and improves survival of a mouse model of Prader-Willi syndrome. *Nat. Med.*, **23**, 213–222.

Knight, E., Greer, E., Draeger, T., Thole, V., Reader, S., Shaw, P. and Moore, G. (2010) Inducing chromosome pairing through premature condensation: Analysis of wheat interspecific hybrids. *Funct. Integr. Genomics*, **10**, 603–608.

Knoll, A., Schröpfer, S. and Puchta, H. (2014) The RTR complex as caretaker of genome stability and its unique meiotic function in plants. *Front. Plant Sci.*, **5**.

Kolb, H.C., Finn, M.G. and Sharpless, K.B. (2001) Click Chemistry: Diverse Chemical Function from a Few Good Reactions. *Angew. Chemie - Int. Ed.*, **40**, 2004–2021.

Komiya, R., Ohyanagi, H., Niihama, M., Watanabe, T., Nakano, M., Kurata, N. and Nonomura, K.I. (2014) Rice germline-specific Argonaute MEL1 protein binds to phasiRNAs generated from more than 700 lincRNAs. *Plant J.*, **78**, 385–397.

Kondo, H., Ozaki, H., Itoh, K., Kato, A. and Takeno, K. (2006) Flowering induced by 5-azacytidine, a DNA demethylating reagent in a short-day plant, *Perilla frutescens* var. *crispa*. *Physiol. Plant.*, **127**, 130–137.

Kovalchuk, I., Kovalchuk, O., Kalck, V., Boyko, V., Filkowski, J., Heinlein, M. and Hohn, B. (2003) Pathogen-induced systemic plant signal triggers DNA rearrangements. *Nature*, **423**, 760–762.

Kron, P. and Husband, B.C. (2012) Using flow cytometry to estimate pollen DNA content: Improved methodology and applications. *Ann. Bot.*, **110**, 1067–1078.

Kubicek, S., O'Sullivan, R.J., August, E.M., et al. (2007) Reversal of H3K9me2 by a Small-Molecule Inhibitor for the G9a Histone Methyltransferase. *Mol. Cell*, **25**, 473–481.

Künzel, G., Korzun, L. and Meister, A. (2000) Cytologically integrated physical restriction fragment

length polymorphism maps for the barley genome based on translocation breakpoints. *Genetics*, **154**, 397–412.

- Lambing, C., Franklin, F.C.H. and Wang, C.J.R.** (2017) Understanding and manipulating meiotic recombination in plants. *Plant Physiol.*, **173**, 1530–1542.
- Lambing, C. and Heckmann, S.** (2018) Tackling plant meiosis: From model research to crop improvement. *Front. Plant Sci.*, **9**.
- Lambing, C., Kuo, P.C., Tock, A.J., Topp, S.D. and Henderson, I.R.** (2020) ASY1 acts as a dosage-dependent antagonist of telomere-led recombination and mediates crossover interference in Arabidopsis. *Proc. Natl. Acad. Sci. U. S. A.*, **117**, 13647–13658.
- Las Heras, J.I. De, King, I.P. and Parker, J.S.** (2001) 5-Azacytidine induces chromosomal breakage in the root tips of wheat carrying the cuckoo chromosome 4SL from *Aegilops sharonensis*. *Heredity (Edinb.)*, **87**, 474–479.
- Law, C.N.** (1963) An effect of potassium on chiasma frequency and recombination. *Genetica*, **33**, 313–329.
- Li, H., Soriano, M., Cordewener, J., Muiño, J.M., Riksen, T., Fukuok, H., Angenent, G.C. and Boutilier, K.** (2014) The histone deacetylase inhibitor trichostatin a promotes totipotency in the male gametophyte. *Plant Cell*, **26**, 195–209.
- Li, X., Li, L. and Yan, J.** (2015) Dissecting meiotic recombination based on tetrad analysis by single-microspore sequencing in maize. *Nat. Commun.*, **6**.
- Li, X., Yu, M., Bolaños-Villegas, P., Zhang, J., Ni, D., Ma, H. and Wang, Y.** (2021) Fanconi anemia ortholog FANCM regulates meiotic crossover distribution in plants. *Plant Physiol.*, **186**, 344–360.
- Lim, E.C., Kim, Jaeil, Park, J., et al.** (2020) DeepTetrad: high-throughput image analysis of meiotic tetrads by deep learning in Arabidopsis thaliana. *Plant J.*, **101**, 473–483.
- Liu, C.H., Finke, A., Díaz, M., Rozhon, W., Poppenberger, B., Baubec, T. and Pecinka, A.** (2015) Repair of DNA damage induced by the cytidine analog zebularine requires ATR and ATM in Arabidopsis. *Plant Cell*, **27**, 1788–1800.
- Liu, H. and Nonomura, K.I.** (2016) A wide reprogramming of histone H3 modifications during male meiosis I in rice is dependent on the Argonaute protein MEL1. *J. Cell Sci.*, **129**, 3553–3561.
- Liu, M., Shi, S., Zhang, S., et al.** (2014) SUMO E3 ligase AtMMS21 is required for normal meiosis and gametophyte development in Arabidopsis. *BMC Plant Biol.*, **14**.
- Liu, S., Yeh, C.T., Ji, T., Ying, K., Wu, H., Tang, H.M., Fu, Y., Nettleton, D. and Schnable, P.S.** (2009) Mu transposon insertion sites and meiotic recombination events co-localize with epigenetic marks for open chromatin across the maize genome. *PLoS Genet.*, **5**.
- Lloyd, A., Morgan, C., Franklin, F.C.H. and Bomblies, K.** (2018) Plasticity of meiotic recombination rates in response to temperature in Arabidopsis. *Genetics*, **208**, 1409–1420.
- Lucht, J.M., Mauch-Mani, B., Steiner, H.Y., Metraux, J.P., Ryals, J. and Hohn, B.** (2002) Pathogen stress increases somatic recombination frequency in Arabidopsis. *Nat. Genet.*, **30**, 311–314.
- Lukaszewski, A.J.** (1992) A comparison of physical distribution of recombination in chromosome 1R in diploid rye and in hexaploid triticale. *Theor. Appl. Genet.*, **83**, 1048–1053.
- Ma, X., Wang, Q., Wang, Y., et al.** (2016) Chromosome aberrations induced by zebularine in triticale. *Genome*, **59**, 485–492.
- Maagd, R.A. de, Loonen, A., Chouaref, J., Pelé, A., Meijer-Dekens, F., Fransz, P. and Bai, Y.** (2020)

CRISPR/Cas inactivation of RECQ4 increases homeologous crossovers in an interspecific tomato hybrid. *Plant Biotechnol. J.*, **18**, 805–813.

- Madic, J., Zocevic, A., Senlis, V., Fradet, E., Andre, B., Muller, S., Dangla, R. and Droniou, M.E.** (2016) Three-color crystal digital PCR. *Biomol. Detect. Quantif.*, **10**, 34–46.
- Mainiero, S. and Pawlowski, W.P.** (2014) Meiotic chromosome structure and function in plants. *Cytogenet. Genome Res.*, **143**, 6–17.
- Marfil, C.F., Asurmendi, S. and Masuelli, R.W.** (2012) Changes in micro RNA expression in a wild tuber-bearing *Solanum* species induced by 5-Azacytidine treatment. *Plant Cell Rep.*, **31**, 1449–1461.
- Marii, L. and Chiriac, G.** (2009) The role of viral infection in inducing variability in virus-free progeny in tomato. *J. Integr. Plant Biol.*, **51**, 476–488.
- Martín, A.C., Shaw, P., Phillips, D., Reader, S. and Moore, G.** (2014) Licensing MLH1 sites for crossover during meiosis. *Nat. Commun.*, **5**.
- Mase, N., Sawamura, Y., Yamamoto, T., Takada, N., Nishio, S., Saito, T. and Iketani, H.** (2014) Direct genotyping of single pollen grains of a self-compatible mutant of Japanese pear (*Pyrus pyrifolia*) revealed inheritance of a duplicated chromosomal segment containing a second S-haplotype. *Euphytica*, **200**, 297–304.
- MATHER, K.** (1934) THE BEHAVIOUR OF MEIOTIC CHROMOSOMES AFTER X-IRRADIATION. *Hereditas*, **19**, 303–322.
- Matsuki, Y., Isagi, Y. and Suyama, Y.** (2007) The determination of multiple microsatellite genotypes and DNA sequences from a single pollen grain: Technical article. *Mol. Ecol. Notes*, **7**, 194–198.
- Mayer, K.F.X., Waugh, R., Langridge, P., et al.** (2012) A physical, genetic and functional sequence assembly of the barley genome. *Nature*, **491**, 711–716.
- Melamed-Bessudo, C. and Levy, A.A.** (2012) Deficiency in DNA methylation increases meiotic crossover rates in euchromatic but not in heterochromatic regions in *Arabidopsis*. *Proc. Natl. Acad. Sci. U. S. A.*, **109**, E981–E988.
- Melamed-Bessudo, C., Yehuda, E., Stuitje, A.R. and Levy, A.A.** (2005) A new seed-based assay for meiotic recombination in *Arabidopsis thaliana*. *Plant J.*, **43**.
- Mercier, R., Mézard, C., Jenczewski, E., Macaisne, N. and Grelon, M.** (2015) The molecular biology of meiosis in plants. *Annu. Rev. Plant Biol.*, **66**, 297–327.
- Meyers, B.C., Tingey, S. V. and Morgante, M.** (2001) Abundance, distribution, and transcriptional activity of repetitive elements in the maize genome. *Genome Res.*, **11**, 1660–1676.
- Mirouze, M., Lieberman-Lazarovich, M., Aversano, R., Bucher, E., Nicolet, J., Reinders, J. and Paszkowski, J.** (2012) Loss of DNA methylation affects the recombination landscape in *Arabidopsis*. *Proc. Natl. Acad. Sci. U. S. A.*, **109**, 5880–5885.
- Modliszewski, J.L., Wang, H., Albright, A.R., Lewis, S.M., Bennett, A.R., Huang, J., Ma, H., Wang, Y. and Copenhaver, G.P.** (2018) Elevated temperature increases meiotic crossover frequency via the interfering (Type I) pathway in *Arabidopsis thaliana*. *PLoS Genet.*, **14**, e1007384.
- Muyt, A. De, Zhang, L., Pilot, T., Kleckner, N., Espagne, E. and Zickler, D.** (2014) E3 ligase Hei10: A multifaceted structure-based signaling molecule with roles within and beyond meiosis. *Genes Dev.*, **28**, 1111–1123.
- Noh, E.J., Lim, D.S., Jeong, G. and Lee, J.S.** (2009) An HDAC inhibitor, trichostatin A, induces a delay

at G2/M transition, slippage of spindle checkpoint, and cell death in a transcription-dependent manner. *Biochem. Biophys. Res. Commun.*, **378**, 326–331.

Nonomura, K.I., Morohoshi, A., Nakano, M., Eiguchi, M., Miyao, A., Hirochika, H. and Kurataa, N. (2007) A germ cell-specific gene of the ARGONAUTE family is essential for the progression of premeiotic mitosis and meiosis during sporogenesis in rice. *Plant Cell*, **19**, 2583–2594.

Nottke, A.C., Kim, H.M. and Colaiácovo, M.P. (2017) Wrestling with chromosomes: The roles of SUMO during meiosis. *Adv. Exp. Med. Biol.*, **963**, 185–196.

Ogneva, Z. V., Suprun, A.R., Dubrovina, A.S. and Kiselev, K. V. (2019) Effect of 5-azacytidine induced DNA demethylation on abiotic stress tolerance in Arabidopsis Thaliana. *Plant Prot. Sci.*, **55**, 73–80.

Onn, I., Heidinger-Pauli, J.M., Guacci, V., Ünal, E. and Koshland, D.E. (2008) Sister chromatid cohesion: A simple concept with a complex reality. *Annu. Rev. Cell Dev. Biol.*, **24**, 105–129.

Osman, K., Algotishi, U., Higgins, J.D., Henderson, I.R., Edwards, K.J., Franklin, F.C.H. and Sanchez-Moran, E. (2021) Distal Bias of Meiotic Crossovers in Hexaploid Bread Wheat Reflects Spatio-Temporal Asymmetry of the Meiotic Program. *Front. Plant Sci.*, **12**.

Paigen, K. and Petkov, P.M. (2018) PRDM9 and Its Role in Genetic Recombination. *Trends Genet.*, **34**, 291–300.

Pandey, P., Daghma, D.S., Houben, A., Kumlehn, J., Melzer, M. and Rutten, T. (2017) Dynamics of post-translationally modified histones during barley pollen embryogenesis in the presence or absence of the epi-drug trichostatin A. *Plant Reprod.*, **30**, 95–105.

Parsons, P.A. (1988) Evolutionary rates: effects of stress upon recombination. *Biol. J. Linn. Soc.*, **35**, 49–68.

Pellicer, J. and Leitch, I.J. (2020) The Plant DNA C-values database (release 7.1): an updated online repository of plant genome size data for comparative studies. *New Phytol.*, **226**, 301–305.

Perrella, G., Consiglio, M.F., Aiese-Cigliano, R., et al. (2010) Histone hyperacetylation affects meiotic recombination and chromosome segregation in Arabidopsis. *Plant J.*, **62**, 796–806.

Phillips, D., Jenkins, G., Macaulay, M., et al. (2015) The effect of temperature on the male and female recombination landscape of barley. *New Phytol.*, **208**, 421–429.

Plough, H.H. (1917) The effect of temperature on crossingover in Drosophila. *J. Exp. Zool.*, **24**, 147–209.

Pratto, F., Brick, K., Khil, P., Smagulova, F., Petukhova, G. V. and Camerini-Otero, D. (2014) Recombination initiation maps of individual human genomes. *Science (80-.)*, **346**.

Preuss, D., Rhee, S.Y. and Davis, R.W. (1994) Tetrad analysis possible in Arabidopsis with mutation of the QUARTET (QRT) genes. *Science (80-.)*, **264**, 1458–1460.

Reid, D.A. (2015) Morphology and Anatomy of the Barley Plant., 73–101.

Rey, M.D., Martín, A.C., Smedley, M., Hayta, S., Harwood, W., Shaw, P. and Moore, G. (2018) Magnesium increases homoeologous crossover frequency during meiosis in ZIP4 (Ph1 gene) mutant wheat-wild relative hybrids. *Front. Plant Sci.*, **9**.

Rommel Fuentes, R., Hesselink, T., Nieuwenhuis, R., et al. (2020) Meiotic recombination profiling of interspecific hybrid F1 tomato pollen by linked read sequencing. *Plant J.*, **102**, 480–492.

Ross, K.J., Fransz, P., Armstrong, S.J., Vizir, I., Mulligan, B., Franklin, F.C.H. and Jones, G.H. (1997) Cytological characterization of four meiotic mutants of Arabidopsis isolated from T-DNA-

- transformed lines. *Chromosom. Res.*, **5**, 551–559.
- Rowan, B.A., Patel, V., Weigel, D. and Schneeberger, K.** (2015) Rapid and inexpensive whole-genome genotyping-by-sequencing for crossover localization and fine-scale genetic mapping. *G3 Genes, Genomes, Genet.*, **5**, 385–398.
- Saini, R., Singh, A.K., Dhanapal, S., Saeed, T.H., Hyde, G.J. and Baskar, R.** (2017) Brief temperature stress during reproductive stages alters meiotic recombination and somatic mutation rates in the progeny of Arabidopsis. *BMC Plant Biol.*, **17**.
- Saintenac, C., Falque, M., Martin, O.C., Paux, E., Feuillet, C. and Sourdille, P.** (2009) Detailed recombination studies along chromosome 3B provide new insights on crossover distribution in wheat (*Triticum aestivum* L.). *Genetics*, **181**, 393–403.
- Saintenac, C., Faure, S., Remay, A., Choulet, F., Ravel, C., Paux, E., Balfourier, F., Feuillet, C. and Sourdille, P.** (2011) Variation in crossover rates across a 3-Mb contig of bread wheat (*Triticum aestivum*) reveals the presence of a meiotic recombination hotspot. *Chromosoma*, **120**, 185–198.
- Sano, H., Kamada, I., Youssefian, S., Katsumi, M. and Wabiko, H.** (1990) A single treatment of rice seedlings with 5-azacytidine induces heritable dwarfism and undermethylation of genomic DNA. *MGG Mol. Gen. Genet.*, **220**, 441–447.
- Santana, I., Wu, H., Hu, P. and Giraldo, J.P.** (2020) Targeted delivery of nanomaterials with chemical cargoes in plants enabled by a biorecognition motif. *Nat. Commun.*, **11**.
- Saze, H., Tsugane, K., Kanno, T. and Nishimura, T.** (2012) DNA methylation in plants: Relationship to small rnas and histone modifications, and functions in transposon inactivation. *Plant Cell Physiol.*, **53**, 766–784.
- Serra, H., Lambing, C., Griffin, C.H., et al.** (2018) Massive crossover elevation via combination of HEI10 and recq4a recq4b during Arabidopsis meiosis. *Proc. Natl. Acad. Sci. U. S. A.*, **115**, 2437–2442.
- Sidhu, G.K., Fang, C., Olson, M.A., Falque, M., Martin, O.C. and Pawlowski, W.P.** (2015) Recombination patterns in maize reveal limits to crossover homeostasis. *Proc. Natl. Acad. Sci. U. S. A.*, **112**, 15982–15987.
- Sidhu, R.K.** (2019) Pollen storage in vegetable crops: A review. *J. Pharmacogn. Phytochem.*, **SP1**, 599–603.
- Sinha, R.P. and Helgason, S.B.** (1969) The action of actinomycin D and diepoxybutane on recombination of two closely linked loci in *Hordeum*. *Can. J. Genet. Cytol.*, **11**, 745–751.
- Solís, M.T., El-Tantawy, A.A., Cano, V., Risueño, M.C. and Testillano, P.S.** (2015) 5-azacytidine promotes microspore embryogenesis initiation by decreasing global DNA methylation, but prevents subsequent embryo development in rapeseed and barley. *Front. Plant Sci.*, **6**.
- Sommermeier, V., Béneut, C., Chaplais, E., Serrentino, M.E. and Borde, V.** (2013) Spp1, a Member of the Set1 Complex, Promotes Meiotic DSB Formation in Promoters by Tethering Histone H3K4 Methylation Sites to Chromosome Axes. *Mol. Cell*, **49**, 43–54.
- Soppe, W.J.J., Jasencakova, Z., Houben, A., Kakutani, T., Meister, A., Huang, M.S., Jacobsen, S.E., Schubert, I. and Fransz, P.F.** (2002) DNA methylation controls histone H3 lysine 9 methylation and heterochromatin assembly in Arabidopsis. *EMBO J.*, **21**, 6549–6559.
- Steffensen, D.** (1955) Breakage of chromosomes in *Tradescantia* with a calcium deficiency. *Proc. Natl. Acad. Sci.*, **41**, 155–160.

- Sun, H., Rowan, B.A., Flood, P.J., Brandt, R., Fuss, J., Hancock, A.M., Michelmore, R.W., Huettel, B. and Schneeberger, K.** (2019) Linked-read sequencing of gametes allows efficient genome-wide analysis of meiotic recombination. *Nat. Commun.*, **10**.
- Sybenga, J.** (1960) The effect of gamma rays on, frequency and localization of chiasmata in *Crotalaria intermedia*. *Eff. gamma rays on, Freq. localization chiasmata Crotalaria intermedia.*, **12**.
- Tachibana, M., Sugimoto, K., Nozaki, M., et al.** (2002) G9a histone methyltransferase plays a dominant role in euchromatic histone H3 lysine 9 methylation and is essential for early embryogenesis. *Genes Dev.*, **16**, 1779–1791.
- Thomas, W.T.B., Bull, H., Booth, A., Hamilton, R., Forster, B.P. and Franckowiak, J.D.** (2019) A practical guide to barley crossing. In *Methods in Molecular Biology*. 21–36.
- Tian, L. and Chen, Z.J.** (2001) Blocking histone deacetylation in Arabidopsis induces pleiotropic effects on plant gene regulation and development. *Proc. Natl. Acad. Sci. U. S. A.*, **98**, 200–205.
- Toby, G.G., Gherraby, W., Coleman, T.R. and Golemis, E.A.** (2003) A Novel RING Finger Protein, Human Enhancer of Invasion 10, Alters Mitotic Progression through Regulation of Cyclin B Levels. *Mol. Cell. Biol.*, **23**, 2109–2122.
- Tottman, D.R.** (1987) The decimal code for the growth stages of cereals, with illustrations. *Ann. Appl. Biol.*, **110**, 441–454.
- Tracy, S.R., Gómez, J.F., Sturrock, C.J., Wilson, Z.A. and Ferguson, A.C.** (2017) Non-destructive determination of floral staging in cereals using X-ray micro computed tomography (μ CT). *Plant Methods*, **13**.
- Twell, D.** (2011) Male gametogenesis and germline specification in flowering plants. *Sex. Plant Reprod.*, **24**, 149–160.
- Underwood, C.J., Choi, K., Lambing, C., et al.** (2018) Epigenetic activation of meiotic recombination near Arabidopsis thaliana centromeres via loss of H3K9me2 and non-CG DNA methylation. *Genome Res.*, **28**, 519–531.
- Volk, G.M.** (2011) Chapter 25: Collecting pollen for genetic resources conservation. In *Collecting plant genetic diversity: technical guidelines 2011 update*. (Guarino L, Ramanatha VR, Goldberg E., eds). Rome: Bioversity International., **115**, 1-10.
- Vorontsova, M., Shaw, P., Reader, S. and Moore, G.** (2004) Effect of 5-azacytidine and trichostatin A on somatic centromere association in wheat. *Genome*, **47**, 399–403.
- Waddington, S.R., Cartwright, P.M. and Wall, P.C.** (1983) A quantitative scale of spike initial and pistil development in barley and wheat. *Ann. Bot.*, **51**, 119–130.
- Wang, H.M., Enns, J.L., Nelson, K.L., Brost, J.M., Orr, T.D. and Ferrie, A.M.R.** (2019) Improving the efficiency of wheat microspore culture methodology: evaluation of pretreatments, gradients, and epigenetic chemicals. *Plant Cell. Tissue Organ Cult.*, **139**, 589-599.
- Wang, J.W., Grandio, E.G., Newkirk, G.M., Demirer, G.S., Butrus, S., Giraldo, J.P. and Landry, M.P.** (2019) Nanoparticle-Mediated Genetic Engineering of Plants. *Mol. Plant*, **12**, 1037–1040.
- Wang, K., Wang, M., Tang, D., Shen, Y., Miao, C., Hu, Q., Lu, T. and Cheng, Z.** (2012) The role of rice HEI10 in the formation of meiotic crossovers. *PLoS Genet.*, **8**.
- Wang, M., Wang, K., Tang, D., Wei, C., Li, M., Shen, Y., Chi, Z., Gu, M. and Cheng, Z.** (2010) The central element protein ZEP1 of the synaptonemal complex regulates the number of crossovers during meiosis in rice. *Plant Cell*, **22**, 417–430.

- Wang, Y. and Copenhaver, G.P.** (2018) Meiotic Recombination: Mixing It Up in Plants. *Annu. Rev. Plant Biol.*, **69**, 577–609.
- Wu, G., Rossivivito, G., Hu, T., Berlyand, Y. and Poethig, R.S.** (2015) Traffic lines: New tools for genetic analysis in *Arabidopsis thaliana*. *Genetics*, **200**, 35–45.
- Wu, K., Malik, K., Tian, L., Brown, D. and Miki, B.** (2000) Functional analysis of a RPD3 histone deacetylase homologue in *Arabidopsis thaliana*. *Plant Mol. Biol.*, **44**, 167–176.
- Xu, C.R., Liu, C., Wang, Y.L., Li, L.C., Chen, W.Q., Xu, Z.H. and Bai, S.N.** (2005) Histone acetylation affects expression of cellular patterning genes in the *Arabidopsis* root epidermis. *Proc. Natl. Acad. Sci. U. S. A.*, **102**, 14469–14474.
- Xue, M., Wang, J., Jiang, L., Wang, M., Wolfe, S., Pawlowski, W.P., Wang, Y. and He, Y.** (2018) The number of meiotic double-strand breaks influence crossover distribution in *Arabidopsis*. *Plant Cell*, **30**, 2628–2638.
- Yamada, S., Ohta, K. and Yamada, T.** (2013) Acetylated Histone H3K9 is associated with meiotic recombination hotspots, and plays a role in recombination redundantly with other factors including the H3K4 methylase Set1 in fission yeast. *Nucleic Acids Res.*, **41**, 3504–3517.
- Yamada, T., Mizuno, K.I., Hirota, K., Kon, N., Wahls, W.P., Hartsuiker, E., Murofushi, H., Shibata, T. and Ohta, K.** (2004) Roles of histone acetylation and chromatin remodeling factor in a meiotic recombination hotspot. *EMBO J.*, **23**, 1792–1803.
- Yang, F., Zhang, L., Li, J., Huang, J., Wen, R., Ma, L., Zhou, D. and Li, L.** (2010) Trichostatin A and 5-azacytidine both cause an increase in global histone H4 acetylation and a decrease in global DNA and H3K9 methylation during mitosis in maize. *BMC Plant Biol.*, **10**, 178.
- Yang, Q., Lu, Z., Singh, D. and Raj, J.U.** (2012) BIX-01294 treatment blocks cell proliferation, migration and contractility in ovine foetal pulmonary arterial smooth muscle cells. *Cell Prolif.*, **45**, 335–344.
- Yant, L., Hollister, J.D., Wright, K.M., Arnold, B.J., Higgins, J.D., Franklin, F.C.H. and Bomblies, K.** (2013) Meiotic Adaptation to Genome Duplication in *Arabidopsis arenosa*. *Curr. Biol.*, **23**, 2151–2156.
- Yao, X., Feng, H., Yu, Y., Dong, A. and Shen, W.H.** (2013) SDG2-Mediated H3K4 Methylation Is Required for Proper *Arabidopsis* Root Growth and Development. *PLoS One*, **8**.
- Yelina, N., Diaz, P., Lambing, C. and Henderson, I.R.** (2015) Epigenetic control of meiotic recombination in plants. *Sci. China Life Sci.*, **58**, 223–231.
- Yelina, N.E., Choi, K., Chelysheva, L., et al.** (2012) Epigenetic Remodeling of Meiotic Crossover Frequency in *Arabidopsis thaliana* DNA Methyltransferase Mutants. *PLoS Genet.*, **8**.
- Yelina, N.E., Lambing, C., Hardcastle, T.J., Zhao, X., Santos, B. and Henderson, I.R.** (2015) DNA methylation epigenetically silences crossover hot spots and controls chromosomal domains of meiotic recombination in *Arabidopsis*. *Genes Dev.*, **29**, 2183–2202.
- Yelina, N.E., Ziolkowski, P.A., Miller, N., Zhao, X., Kelly, K.A., Muñoz, D.F., Mann, D.J., Copenhaver, G.P. and Henderson, I.R.** (2013) High-throughput analysis of meiotic crossover frequency and interference via flow cytometry of fluorescent pollen in *Arabidopsis thaliana*. *Nat. Protoc.*, **8**.
- Yoshida, M., Kijima, M., Akita, M. and Beppu, T.** (1990) Potent and specific inhibition of mammalian histone deacetylase both in vivo and in vitro by trichostatin A. *J. Biol. Chem.*, **265**, 17174–17179.
- You, B.R. and Park, W.H.** (2012) Zebularine inhibits the growth of HeLa cervical cancer cells via cell cycle arrest and caspase-dependent apoptosis. *Mol. Biol. Rep.*, **39**, 9723–9731.

- Zadoks, J.C., Chang, T.T. and Konzak, C.F.** (1974) A decimal code for the growth stages of cereals. *Weed Res.*, **14**, 415–421.
- Zelkowski, M., Olson, M.A., Wang, M. and Pawlowski, W.** (2019) Diversity and Determinants of Meiotic Recombination Landscapes. *Trends Genet.*, **35**, 359–370.
- Zhang, L., Wang, S., Yin, S., Hong, S., Kim, K.P. and Kleckner, N.** (2014) Topoisomerase II mediates meiotic crossover interference. *Nature*, **511**, 551–556.
- Zhang, P., Zhang, Y., Sun, L., et al.** (2017) The rice AAA-ATPase *osfign1* is essential for male meiosis. *Front. Plant Sci.*, **8**.
- Zhou, G., Zhang, Q., Tan, C., Zhang, X. qi and Li, C.** (2015) Development of genome-wide InDel markers and their integration with SSR, DArT and SNP markers in single barley map. *BMC Genomics*, **16**.
- Zhou, L., Cheng, X., Connolly, B.A., Dickman, M.J., Hurd, P.J. and Hornby, D.P.** (2002) Zebularine: A novel DNA methylation inhibitor that forms a covalent complex with DNA methyltransferases. *J. Mol. Biol.*, **321**, 591–599.
- Zhu, T., Li, L., Feng, L., Mo, H. and Ren, M.** (2020) Target of Rapamycin Regulates Genome Methylation Reprogramming to Control Plant Growth in Arabidopsis. *Front. Genet.*, **11**.
- Zhu, Y., Zhang, Y.X., Liu, W.W., Ma, Y., Fang, Q. and Yao, B.** (2015) Printing 2-Dimensional Droplet Array for Single-Cell Reverse Transcription Quantitative PCR Assay with a Microfluidic Robot. *Sci. Rep.*, **5**.
- Zickler, D. and Kleckner, N.** (1999) Meiotic chromosomes: Integrating structure and function. *Annu. Rev. Genet.*, **33**, 603–754.
- Ziolkowski, P.A., Berchowitz, L.E., Lambing, C., et al.** (2015) Juxtaposition of heterozygous and homozygous regions causes reciprocal crossover remodelling via interference during Arabidopsis meiosis. *Elife*, **4**.
- Ziolkowski, P.A., Underwood, C.J., Lambing, C., et al.** (2017) Natural variation and dosage of the HEI10 meiotic E3 ligase control Arabidopsis crossover recombination. *Genes Dev.*, **31**, 306–317.

10. Abbreviations

CO: Crossover
Crystal dPCR: Crystal Digital PCR
DAPI: 4',6-diamidino-2-phenylindole
dHj: Double Holliday junction
D-loop: Displacement loop
DSBs: Double strand breaks
EDTA: Ethylenediamine tetra-acetic acid
EdU: 5-ethynyl-2'deoxyuridine
FACS: Fluorescence-activated cell sorting
FTLs: Fluorescent transgenic lines
GBS: Genotyping-by-sequencing
HR: Homologous recombination
KASP: Kompetitive Allele-Specific PCR
LE: Lateral elements
NCO: Non-crossover
PTMs: Post-translational modifications
qPCR: Quantitative PCR
SC: Synaptonemal complex
SDSA: Synthesis-dependent strand annealing
SUMO: Small ubiquitin-like modifier
TF: Transverse filaments
TSA: Trichostatin A
WGA: Whole-genome amplification
WT: Wild type

11. Acknowledgements

I am extremely grateful that one of the milestones in my life is finishing. To come to this point, I have received supports from countless people. I would like to thank my supervisor, Stefan Heckmann, who must have gone through hard time (I would like to say not too often!) supervising me! I deeply appreciated his way of supervising a PhD student into an independent scientist, and the fact that I was able to talk to him whenever I wanted to. This is the biggest advantage of being his student, that I know I can discuss problems with him. Therefore, I sincerely appreciate his supports throughout this journey.

Andreas Houben, who always shared great jokes, warm greetings and rational advices as a supervisor. His insights and comments were always something that I missed, and I couldn't be more appreciated for his help on this. I also had no problem to talk or discuss any problems with him, and I am aware of his effort to look out for everyone as much as possible. Most importantly, if he ignored my email in 2017, I couldn't even thought that I would do PhD in IPK.

And Jörg Fuchs, a mentor, a scientist, a supervisor, a dark-fur-business CEO, a Glühwein controller and so on (I will stop here to save his social reputation). I honestly think it would have been impossible for me to come to this point if he wasn't there. There are plenty of things I would like to thank him, but the flow-sorting pollen nuclei appointments were the most fruitful scientific&philosophical discussions I would miss the most! And I would like to notify him again here, that the way to my greenhouse is shorter when you take the library road, not through the building. End of discussion. And I hope he keeps my lottery payout, I will check it when I visit Germany again. Together with another fur business CEO, Ivona Kubalova, we had wonderful evenings through running (?) rituals. Both of them claim that I do not listen to them while they are talking, which is not true at all, I would like to demonstrate the situation again. I will miss all the great times we shared together.

And last but not least, team Meiosis. There were always Jana Lorenz, Franziska Hartmann and Marius Dölling who took the trouble to help my work, the biggest help in the lab. I may have not expressed it enough, I truly admired their dedication. And my fellow PhD students, Mohammad Ayoub and Stefan Steckenborn, I know for sure we all will be alright. And I will miss the chats I shared with Mo, who was my office mate! Furthermore, I have received big help from gardeners, especially Kathrin Tiemann, on raising barley plants in such a great condition so that I was able to perform experiments without problems. And I thank Britt Leps, who helped me tremendously from the start to the end.

마지막으로 저의 가족과 친구들에게 감사합니다. 부족한 저를 항상 믿어주시고, 위로해주시고 곁에 있어주셔서 감사합니다. 소중한 이 경험을 토대로 앞으로 더 큰 사람으로, 스스로 살피고 주변도 잘 돌보는 사람으로 성장하겠습니다. 감사합니다.

Yun-Jae Ahn

Date of Birth: 1993. 01. 21.
E-mail: yjahn0121@gmail.com
Cell: +82 1067605153

Education

- Ph.D. Student** Plant Meiosis and Breeding
Leibniz Institute of Plant Genetics and Crop Plant Research (IPK), Germany
(2018. 01. - 2021. 06.)
Thesis title: Development and application of Crystal Digital PCR-based single pollen nucleus genotyping to measure meiotic recombination rates in barley (*Hordeum vulgare*) in high-throughput
Advisor: Dr. Stefan Heckmann and Prof. Dr. Andreas Houben
- M.Sc.** Flower Genetics and Breeding (Horticultural Science)
Kyungpook National University, Republic of Korea
(2015. 03. - 2017. 02.)
Thesis title: Investigation of Karyotypic Composition and Evolution in *Lilium* Species belonging to Section Martagon
Advisor: Prof. Dr. Ki-Byung Lim
Final Grade: 4.1/4.3
- B.Sc.** Horticultural Science
Kyungpook National University, Republic of Korea
(2011. 03 - 2015. 02)
Final Grade: 3.61/4.3

Research and Work Experience

Institute for Basic Science (IBS), Daegu, Republic of Korea

- *Researcher* 2017. 05 - 2017. 10.

Center for Plant Aging Research

- Focus on the flower senescence of *Arabidopsis* via RNA *in situ* hybridization

List of Publications from PhD Thesis

- 1) **YJ. Ahn**, J. Fuchs, A. Houben and S. Heckmann "High-throughput Measuring of Meiotic Recombination Rates in Barley Pollen Nuclei using Crystal Digital PCR™", *The Plant Journal* (2021)
- 2) **YJ. Ahn**, M. Cuacos, M. A. Ayoub, J. Kappermann, A. Houben and S. Heckmann "*In planta* Delivery of Chemical Compounds into Barley Meiocytes: EdU as Compound Example", *Plant Meiosis* (2020)

List of Other Publications (ORCID ID: <https://orcid.org/0000-0002-6510-3532>)

- 1) **YJ. Ahn**, YJ. Hwang, A. Younis, MS. Sung, F. Ramzan, MJ Kwon, YI Kang, CK. Kim and KB. Lim “Investigation of Karyotypic Composition and Evolution in *Lilium* Species belonging to the Section Martagon”, Plant Biotechnology Reports (2017)
- 2) MJ. Kwon, F. Ramzan, **YJ. Ahn**, YJ. Hwang, YI. Kang, CK. Kim, A. Younis and KB. Lim “Chromosomal Analysis of *Lilium Longiflorum*×Asiatic Hybrids using GISH (Genomic *in situ* hybridization)”, Horticulture, Environment, and Biotechnology (2017)

Abstracts

- 1) **YJ. Ahn**, J. Fuchs, A. Houben and S. Heckmann “Measuring meiotic recombination rates in barley pollen nuclei in high-throughput with Crystal Digital PCR” Korean Breeding Science Conference (2021)
- 2) **YJ. Ahn**, M. Ayoub, M. Cuacos, S. Dreissig, C. Feng, J. Lorenz, S. Steckenborn and S. Heckmann “Towards Harnessing Meiosis in Barley” Plant and Animal Genome XXVII Conference (2019)
- 3) **YJ. Ahn**, Min-Ji Kwon, Fahad Ramzan, Young-Kwan Jo, Ki-Byung Lim. Cytogenetic Analysis of Repetitive Sequences in *L. hansonii*. HORTICULTURE ABSTRACTS (2016)
- 4) **YJ. Ahn** Genetic and Cytogenetic Analysis of section Martagon *Lilium* species in Jeju Island, S.Korea (2016)
- 5) **YJ. Ahn**, Min-Ji Kwon, Fahad Ramzan, Ge Guo, Ki-Byung Lim. Karyotype Analysis of Several *Lilium* Species in Archelirion Section. HORTICULTURE ABSTRACTS (2015)
- 6) **YJ. Ahn**, Yoon-Jung Hwang, Min-Ji Kwon, Fahad Ramzan, Ge Guo, Ki-Byung Lim. “Genetic Diversity of an Unidentified Wild Species of Martagon Section *Lilium* Domesticated in Jeju Island Revealed by FISH.” HORTICULTURE ABSTRACTS (2015)

Selected Honors and Rewards

- 1) **Early-Stage Researcher (ESR) MEICOM network: Marie Skłodowska-Curie Actions Innovative Training Network (ITN) H2020-MSCA-ITN-2017** (PhD project)
- 2) Outstanding Oral Presentation award, Korean Breeding Science Conference, 2021

Skills and Techniques

- 1) Digital PCR/Real-time quantitative PCR and PCR based genotyping
- 2) Quantitative Reverse Transcription PCR
- 3) Flowcytometry
- 4) Pollen/leaf/root nuclei isolation & DNA/RNA isolation
- 5) Fluorescence microscopy/Stereo microscopy
- 6) Crossing/Cultivation
- 7) Cloning/Transformation
- 8) Tissue culture/Cell culture
- 9) Karyotyping and *In situ* hybridization (FISH/GISH/RISH)
- 10) Microtome dissection
- 11) *In planta* injection

Secondments

- 1) University of Leicester, United Kingdom (2019. 02)
Training in molecular cytogenetics in barley and wheat
-

Trainings

- 1) Inaugural Meeting, Birmingham, United Kingdom (2018.07)
Workshop on Plant Meiotic Recombination
 - 2) MEICOM Bioinformatics Workshop, Wageningen University and Research, Netherlands (2019. 02)
 - 3) MEICOM 1st Annual Meeting, Madrid, Spain (2019. 06)
Workshop in Advances in Meiotic Recombination
Workshop in Presentation Skills
 - 4) Droplet Digital PCR System Training, Stilla Technologies, France (2018. 04)
 - 5) Droplet Digital PCR System Training, IPK Gatersleben, Germany (2018. 06 and 2018. 11)
 - 6) Annual Report with thesis committees and MEICOM network
-

Teaching Experiences

- 1) Supervising three master students, IPK Gatersleben, Germany (2018-2020)
 - 2) Student Tutoring in Control of Diseases and Insect Pests (2014)
 - 3) Student Tutoring in General Botany, Kyungpook National University (2013)
 - 4) Student Tutoring in Plant Growth Regulator, Kyungpook National University (2013)
-

Outreach

- 1) Think Tank “Meet the Scientist”, Think Tank Museum of Birmingham, United Kingdom (2019)
-

Conferences & Talks

- 1) Oral presentation, Korean Breeding Science Conference, Republic of Korea (2021)
 - 2) Poster, EMBO workshop in Meiosis, La Rochelle, France (2019)
 - 3) Poster, 22nd International Chromosome Conference, Prague, Czech Republic (2018)
 - 4) Poster, 14th Plant Science Student Conference (PSSC), IPK, Germany (2018)
 - 5) Poster, EMBO workshop in Plant Genome Stability and Change, IPK, Germany (2018)
 - 6) Webinar on nucleus genotyping using Crystal Digital PCRTM, Global engagement&Stilla Technologies (2021)
-

References

- 1) Dr. Stefan Heckmann (Meiosis, IPK Gatersleben, Germany)
e-mail: heckmann@ipk-gatersleben.de
- 2) Prof. Dr. Andreas Houben (Chromosome Structure and Function, IPK Gatersleben, Germany)
e-mail: houben@ipk-gatersleben.de
- 3) Dr. Joerg Fuchs (Chromosome Structure and Function, IPK Gatersleben, Germany)
e-mail: fuchs@ipk-gatersleben.de
- 4) Prof. Dr. Ki-Byung Lim (Horticultural Science Department, Kyungpook National University, Republic of Korea)
e-mail: kblim@knu.ac.kr

Eidesstattliche Erklärung / Declaration under Oath

Ich erkläre an Eides statt, dass ich die Arbeit selbstständig und ohne fremde Hilfe verfasst, keine anderen als die von mir angegebenen Quellen und Hilfsmittel benutzt und die den benutzten Werken wörtlich oder inhaltlich entnommenen Stellen als solche kenntlich gemacht habe.

I declare under penalty of perjury that this thesis is my own work entirely and has been written without any help from other people. I used only the sources mentioned and included all the citations correctly both in word or content.

Datum / Date

Unterschrift des Antragstellers / *Signature of the applicant*

13. Appendix

Appendix 1. Measured meiotic recombination rates within four chromosomal intervals: Ic 1, Ic 3, Id 3-1 and Id 3-2.

Interval Ic 1 (1029 + 1076)													
Plant	Ch.	Positive droplets			Double nuclei encapsulations				B+M calls w/o nuclei	Corrected + normalized values		Rec. call rate	Rec. rate
		B+B	M+M	B+M	total	no signal	B+B/M+M	B+M		Parental calls	Recomb. calls		
M1 + B1	1	142	119	12	9	0	0	9	0	238	3		
	2	173	78	4	3	0	0	3	0	156	1		
	3	142	129	5	4	1	2	1	0	256	4		
	4	92	99	24	49	19	10	20	0	174	4		
	5	111	161	21	35	10	6	19	0	217	2		
	6	167	147	9	6	2	0	4	0	294	5		
	sum									1335	19		
M2 + B2	7	117	156	2	4	1	2	1	0	232	1		
	8	133	199	4	6	1	2	3	0	264	1		
	9	165	135	3	5	1	3	1	0	267	2		
	10	157	162	12	18	3	4	11	0	310	1		
	11	176	110	5	5	1	2	2	0	218	3		
	12	146	126	8	6	1	2	3	0	250	5		
	sum									1541	13		
M3 + B3	13	133	137	7	7	2	3	2	0	263	5		
	14	143	169	10	7	2	3	2	0	283	8		
	15	119	116	6	5	1	2	2	0	230	4		
	16	115	95	2	4	1	3	0	0	187	2		
	17	129	104	7	6	1	2	3	0	206	4		
	18	94	106	7	7	2	2	3	0	186	4		
	sum									1355	27		
M4 + B4	19	81	102	2	5	1	3	1	0	159	1		
	20	87	119	1	7	2	4	1	0	171	0		
	21	64	116	3	7	2	3	2	0	126	1		
	22	83	109	1	5	2	2	1	0	164	0		
	sum									620	2		
M5 + B5	23	88	89	5	6	2	2	2	0	174	3		
	24	98	134	9	6	2	3	1	0	193	8		
	25	108	116	14	4	2	2	0	0	214	14		
	26	104	128	7	5	1	3	1	0	205	6		
	sum									786	31		
M6 + B6	27	114	116	2	1	0	0	1	0	228	1		
	28	115	125	1	1	0	0	1	0	230	0		
	sum									458	1		
Total										6095	93	1.5	

Interval Ic 1 (1029 + 1076)													
Plant	Ch.	Positive droplets			Double nuclei encapsulations				B+M calls w/o nuclei	Corrected + normalized values		Rec. call rate	Rec. rate
		B+B	M+M	B+M	total	no signal	B+B/M+M	B+M		Parental calls	Recomb calls		
H1	1	176	160	41	6	0	0	6	0	320	35		
	2	203	216	36	9	2	4	3	0	402	33		
	3	185	151	42	7	1	1	5	0	301	37		
	4	139	172	55	45	10	15	20	0	265	35		
	sum										1288	140	9.8
H2	5	83	87	17	3	0	3	0	0	164	17		
	6	111	104	31	6	2	3	1	0	206	30		
	7	90	85	12	4	1	3	0	0	168	12		
	8	131	158	31	8	2	0	6	0	262	25		
	9	133	120	29	9	3	2	4	0	238	25		
	10	160	210	35	13	2	4	7	0	316	28		
sum										1354	137	9.2	7.7
H3	11	129	132	28	5	1	1	3	0	258	25		
	12	153	159	18	4	1	3	0	0	304	18		
	13	82	87	18	5	0	2	3	0	162	15		
	14	127	132	31	7	0	2	5	0	252	26		
	15	116	114	24	8	2	2	4	0	226	20		
	16	120	116	31	9	2	2	5	0	230	26		
sum										1432	130	8.3	6.8
H4	17	203	212	35	5	1	1	3	0	406	32		
	18	150	157	34	7	2	3	2	0	298	32		
	sum										704	64	8.3
H5	19	128	101	38	10	3	2	5	0	200	33		
	20	123	122	16	10	3	3	4	0	242	12		
	21	130	131	30	8	3	3	2	0	258	28		
	22	147	125	22	7	2	3	2	0	248	20		
sum										948	93	8.9	7.4
H6	23	125	148	20	1	0	0	1	3	248	19		
	24	127	131	19	2	0	0	2	2	252	17		
	25	56	95	11	1	0	0	1	0	112	10		
	26	103	119	17	5	0	0	5	0	206	12		
	27	135	130	29	6	0	0	6	0	260	23		
	28	120	109	21	1	0	0	1	1	218	20		
sum										1296	101	7.2	5.7
Total										7022	665	8.6	7.1

Interval Ic 3 (3039 + SNP6)													
Plant	Ch.	Positive droplets			Double nuclei encapsulations				B+M calls w/o nuclei	Corrected + normalized values		Rec. call rate	Rec. rate
		B+B	M+M	B+M	total	no signal	B+B/M+M	B+M		Parental calls	Recomb. calls		
M1 + B1	1	227	225	5	5	1	1	3	0	450	2		
	2	223	237	9	8	3	3	2	0	444	7		
	3	201	191	14	5	1	1	3	0	382	11		
	4	184	220	11	7	1	2	4	0	366	7		
	5	199	249	13	7	2	3	2	0	396	11		
	6	292	223	15	4	1	0	3	0	446	12		
	sum										2484	50	
M2 + B2	7	109	142	5	5	1	1	3	0	218	2		
	8	107	105	3	7	2	3	2	0	208	1		
	9	129	118	4	6	3	1	2	0	236	2		
	10	91	70	6	4	0	0	4	0	140	2		
	11	42	50	17	16	2	2	12	0	82	5		
	12	41	60	20	11	3	2	6	0	80	14		
	sum										964	26	
M3 + B3	13	117	109	7	5	1	3	1	0	216	6		
	14	97	79	10	5	0	1	4	0	158	6		
	15	112	123	3	6	2	3	1	0	222	2		
	16	114	69	16	10	2	2	6	0	136	10		
	17	98	77	22	7	0	2	5	0	152	17		
	18	108	96	23	7	1	2	4	0	190	19		
	sum										1074	60	
M4 + B4	19	102	71	3	4	1	1	2	0	142	1		
	20	79	70	0	6	3	3	0	0	138	0		
	21	95	61	0	6	2	4	0	0	118	0		
	sum										398	1	
M5 + B5	22	76	92	8	7	2	2	3	0	150	5		
	23	77	86	18	10	3	4	3	0	150	15		
	24	92	115	19	7	2	1	4	0	184	15		
	25	113	142	7	9	2	3	4	0	224	3		
	26	109	110	27	8	3	2	3	0	216	24		
	sum										924	38	
M6 + B6	27	97	92	2	0	0	0	0	0	184	2		
	28	121	132	5	2	0	0	2	0	242	3		
	sum										426	5	
Total										6270	180	2.8	

Interval Ic 3 (3039 + SNP6)													
Plant	Ch.	Positive droplets			Double nuclei encapsulations				B+M calls w/o nuclei	Corrected + normalized values		Rec. call rate	Rec. rate
		B+B	M+M	B+M	total	no signal	B+B/M+M	B+M		Parental calls	Recomb. calls		
H1	1	145	129	19	5	1	2	2	0	256	17		
	2	114	100	27	5	1	1	3	0	200	24		
	3	130	119	35	8	2	1	5	0	238	30		
	4	128	102	21	6	1	5	0	0	200	21		
	5	133	117	13	6	2	4	0	0	230	13		
	6	159	118	25	5	1	2	2	0	230	23		
	sum										894	92	9.3
H2	7	120	135	55	25	3	6	16	0	238	39		
	8	136	158	35	12	2	2	8	0	270	27		
	9	106	95	38	8	0	2	6	0	188	32		
	10	135	64	55	22	2	3	17	0	126	38		
	11	112	72	46	35	10	7	18	0	138	28		
	12	104	87	38	25	5	5	15	0	170	23		
	sum										1130	187	14.2
H3	13	143	153	25	9	1	1	7	0	286	18		
	14	154	173	24	10	2	2	6	0	306	18		
	15	162	147	16	7	3	2	2	0	292	14		
	16	177	129	32	9	2	2	5	0	256	27		
	17	107	96	42	9	1	1	7	0	192	35		
	18	97	102	10	3	0	3	0	0	192	10		
	sum										1524	122	7.4
H4	19	199	219	30	11	3	3	5	2	394	23		
	20	244	244	48	15	2	5	8	3	480	37		
	21	188	185	32	13	2	4	7	2	364	23		
	sum										874	60	6.4
H5	22	102	98	20	7	1	3	3	0	194	17		
	23	105	90	16	6	2	4	0	0	176	16		
	24	93	121	29	7	2	2	3	0	184	26		
	sum										554	59	9.6
H6	25	133	123	18	5	0	0	5	1	246	12		
	26	119	120	20	3	0	0	3	1	238	16		
	27	111	96	22	4	0	0	4	1	192	17		
	28	106	105	15	1	0	0	1	2	208	12		
	29	86	91	11	2	0	0	2	0	172	9		
	30	100	118	12	3	0	0	3	0	200	9		
	sum										1256	75	5.6
Total										6232	595	8.8	6.0

Interval Id 3-1 (3118 + 3135)													
Plant	Ch.	Positive droplets			Double nuclei encapsulations				B+M calls w/o nuclei	Corrected + normalized values		Rec. call rate	Rec. rate
		B+B	M+M	B+M	total	no signal	B+B/M+M	B+M		Parental calls	Recomb. calls		
M1 + B1	1	179	203	3	13	3	8	2	0	350	1		
	2	188	171	2	8	5	2	1	0	340	1		
	3	215	204	5	5	2	0	3	1	408	1		
	4	206	207	6	6	3	1	2	1	412	3		
	sum										1510	6	
M2 + B2	5	157	152	1	11	3	7	1	0	298	0		
	6	216	144	5	8	2	4	2	0	284	3		
	7	153	158	2	6	2	3	1	0	304	1		
	8	226	121	8	15	8	4	3	0	240	5		
	sum										1126	9	
M3 + B3	9	225	219	1	2	1	1	0	0	438	1		
	10	299	365	1	2	0	1	1	0	598	0		
	11	189	386	6	8	2	2	4	0	376	2		
	12	299	391	9	13	7	0	6	0	598	3		
	sum										2010	6	
M4 + B4	13	152	345	1	3	1	2	0	0	302	1		
	14	145	361	4	1	0	0	1	0	290	3		
	15	150	290	2	7	3	3	1	0	298	1		
	16	244	354	8	8	3	5	0	0	484	8		
	17	185	190	3	3	0	0	3	0	370	0		
	18	127	205	3	11	6	2	3	0	252	0		
	19	148	97	0	3	2	1	0	0	194	0		
	20	155	136	8	4	0	0	4	0	272	4		
	sum										2462	17	
M5 + B5	21	295	214	4	4	1	1	2	0	428	2		
	22	198	216	4	10	5	1	4	0	396	0		
	23	188	208	3	3	0	0	3	0	376	0		
	24	197	164	0	10	4	6	0	0	322	0		
	sum										1522	2	
M6 + B6	25	252	157	4	5	1	1	3	0	314	1		
	26	314	185	4	5	1	1	3	0	370	1		
	27	203	124	1	4	1	2	1	0	246	0		
	28	360	242	6	7	1	3	3	0	482	3		
	29	423	233	3	6	1	3	2	0	464	1		
	30	464	235	3	7	2	2	3	0	468	0		
	sum										2344	6	
M7 + B7	31	150	248	3	3	1	1	1	0	300	2		
	32	68	211	4	4	0	0	4	0	136	0		
	33	93	307	3	2	1	0	1	0	186	2		
	34	129	155	6	3	0	0	3	0	258	3		
	35	109	198	6	2	0	0	2	0	218	4		
	36	143	277	2	5	1	2	2	0	284	0		
	sum										1382	11	

Interval Id 3-1 (3118 + 3135)														
	Plant	Ch.	Positive droplets			Double nuclei encapsulations				B+M calls w/o nuclei	Corrected + normalized values		Rec. call rate	Rec. rate
			B+B	M+M	B+M	total	no signal	B+B/M+M	B+M		Parental calls	Recomb. calls		
Parental genotypes mixed 1:1	M8 + B8	37	116	158	3	7	2	5	0	0	228	3		
		38	92	139	18	3	1	0	2	0	184	16		
		39	79	172	5	1	0	0	1	0	158	4		
		40	106	190	8	3	0	0	3	0	212	5		
		sum										782	28	
	M9 + B9	41	168	81	2	1	0	0	1	0	162	1		
		42	107	74	1	0	0	0	0	0	148	1		
		43	66	89	0	0	0	0	0	0	132	0		
		sum										442	2	
	Total										13580	87	0.6	

Id 3-1 heterozygous	H1	1	129	144	41	4	1	3	0	0	256	41		
		2	150	123	48	4	0	4	0	0	242	48		
	3	156	180	46	8	4	4	0	0	308	46			
	4	165	145	37	1	0	1	0	0	290	37			
	sum										1096	172	13.6	12.9
	H2	5	134	187	48	8	3	5	0	0	264	48		
		6	152	209	60	10	4	6	0	0	298	60		
		7	67	64	32	7	5	2	0	0	126	32		
		8	148	157	59	6	3	3	0	0	294	59		
	sum										982	199	16.9	16.2
	H3	9	208	175	45	1	0	1	0	0	350	45		
		10	172	186	51	2	0	2	0	0	342	51		
		11	176	175	35	5	2	3	0	0	348	35		
12		291	267	60	9	4	5	0	0	530	60			
sum										1570	191	10.8	10.2	
H4	13	167	116	33	10	5	5	0	0	228	33			
	14	151	136	39	5	3	2	0	0	270	39			
	15	145	124	38	12	7	5	0	0	244	38			
	16	148	122	31	1	0	1	0	0	244	31			
	17	275	201	48	22	12	5	5	0	398	43			
	18	318	255	69	6	0	0	6	0	510	63			
	19	144	121	29	12	6	3	3	0	240	26			
	20	182	167	51	12	7	2	3	0	332	48			
	21	152	90	26	15	4	7	4	0	174	22			
	22	88	70	23	7	1	0	6	0	140	17			
	23	130	214	55	8	2	1	5	0	260	50			
24	171	209	57	6	1	0	5	0	342	52				
sum										3382	462	12.0	11.4	
H5	25	98	211	29	8	5	1	2	0	196	27			
	26	132	243	26	6	3	0	3	0	264	23			
	27	104	292	25	2	0	0	2	0	208	23			
	28	105	308	33	8	5	0	3	0	210	30			
	29	176	329	36	3	0	0	3	0	352	33			
sum										1230	136	10.0	9.3	

Interval Id 3-1 (3118 + 3135)															
	Plant	Ch.	Positive droplets			Double nuclei encapsulations				B+M calls w/o nuclei	Corrected + normalized values		Rec. call rate	Rec. rate	
			B+B	M+M	B+M	total	no signal	B+B/M+M	B+M		Parental calls	Recomb. calls			
Id 3-1 heterozygous	H6	30	382	362	90	6	1	1	4	0	724	86			
		31	312	300	85	6	2	1	3	0	600	82			
		32	340	411	97	7	2	2	3	0	678	94			
		33	389	381	98	6	2	1	3	0	762	95			
		34	404	452	133	9	3	1	5	0	808	128			
		35	378	382	97	6	1	1	4	0	756	93			
		sum										4328	578	11.8	11.1
	H7	36	313	313	75	5	1	2	2	0	624	73			
		37	342	349	98	6	0	2	4	0	682	94			
		38	344	332	96	5	0	0	5	0	664	91			
		39	279	298	75	6	3	1	2	0	558	73			
		40	341	360	70	7	1	3	3	0	680	67			
		41	261	281	63	2	0	0	2	0	522	61			
		sum										3730	459	11.0	10.3
	H8	42	215	250	61	11	3	8	0	0	422	61			
		43	168	247	46	3	0	3	0	0	334	46			
		44	166	218	47	3	0	0	3	0	332	44			
		45	180	203	63	3	0	0	3	0	360	60			
			sum										1448	211	12.7
	H9	46	117	130	43	3	0	0	3	0	234	40			
47		114	152	43	2	0	0	2	0	228	41				
48		45	49	17	3	0	0	3	0	90	14				
		sum										552	95	14.7	14.0
	Total										18318	2503	12.6	12.0	

Interval Id 3-2 (3135 + 3152)															
	Plant	Ch.	Positive droplets			Double nuclei encapsulations				B+M calls w/o nuclei	Corrected + normalized values		Rec. call rate	Rec. rate	
			B+B	M+M	B+M	total	no signal	B+B/M+M	B+M		Parental calls	Recomb. calls			
Parental genotypes mixed 1:1	M1 + B1	1	142	102	4	2	0	0	2	0	204	2			
		2	152	106	2	1	0	0	1	0	212	1			
		sum										416	3		
	M2+ B2	3	176	90	5	3	0	0	3	0	180	2			
		4	213	143	9	4	0	0	4	0	286	5			
		sum										466	7		
	M3 + B3	5	161	184	2	1	0	0	1	0	322	1			
		6	118	94	1	1	0	0	1	0	188	0			
		sum										510	1		
		Total										1392	11	0.8	

Id 3-2 heterozygous	H1	1	141	83	33	12	4	2	6	3	162	24			
		2	122	77	31	2	0	0	2	3	152	26			
		3	111	85	18	2	2	0	0	1	170	17			
		sum											484	67	12.2
	H2	4	139	136	42	3	0	0	3	2	276	37			
		5	159	151	46	0	0	0	0	0	302	46			
		6	91	70	28	1	0	0	1	0	140	27			
		7	135	101	21	1	0	0	1	0	202	20			
	sum											920	130	12.4	11.6
	H3	8	204	150	32	2	0	0	2	0	300	30			
		9	208	170	38	1	0	0	1	0	340	37			
		10	194	125	45	1	0	0	1	0	250	44			
		11	213	136	30	2	0	0	2	0	272	28			
		12	204	137	49	3	0	0	3	0	274	46			
		13	170	112	31	1	0	0	1	1	224	29			
	sum											1660	214	11.4	10.6
	H4	14	124	114	32	7	2	4	1	0	224	31			
		15	147	133	30	5	1	4	0	0	262	30			
		16	137	131	32	5	1	3	1	0	260	31			
		17	149	116	17	9	2	7	0	0	226	17			
		18	142	122	30	2	1	0	1	0	244	29			
		19	147	136	25	4	1	3	0	0	270	25			
	sum											1486	163	9.9	9.1
	H5	20	121	101	25	5	2	1	2	0	202	23			
		21	165	159	52	5	0	3	2	0	316	50			
		22	118	113	47	12	5	6	1	0	220	46			
		23	152	112	46	4	2	1	1	2	222	43			
24		118	98	35	7	4	2	1	1	194	33				
25		151	160	48	11	3	7	1	0	296	47				
sum											1450	242	14.3	13.5	
H6	26	61	47	15	2	0	0	2	0	94	13				
	27	45	50	12	2	0	0	2	0	90	10				
	sum											184	23	10.0	9.2
Total											6184	816	11.7	10.9	

Appendix 2. Measured meiotic recombination rates within four chromosomal intervals: Ic 1 and Id 3-1 from chemical compounds injected plants.

Plant	Ch.	Interval Ic 1 (1029+1076)					Interval Id 3-1 (3118+3135)					Rec. call rate	
		Positive droplets			Corrected + normalized values		Positive droplets			Corrected + normalized values			
		B+B	M+M	B+M	Parental calls	Recomb. calls	B+B	M+M	B+M	Parental calls	Recomb. calls		
uninjected	H1	1	97	121	20	194	20	n.d.					
		2	81	99	16	162	16						
		3	42	55	4	90	4						
		4	67	81	13	134	13						
		5	71	65	12	130	12						
		6	49	46	9	92	9						
		sum				802	74	8.4					
	H2	1	129	136	8	258	8	77	105	21	154	21	
		2	192	168	8	332	8	96	131	33	192	33	
		3	126	120	13	226	13	76	86	36	152	36	
		4	116	126	20	232	20	113	141	47	226	47	
		5	121	132	8	242	8	79	121	22	158	22	
		6	149	132	18	264	18	126	157	32	252	32	
		7	127	160	14	254	14	95	89	26	178	26	
			sum				1808	89	4.7			1312	
	H3	1	102	89	8	178	8	92	129	27	184	27	
		2	102	92	13	184	13	84	102	24	168	24	
		3	212	235	32	424	32	212	286	70	424	70	
		4	196	183	20	366	20	187	239	72	374	72	
			sum				1152	73	6.0			1150	
H4	1	104	104	11	208	11	145	168	60	290	60		
	2	151	195	18	302	18	191	223	85	382	85		
	3	193	215	13	386	13	245	265	80	490	80		
	4	183	135	13	270	13	224	199	89	398	89		
		sum				1166	55	4.5			1560		314
Water	H5	1	57	71	11	114	11	88	86	30	172	30	
		2	121	157	22	242	22	165	199	49	330	49	
		3	202	208	44	404	44	245	186	73	372	73	
		4	102	127	15	204	15	134	103	36	206	36	
			sum				964	92	8.7			1080	
	H6	1	154	151	22	302	22	156	155	35	310	35	
		2	126	126	23	252	23	144	127	35	254	35	
		3	89	110	34	118	34	139	145	47	278	47	
		4	49	56	2	98	2	40	71	13	80	13	
	sum				770	81	9.5			922	130	12.4	

Plant	Ch.	Interval Ic 1 (1029+1076)					Rec. call rate	Interval Id 3-1 (3118+3135)					Rec. call rate	
		Positive droplets			Corrected + normalized values			Positive droplets			Corrected + normalized values			
		B+B	M+M	B+M	Parental calls	Recomb. calls		B+B	M+M	B+M	Parental calls	Recomb. calls		
0.05% Silwet L-77	H7	1	42	53	8	84	8	n.d.						
		2	126	121	24	242	24	n.d.						
		sum				326	32	8.9						
	H8	1	162	177	24	324	24	196	227	55	392	55		
		2	162	182	13	324	13	243	219	46	438	46		
		3	160	225	17	320	17	289	271	63	542	63		
		4	175	173	23	346	23	196	188	52	376	52		
		5	143	147	20	286	20	144	174	30	288	30		
		6	242	253	26	484	26	241	231	82	462	82		
		7	153	166	12	306	12	201	257	50	402	50		
		8	239	199	18	398	18	190	228	52	380	52		
		9	176	126	16	252	16	190	247	56	380	56		
		10	163	187	12	326	12	214	237	48	428	48		
	sum				3366	181	5.1				4088	534	11.6	
	H9	1	347	327	55	654	55	n.d.						
		2	299	286	44	572	44	n.d.						
		3	255	286	16	510	16	n.d.						
		4	287	252	34	504	34	n.d.						
		5	292	354	24	584	24	n.d.						
		6	208	209	30	416	30	n.d.						
		7	237	225	37	450	37	n.d.						
		8	308	286	57	572	57	n.d.						
		9	390	353	66	706	66	n.d.						
		10	341	315	49	630	49	n.d.						
		11	299	264	34	528	34	n.d.						
		12	315	363	49	630	49	n.d.						
		13	178	199	28	356	28	n.d.						
	sum				7112	523	6.9							
	Zebularine 0.5µM	H10	1	161	180	50	322	50	n.d.					
			2	228	229	91	456	91	n.d.					
			3	129	144	42	258	42	n.d.					
			4	160	165	42	320	42	n.d.					
			5	175	197	43	350	43	n.d.					
6			188	164	43	328	43	n.d.						
7			107	97	26	194	26	n.d.						
8			111	107	48	214	48	n.d.						
sum					2442	385	13.6							
H11		1	199	197	68	394	68	n.d.						
		2	187	173	63	346	63	n.d.						
		3	174	195	71	348	71	n.d.						
		4	64	71	30	128	30	n.d.						
		5	52	66	25	104	25	n.d.						
		6	55	50	20	100	20	n.d.						
sum				1420	277	16.3								

Plant	Ch.	Interval Ic 1 (1029+1076)					Rec. call rate	Interval Id 3-1 (3118+3135)					Rec. call rate	
		Positive droplets			Corrected + normalized values			Positive droplets			Corrected + normalized values			
		B+B	M+M	B+M	Parental calls	Recomb. calls		B+B	M+M	B+M	Parental calls	Recomb. calls		
Zebularine 0.5µM	H12	1	158	182	32	316	32	237	209	60	418	60		
		2	176	188	26	352	26	236	220	51	440	51		
		3	28	42	4	56	4	32	30	6	60	6		
		4	118	144	17	236	17	109	166	24	218	24		
		sum				960	79	7.6				1136		141
	H13	1	148	151	30	296	30	n.d.						
		2	145	174	25	290	25	n.d.						
		sum				586	55	8.6						
	H14	1	100	119	39	200	39	n.d.						
		2	70	67	17	134	17	n.d.						
		3	83	100	24	166	24	n.d.						
		4	79	65	17	130	17	n.d.						
		sum				630	97	13.3						
	H15	1	180	228	33	360	33	296	302	69	592	69		
		2	174	192	42	348	42	331	320	76	640	76		
		3	246	207	44	414	44	301	352	73	602	73		
		4	204	196	40	392	40	324	378	98	648	98		
		sum				1514	159	9.5				2482		316
	H16	1	87	119	13	174	13	168	228	66	336	66		
		2	156	138	32	276	32	206	284	61	412	61		
3		206	207	21	412	21	248	334	66	496	66			
4		172	126	20	252	20	268	318	81	536	81			
sum					1114	86	7.2				1780	274		13.3
Trichostatin A 0.5nM	H17	1	283	261	51	522	51	234	191	66	382	66		
		2	278	265	34	530	34	215	228	52	430	52		
		3	254	291	43	508	43	203	259	81	406	81		
		4	78	83	8	156	8	58	73	21	116	21		
		5	193	194	23	386	23	177	196	48	354	48		
		6	164	155	18	310	18	125	163	40	250	40		
		7	186	178	28	356	28	107	154	38	214	38		
		8	129	140	17	258	17	116	143	33	232	33		
		sum				3026	222	6.8				2384		379
	H18	1	103	118	14	206	14	73	71	24	116	24		
		2	94	102	7	188	7	81	82	17	162	17		
		3	117	134	11	234	11	71	90	25	142	25		
		4	96	84	4	168	4	53	66	14	106	14		
		5	81	78	7	156	7	56	65	20	112	20		
		6	106	82	13	164	13	64	82	19	128	19		
7		100	109	12	200	12	73	71	24	142	24			
8		89	66	7	132	7	52	67	19	104	19			
9		60	61	12	120	12	55	56	16	110	16			
10		96	108	14	192	14	63	84	24	126	24			
11		83	60	5	120	5	50	45	14	90	14			
sum				1880	106	5.3				1338	216	13.9		

Plant	Ch.	Interval Ic 1 (1029+1076)					Rec. call rate	Interval Id 3-1 (3118+3135)					Rec. call rate	
		Positive droplets			Corrected + normalized values			Positive droplets			Corrected + normalized values			
		B+B	M+M	B+M	Parental calls	Recomb. calls		B+B	M+M	B+M	Parental calls	Recomb. calls		
Trichostatin A 0.5nM	H19	1	101	114	14	202	14		95	128	31	190	31	
		2	85	94	10	170	10		86	129	29	172	29	
		3	65	89	9	130	9		79	132	10	158	10	
		sum				502	33	6.2				520	70	11.9
	H20	1	153	135	27	270	27		179	198	41	358	41	
		2	45	38	7	76	7		39	52	13	78	13	
sum					346	34	8.9				436	54	11.0	
BIX-01294 0.5µM injected	H21	1	85	101	21	170	21		116	103	29	206	29	
		2	144	173	30	288	30		131	166	46	262	46	
		3	179	168	31	336	31		138	161	40	276	40	
		4	103	135	14	206	14		105	133	23	210	23	
		5	178	165	23	330	23		125	155	44	250	44	
		6	125	108	12	214	12		101	125	34	202	34	
		7	146	125	17	248	17		119	147	39	238	39	
		8	140	103	14	204	14		83	113	42	166	42	
		9	116	102	20	204	20		91	84	29	168	29	
		10	119	125	9	236	9		94	119	32	188	32	
		11	127	122	12	240	12		112	117	35	224	35	
		sum				2676	203	7.1				2390	393	14.1
	H22	1	103	126	23	206	23		n.d.					
		2	70	85	20	140	15							
3		88	83	22	166	18								
4		50	55	9	100	9								
		sum				612	65	9.6						
H23	1	162	213	18	324	18		n.d.						
	2	246	275	20	292	20								
	3	311	344	36	622	36								
	4	93	112	13	186	13								
	5	168	161	47	322	47								
		sum				1746	134	7.1						
Total					36920	3135					22578	3419		